Evaluation of Biomass Burning in China Using Satellite Remote Sensing Data

衛星リモートセンシングによる中国における バイオマス火災の評価に関する研究

Presented to the Faculty of the Graduate School of Agriculture

The Hokkaido University at Sapporo, Japan

for the degree Doctor of Philosophy

in Agriculture

by

Yi Kunpeng

(伊　坤朋)

共生基盤学専攻　　博士後期課程

星星之火,可以燎原。
小さな火花も広野を焼き尽くすことができる。
How small a spark it takes to set fire to a vast forest.

Abstract

Biomass burning (Fire) is one of the disasters causing threats to diverse ecosystems throughout the world. The majority of fires around the globe are caused by human activities, such as discarded cigarettes, campfire or sparks from equipment. Lightning is probably the most common natural cause of fire, especially in boreal forests. Fire has played, and will continue to play, a major role in shaping vegetation ecosystems throughout the world. Fire is a paradox. It is an essential factor for forest regeneration and nutrient recycling. For centuries, fire is one of the oldest tools known to humans and has been used as a management technique in land clearance. However, it is important to remember that fires can be devastating to diverse ecosystems under extreme weather conditions. The impacts of fires can have global consequences: biomass burning also produces gaseous and particle emissions that affect the composition of global atmosphere exacerbating climate change. Fires can produce local extinctions of species, alter species compositions and successional stages and bring about substantial changes in ecosystem functioning. Therefore, there is a strong impetus for an improved understanding of long-term fire regime and effects on both atmosphere and vegetation ecosystems.

Generally, most of fires occurred in the wild land regions including the most remote and inaccessible places. It is hard to be detected in time or managed efficiently in pre-satellite era. Nowadays, fires can be monitored and analyzed over large areas in a timely and cost-effective manner by using satellite sensor imagery in combination with spatial analysis as provided by Geographical Information Systems (GIS).

Information derived from satellite remote sensing systems provide a sound alternative to derive critical information for fire scientists and decision makers. This information is spatially comprehensive, and provides the capability for periodical updating.

Many previous research efforts have been addressed to wildfire in China. Tian et al. (2011a, b) focus on future impacts of climate change on forest fire danger in northeastern China. Liu et al. (2012) emulated natural fire effects using harvesting in an eastern boreal forest landscape of northeast China. Yang et al. (2004) simulated temporal patterns of fire regimes by using a hierarchical fire frequency model named LANDIS. A Fire danger assessment with remote sensing was also carried out in Northern China (Wang et al., 2013). However, these studies only focus on some particular regions, specific fire cases or specific fire period (pre-fire or post-fire). Remote sensing technologies have not been well studied in fire-related researches in China. A general and all rounds fire situations in china by using improved remote sensing satellite data and models should be addressed more efforts in this field. Therefore, the whole paper is designed in the descending order of the spatial study area from the country's macro management to the micro operation: China, Northeast region, the Great Xing'an Mountains, a study case of the 1987 fire. In time axis, the work is designed to follow time sequence, i.e. what the remote sensing can contribute to fire in different periods (pre-fire, during fire and post-fire).

In this study, I combine some unique methods and techniques such as quantitative analyses (e.g., time series analysis, statistical and geophysical methods) of observational and remote sensing data (e.g., MODIS, LANDSAT, NOAA-AVHRR) with physical modeling of fire-vegetation processes. Satellite and GIS data will be

used in situ burned area observations information to understand fire-induced vegetation processes and fire consequence on atmospheric environment. There are mainly two objectives of this work. As we know, it is impossible to effectively manage fires without a clear and correct understanding of the distribution and dynamics of fire. Therefore, it is vital to have correct and timely knowledge of the total area burned and the spatial pattern of fire in China. This is the first motivation of this study. In addition, biomass burning also leads to an increase in greenhouse gas emissions, such as carbon dioxide (CO_2) and methane (CH_4). At both global and regional scale, biomass burning events have a devastating impact on limited forest resources and atmospheric quality. As such, the second research objective is to seek an improved understanding the biomass burning effects of fire on both atmosphere and landscape-scale dynamics in vegetation ecosystems. To be specific, the objectives of this study were to identify spatial and temporal patterns of burned area China; to map the fire risk and danger in the northeast of China by combining remote sensing data and meteorological data; to estimate the potential range and spatial-temporal patterns of biomass burning emissions in the Great Xing'an Mountain area; to describe the long-term effects on vegetation following a typical fire disturbance.

This article is organized in six chapters. Chapter 1 summarizes major biomass burning effects, challenges of biomass burning monitoring, the objectives and organization throughout the whole paper. In Chapter 2, I identify spatial and temporal patterns of burned area China by using historical statistical data and MODIS fire product. A general picture of the fire situations in China will be shown in this chapter. Chapter 3 presents a fire risk mapping method which is based on satellite data and

meteorological data. In chapter 4, I estimate the potential range and spatial-temporal patterns of biomass burning emissions in the Great Xing'an Mountain area. Chapter 5 assesses the fire damage of the entire fire-affected areas in the Great Xing'an Mountains from the 1987 fire event. Both intra- and inter-annual variations in satellite observations were analyzed to better understand how vegetation responds to fire disturbance. The chapter 6 presents whole conclusions and the limitations of the thesis.

Chapter 2 presents an analysis of the spatial and temporal patterns of burned area in China by combining national historic records and satellite fire data. It is the first to consider the larger picture of open fires for the entirety of China. Both spatial patterns and temporal trends are analyzed in nine sub-regions spanning a diverse array of ecosystems. An analysis of the fire products shows that, during the period 2001–2012, an average of 3.2×10^6 ha (32,000 km^2) yr^{-1} area was burned in China. The majority of these fires occurred in the northeast and in the southwest regions. Fires in southwest China are characterized by frequent burns with light damage. While the northeast region accounts for less fire occurrences, but larger and cause more serious damage than southwest China. The inter- and intra-annual fire trends and variations of nine sub-regions are reported by analyzing regional climate characteristics. Monthly meteorological data at 130 stations in China are used over a 50-year period (1952-2013). The monthly burned area profiles of each sub-region exhibit a distinctive seasonality. Spring and autumn are the two peak fire seasons in each year for the entirety of China. Fire season duration and fire severity are closely related to modes of regional climate variability in the northeast and southwest China and Inner

Mongolia. Crop residue burning plays an important role in southeast and north China, especially concentrated in the Yangtze River and the North China plains. Therefore, the fire activities are dominantly governed by agricultural activities and are less affected by regional climate in southeast and north China.

In chapter 3, a fire disturbance index (FDI) algorithm is designed to capture long-term variations in the ratio of Land Surface Temperature (LST) to Enhanced Vegetation Index (EVI) on a pixel-by-pixel basis. There is a dramatic difference in the LST-EVI relationship between pre-fire and post-fire values in the case of a fire that occurred in 2003. The algorithm is tested using data from a Moderate Resolution Imaging Spectroradiometer (MODIS) data to explore continuous spatio-temporal patterns of fire disturbances. The findings suggest that the FDI can be used to detect pixels corresponding to burned regions. However, it often overestimates the fire-affected area with a large amount of noises. The fire disturbance patterns are also analyzed using meteorological parameters in Northeast China.

Biomass burning emissions in the boreal region yield an important contribution to the chemical budget of the troposphere. Thus, chapter 4 assesses the contribution of biomass burning to the emissions of atmospheric trace species in the Great Xing'an Mountains (GXM), which is also the most severe fire-prone area in China. I estimate various biomass burning activities by combining explicit remote sensing data with fire-induced emission models. We derived 9998 fire scars with 46,096 km^2 from the years 1986 to 2010. The years 1987 and 2003 contributed 33.2% and 22.9%, respectively, in burned area during the 25 years. Fire activity is the strongest in May. Most large fires occurred in the north region of GXM between 50ºN and 54ºN latitude

due to much drier weather and higher fire danger in the northern region than in the southern region of the study domain. Evergreen and deciduous needleleaf forest and deciduous broadleaf forest are main sources of emissions, accounting for 84%, 81%, 84%, 87%, 89%, 86%, 85% and 74% of the total annual CO_2, CH_4, CO, PM_{10}, $PM_{2.5}$, SO_2, BC and NOx emissions, respectively. Fire emissions from shrubland, grassland and cropland only account for a small fraction of the total emissions level (approximately 4%-11%). Comparisons of our results with other published estimates of biomass burning emissions show reasonable agreement. However, substantial uncertainties remain concerning the modeling parameters.

Chapter 5 assesses fire effect on vegetation of a typical fire event. I pick up the catastrophic fire as a study case, which occurred in 1987 on the northern Great Xing'an Mountain in China. This chapter describes the long-term effects on vegetation following the catastrophic fire by analyzing the AVHRR GIMMS 15-day composite normalized difference vegetation index (NDVI) dataset. Both temporal and spatial characteristics are analyzed for natural regeneration and tree planting scenarios from 1984 to 2006. Regressing post-fire NDVI values on the pre-fire values helped to identify the NDVI for burnt pixels in vegetation stands. Stand differences in fire damage are classified into five levels: Very High (VH), High (H), Moderate (M), Low (L) and Slight (S). Furthermore, intra-annual and inter-annual post-fire vegetation recovery trajectories are analyzed by deriving a time series of NDVI and stand regrowth index (SRI) values for the entire burned area. The results show that October is a better month for distinguishing the post- and pre-fire vegetation conditions using the NDVI signals because colored leaves of grasses and shrubs fall down, while the

leaves on healthy trees remain green in October. Because of tree planting primarily were mainly carried out in the severely burned area following the 1987 fire, the high and very high burned pixels exhibited a better recovery trend than the lightly burned regions.

Acknowledgement

In this moment, when I sit down to write these final sentences, I realize that my PhD life in the Hokkaido University as well as my entire schooldays come to an end. The years have become remote, more than twenty years past in a twinkle. All my feelings and inspirations are concentrated in the long way of seeking knowledge. The sweets, bitters and all kinds of feelings well up in this road. No matter how hard the days I faced, I finally chose be strong. Be strong is not because how strong I am, but because there are so many people constantly gave me the strength to proceed, who also taught me a lot about life. Thanks and appreciates are words too light to carry my deep gratitude in my heart. But now, I can only do this to everyone, to express my sincere affection.

I would like to thank my dissertation director, Dr. Tani Hiroshi. I will always be grateful to you for providing me this valuable opportunity to have studied in this lab as an international PhD student. Thanks for your guidance, constructive criticism and patience to guide me through my research. Thanks for your scientific research cultivate spirits that encourage innovation, respect disagreements and inclusive failures. It has been excellent opportunity for me and I have learned a lot from you. You are my inspiration, not only in the academic and research fields, but also in your leadership and entrepreneurship. I would also like to express my special thanks to Prof. Osaki Mitsuru and Prof. Noguchi Noboru for their professional suggestions and comments on my dissertation.

I owe a very big thanks to my daily supervisor, Dr. Wang Xiufeng. Thanks for your guidance on all sides of my daily life in Japan. Each international student likes a

lonely and helpless boat, when he/she starts the first step in a foreign land. You are here like an anchor, which makes us feel poised and calm to face tempestuous storms and terrible waves. You covered us to seek our studies without any other daily life troubles. Wish you can enjoy a peaceful and nice time in the coming years, be healthy and be beautiful forever.

I would like to thank all of my colleagues in the lab of Remote Sensing Group (RSG) of : Liu yang, Guo meng, Jiang shiming, Zhong guosheng, Kojima, Sonobe, Koita, Soma, Araki, Ooki, Duerblt, Laju, Yoki, Tony. This room is full of the fragrance smell of books. All the serious discussions and funny jokes with you guys, carved the edges and corners of my memories about this lab. I have confident this friendship will continue for many years to come.

I would like to thank my Master adviser, Prof. Zhang Jiquan who works in Northeast Normal University, Changchun, China. Thanks for your offer me a great opportunity to study abroad that giving me a new starting line in my life. I will remember my original intentions, no matter how far I reach in the future.

I would like to thank my mother. I brought you a toilsome10-month pregnancy first, when I haven't yet come to this world. From the baby babbles to contradict you, until I travel in distant parts in the name of seeking knowledge, I failed to take the responsibility of filial piety in a Chinese traditional way that require a son to company with parents. That would be two weeks after your sixty years old birthday, when you read these words. I hope you can feel a little bit of relief and console when you see mine grow up through the time. Mama, I wish you be happy and be healthy forever. If

time and tide have to climb on your face, then please smile out many wrinkles to give the coming years some stairs, welcome them.

I would like to thank my father. I brought you many pressures and troubles. I deservedly should bring you much more expects and hopes as well. From a baby toddler to a free running, my footsteps get quicken gradually, while your actions turn to slow. You vouchsafed me a name of Kunpeng with a huge hope of future, I will do my best to earn a parallel life.

I would like to thank my girlfriend for being very supportive and your moral supports have been inspirational throughout the course of my PhD study. And despite the very tough challenges facing us some days, you have always stood by me, continues to energize me with a sense of hope and optimism, and a belief that if we chose be strong, we can build a better life for ourselves.

Finally, I would like to express my tremendous gratitude to the Chinese Top University Graduate Students Studying Abroad program, which sponsored me to finish my PhD study in Japan.

Yi Kunpeng

In Hokkaido University

Table of Content

List of figures

Chapter 1. General introduction

1.1 WHAT IS BIOMASS BURNING?

Biomass consists of living or once-living biological material. However, when we use the term in this study, we are referring to living or dead vegetation in most cases. Biomass burning is the act of burning living or once living biological material. Biomass burning results from either natural processes, such as ignition by lightning strikes, or anthropogenic sources, i.e. human-induced, activity, such as prescribed fires used for agricultural, eco-logical control or other similar purposes. Fires are estimated to burn up to 500 million hectares of woodland, open forests, tropical and sub-tropical savannas, 10-15 million hectares of boreal and temperate forest and 20 to 40 million hectares of tropical forests annually (Stephens et al., 2008). Wildfires are a natural phenomenon; however, an increase in non-sustainable vegetation burning has scarred the Earth to a much greater extent in the last several decades than in prior times. Wildfires are a paradox for many terrestrial ecosystems. Fire is essential to maintain ecosystem dynamics, biodiversity and productivity. They are nature's way of recycling the essential nutrients, especially nitrogen. For many boreal forests, fire is a natural part of the cycle of the forest and some tree species. Fire is one of the oldest tools known to humans; it has been used as a management technique in land clearance for centuries (Stephens et al., 2010). Conversely, fires destroy tens of thousands of hectares of forests, woodlands and other vegetation, resulting in the loss of many human and animal lives and immense economic damage.

1.2 BIOMASS BURNING EFFECT

Fire in the natural context is an important part of ecosystem services that provides nutrients and recycling material. Fires have also always resulted in the emissions of some gases and aerosols to the atmosphere (Keywood et al., 2013). Biomass burning is known as a major source of aerosols and trace gases in the atmosphere (Marshall et al., 1996; Jacobson et al., 2009). Smoke emitted by fires consists of aerosol particulate matter (PM) and numerous trace gases, including carbon monoxide (CO), carbon dioxide (CO_2), methane (CH_4) and nitrogen oxides (Knox and Clarke). Globally, biomass burning contributes approximately 50% of the total direct CO emissions and approximately 15% of surface NO_X emissions (Levine et al., 1995; Ito and Penner, 2004). Most of this particulate matter and trace gases can significantly impact the air quality and human health as well as the climate, with a potential feedback on air quality. For example, smoke PM can influence the precipitation processes to result in delayed, suppressed, or invigorated rainfall, a change in the cloud albedo, and scatter and absorb solar radiation, which affects atmospheric warming or cooling and contributes to climate change (Liu et al.; Crimmins, 2004; Aldersley et al., 2011). Figure 1-1 shows the wildfire situation in the boreal forest near the border between Russia and China. This image shows a number of fires that are simultaneously burning in this region. This situation is not exceptional; many fire spots appear almost daily during the fire season. Scientists also fear that human beings are instigating a catastrophic feedback loop in which greenhouse gasses accumulate to result in a warmer, drier climate, which, in turn, causes more wildfires, thereby accelerating the increase in greenhouse gases.

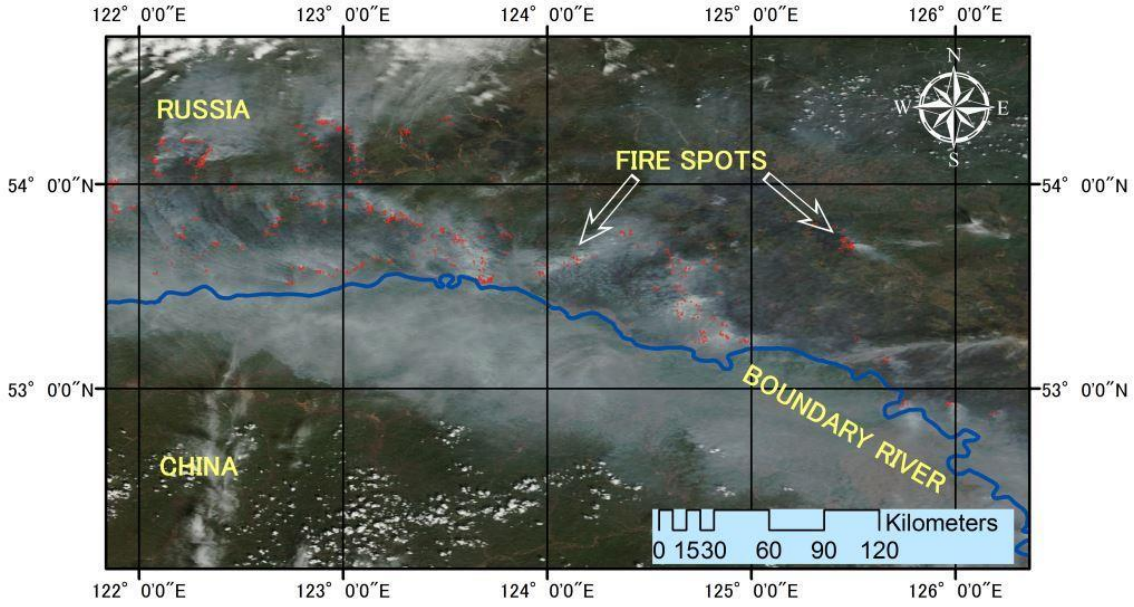

Figure 1-1 MODIS True Color of fires and smoke near the border between China and Russia on May 17, 2012 (RGB composition: band1-band4-band3)

Wildfire is an important process in regulating vegetation succession, plant regeneration and species composition in boreal forest ecosystems (Kang et al., 2006; Wulder et al., 2009; Beck et al., 2011). Large areas of the boreal forest zone, which natural fire has shaped over several millennia, are burned every year. The industrial and recreational use of boreal forests and forest fire suppression capabilities have dramatically increased over the past century (Cahoon et al., 1994). Northeast China maintains abundant forest resources, with a forest area of ~ 47.0×10^4 km^2 that occupies 31% of China's total forest area (Tan et al., 2007). This region stores 1.0-1.5 Pg C and contributes to approximately 24–31% of the total carbon storage in China (Fang et al., 2001). Figure 1-2 shows the burned area of a 2010 fire event in the Great Xing'an Mountain in the Northeast region of China. This photo was taken one year after the fire during our field survey in August 2011. Most carbon is stored in living trees. For thousands of years, wildfires have been the predominant disturbances in this

region, which has been strongly modified by humans during the latter half of the last century.

Figure 1- 2 Burned area of 2010 fire in the Great Xing'an Mountain, Northeast region of China (The photo was taken on August 20, 2011)

1.3 REMOTE SENSING CONTRIBUTES

Thirty years after the pioneering work, a number of research coordination activities have contributed to the understanding of biomass burning, including the Global Fire Monitoring Center and the European Commission via the Forest Fire Information System, both of which facilitate the monitoring and assessment of biomass burning activity. Satellite remote sensing technology has the potential to play an important role in monitoring fires and their consequences as well as in operational fire management (Akther and Hassan, 2011). Space-based observation is the best method for acquiring global quantitative information and the spatial distribution of wildfire events. A number of satellite-based observations have been available since early 1982 to constrain fire activity from space. The majority of satellite-based sensors employ

passive techniques, observing either solar backscatter or thermal emissions. Remote sensing data include observations of fire activity (ignition, location, and burnt area) and products, such as the temperature, precipitation, solar radiation, vegetation type, and Normalized Difference Vegetation Index. When fed into biogeochemical models or used with vegetation classification systems, this information enables the evaluation of fuel load and combustion completeness (van der Werf et al., 2006). The main biomass burning products derived from remote sensing include the fire activity (or hotspots) and area burned. The fire activity provides information on the spatial and temporal distributions enabling near real-time fire monitoring. The duration of a fire can be estimated because small fires can generally be detected.

Table1-1 Satellite measurement of variables related to wildfire and burned surfaces

Variable	Sensor (satellite)	Spatial resolution	Spatial coverage	Date period
Fire location	OLS(DMSP)			
	AVHRR (NOAA)	2.7×2.7km	Global	1979-1992
	MODIS(Terra/Aqua)	1×1km	Global	1992-present
	VIRS (TRMM)	1×1km	Global	2000-present
	ASTER (Diaz-Delgado *et*	2.4×2.4km	40°N-40°S	1997–present
	al.)	0.03×0.03km	Global	2000–present
	HSRS (BIRD)	0.37×0.37km		
Fire radiate power	IMG (GOES)	4×4km	North and	
	SEVIRI (MSG)	3×3 km	Africa and	2004–present
	MODIS (Terra & Aqua)	1×1 km	Global	2000–present
	HSRS (BIRD)	0.37 × 0.37 km		
Temperature	SEVIRI (MSG)	3×3 km	Africa and	2004–present
	IMG (GOES)	4×4 km	North and	
Burned area	ASTER (Diaz-Delgado *et*	0.03 × 0.03 km	Global	2000–present
	al.)	0.5×0.5 km	Global	2000–present
	MODIS (Terra & Aqua)	1×1 km	Global	2000– present
Burned severity	VEG (SPOT)	0.03 × 0.03 km	Global	1972–present
	TM, ETM (Woodcock *et al.*)			

Table 1-1 lists the fire activity and burned area products presently available. Products have progressed from single to multiyear products, enabling an understanding of inter-annual variability in areas burned with the combination of regionally active fires. In addition, discrepancies in burned areas derived from different sensor products result in differences in the emission estimates of pyrogenic chemical species. For example, a validation of GLOBCARBON, MODIS, and L3JRC burned-area products using standard independent reference data and reporting protocols for Southern Africa showed that the MODIS product was most accurate, most likely due to its higher spatial resolution, which enables the detection of smaller and fragmented fires (Kaiser et al., 2012).

1.4 CHALLENGE OF BIOMASS BURNING MONITORING AND MANAGEMENT

The worldwide fire crisis during the El Niño episode of 1997-98 and a number of large fire disasters on the Balkan, in the Mediterranean Region, North America, Eurasia, Australasia and Africa between 1998 and 2001 revealed that an international wildland fire network was needed to facilitate information sharing and wildland fire disaster assistance. To avoid undesirable consequences of fires, the prevention, monitoring, and management of fires are required. Information on fire behavior and location is vital to predict fire occurrence and emissions (Keywood et al., 2013). As mentioned above, remote sensing from space is especially suited for forest fire research. Even though satellite remote sensing technology has been successfully applied to wildfire research and management in many ways, some aspects still require improvement:

i. Cloud cover and smoke may mask fire activity. The advantage of detecting products of the burned area over active fire detection is that observational gaps due to cloud cover and satellite revisiting time can be filled due to the persistence of the burn scar. However, the area burned may be underestimated because a substantial part of the grid cell must be burned to be counted. The advantages and limitations of fire activity and products of the burned area suggest that the combination of these products would improve global estimates of biomass burning emissions (Keywood et al., 2013).

ii. The quantification of fire risk often is a difficult and contentious task due to: the complexity of fire events across multiple time and space scales, the effects of these fires on the ecosystem, and (Ardizzone et al.) the diverse fire regimes that are created by these fire events over time (Keane et al., 2010).

iii. Quantifying biomass burning emissions represents a challenge, and current estimates are only available at a coarse spatial resolution with large uncertainty.

Although, satellite-based technologies have been wildly used in burn area mapping in United States and Canada, large gaps remain between developing countries and these developed countries. For example, an accurate and national history of burned area maps in China has not been well documented, even though many fires have occurred across divers plant ecosystems in this country.

1.5 GOALS AND OBJECTIVES

At both the global and regional scale, biomass burning events have a devastating impact on limited forest resources and atmospheric quality. As such, understanding the effects of wildfire on the environment is one of my research interests. I combine unique methods and techniques, such as quantitative analyses (e.g. time series analysis, statistical and geophysical methods) of observational and remote sensing data (e.g. MODIS, LANDSAT, SPOT, PALSAR) with physical models of fire-vegetation processes. I will use satellite and GIS data as well as in situ burned area observation information to understand fire-induced vegetation processes and interactions of fire-climate systems, improve our model capability to predict fire risk and assess current and future fire impacts and consequences on our environment.

The objective of this study was to identify the spatial and temporal patterns of burned areas in China, map the fire risk and danger in Northeast China by combining remote sensing data and meteorological data, and estimate the potential range and spatial-temporal patterns of biomass burning emissions in the Great Xing'an Mountain area. Specifically, I will assess the fire damage of all fire-affected areas in the Great Xing'an Mountains from the 1987 fire event (ii) to better understand how vegetation responds to fire disturbances by analyzing intra- and inter-annual variability in satellite observations and (iii) to characterize the spatial pattern of post-fire vegetation trends using the AVHRR GIMMS NDVI record over the period 1986-2006.

1.6 ORGANIZATION

This article is organized into seven main sections. Figure 1-3 represents the structure of the entire thesis. The entire paper was designed in descending order of the spatial study area from the country's macro management to the micro operation: China, northeast region, the Great Xing'an Mountains, 1987 fire scar. In the time dimension, the work was designed to follow a time sequence, i.e. what the remote sensing can contribute to fire in different periods (pre-fire, during fire and post- fire.)

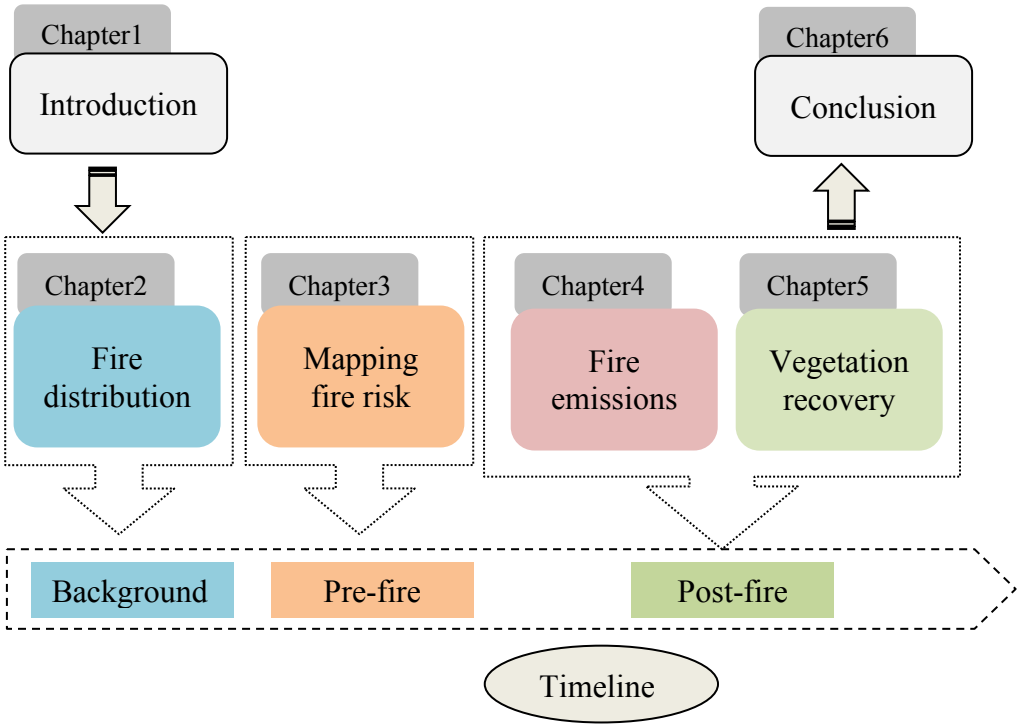

Figure 1- 3 Structure of the thesis

In Chapter 1, I overview major biomass burning effects and the challenges monitoring biomass burning, and I summarize the objectives and outline organization throughout the entire paper. In Chapter 2, I identify the spatial and temporal patterns of the burned area in China by using historic statistical data and the MODIS fire

product. This chapter will show a general picture of the fire situation in China. Chapter 3 presents a fire risk mapping method that is based on satellite and meteorological data. In chapter 4, I estimate the potential range and spatial-temporal patterns of biomass burning emissions in the Great Xing'an Mountain area. Chapter 5 assesses the fire damage of the entire fire-affected areas in the Great Xing'an Mountains from the 1987 fire event. Both the intra- and inter-annual variabilities in satellite observations were analyzed to better understand how vegetation responds to fire disturbances. Chapter 6 presents overall conclusions and the limitations of the thesis.

Chapter 2. Assessing spatial patterns and temporal trends of burned area in China

ABSTRACT

In this chapter, we present an analysis of the spatial and temporal patterns of burned area in China by combining national historic records (1950-2010) and satellite fire products (2000-2010). Our study is the first to consider the larger picture of open fires for the entirety of China, analyzing fire spatial patterns and temporal trends from nine sub-regions whose territories span a diverse array of ecosystems. This scale is commensurate with that of some important climate variations, yet still allows us to make comparisons across diverse ecosystems. An analysis of the fire products showed that, during the period 2001–2012, an average of 3.2×10^6 ha (32,000 km^2) yr^{-1} of fires occurred in China. The majority of these fires occurred in northeast China and in the southwest provinces. Southwest China is characterized by many small fires and more casualties. Although the northeast has fewer fires, they are larger and cause more serious damage. The inter- and intra-annual fire trends and variations of nine sub-regions were reported by analyzing regional climate characteristics. Monthly meteorological data at 130 stations in China were used over a 50-year period (1952-2013). The monthly burned area profiles of each sub-region exhibit a distinctive seasonality. Spring and autumn are the two peak fire seasons each year for the entirety of China. Fire season duration and fire severity are closely related to modes of regional climate variability in Northeast and Southwest China and Inner Mongolia. Crop residue burning plays an important role in southeast and north China, especially

concentrated in the middle and lower Yangtze River and the North China plains. Therefore, the fire activities are dominantly governed by agricultural activities and are less affected by regional climate in southeast and north China.

KEYWORDS:

Fire frequency, crop residues burning, climate, spatial trend, temporal pattern

2.1 INTRODUCTION

Vegetation burning in China is a threat to its limited forest resources and the environment, causing not only local ecological, economic and social impacts but also large-scale implications for global change. The effects of fire on vegetation, soil and the atmosphere are strongly associated with fire characteristics (e.g., density, frequency, severity, seasonality, size distribution), which are commonly grouped under the general term fire regimes (Stocks et al., 2002). Fire regimes refer to average fire conditions occurring over a long period of time. Fire density is commonly measured as the number of fires within a given area. Fire frequency is related to the return interval of fire, measured on a given time scale (Chuvieco et al., 2008). Mapping the timing and extent of vegetation fires is crucial, as fire is a major disturbance factor reshaping ecosystem landscape structure and the cycling of carbon. Over the past several decades, there has been growing concern about the relationship between fires and climate change (Westerling et al., 2003; Randerson et al., 2006; Keywood et al., 2013) and a perceived increasing incidence, extent, and severity of uncontrolled burning globally (Hoelzemann, 2004; Giglio et al., 2006; Chuvieco et al., 2008), which has led to calls for international environmental policies concerning

fires (FAO, 2006). Therefore, there is a strong impetus for datasets of long term burned area with explicit spatial and temporal resolution.

The monitoring of biomass burning using satellite data at regional to global scales has been prevalent over the last two decades. The locations of active fires and the spatial extent of the areas affected by fires can be detected at the time of satellite overpass. The NASA Moderate Resolution Imaging Spectroradiometer (MODIS) on the Terra (morning) and Aqua (afternoon) satellites has specific features for fire monitoring and has been used to systematically generate a suite of global MODIS land products, including a 1 km active fire product (Giglio et al., 2009; Urbanski et al., 2009) and, more recently, a burned area product that maps the approximate day and extent of burning at 500 m resolution (Roy et al., 2008). The first global burned area product is now being generated as part of the MODIS Land Collection 5 product suite and is currently available.

One of the most interesting topics in fire-related research is the analysis of the spatial pattern of fire distribution and fire regimes and whether these regimes are originally shaped by regional climate characteristics. The main purpose of this study was to identify patterns of burned area in China by combining national statistics for China (1950-2010) with the MODIS burned area product (2001-2012). The MODIS fire product provides a more consistent spatial and temporal basis for interpretation than national statistics. Seasonal and inter-annual burned area temporal patterns were analyzed to obtain fire frequency and periodicity in the burn cycle. We also determined whether burned area increased or decreased for any month or annually over the 60 years across the entirety of China and for 9 sub-regions. The fire patterns

were correlated with regional climate characteristics to explain fire occurrence and frequency in relation to, for example, land cover, spatial distribution, elevation and sea influence.

2.2 DATA SOURCE AND PREPROCESSING

2.2.1 MODIS burned area product MCD45

The Moderate Resolution Imaging Spectroradiometer (MODIS) was launched on the Terra platform in December 1999 as part of NASA's Earth Observing System (Quarmby *et al.*). The MODIS instrument, which began collecting image data in February 2000, is generating a number of land surface products to meet the goals of NASA's Earth Science Enterprise (Justice *et al.*, 1998). The fire products now available from MODIS include the only current global daily active fire product (Justice *et al.*, 2002). In this study, fire-affected areas of China were taken from the recently developed MODIS MCD45A1 Burned Area. This fire product is produced from a change detection algorithm based on a bidirectional reflectance distribution function (BRDF) model (Roy *et al.*, 2005; Roy *et al.*, 2008). MCD45A1 is a monthly product at 500 m resolution and has been available online since April 2000. The product reports the approximate day of burning with 8-day precision. A statistical measure is used to determine whether the difference between the observed reflectance and the BRDF model predicted reflectance in the near and middle infrared bands indicates a significant change of interest. This approach is repeated independently for each pixel, moving through the reflectance time series in daily steps. A temporal constraint is used to differentiate between temporary changes, such as shadows, which are spectrally similar, to more persistent fire-induced changes. The identification of

the date of burning is constrained by the frequency and occurrence of missing observations, and to reflect this, the algorithm is run to report the burn date with an eight-day precision.

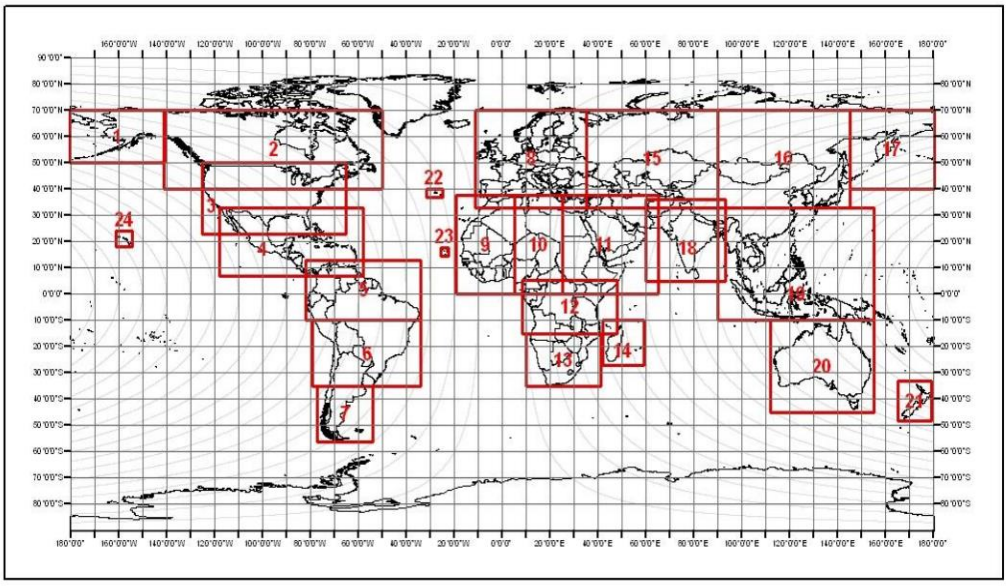

Figure 2- 1 Geotiffs covering a set of sub-continental windows

2.2.2 Historic fire statistical data

The forests of China represent a significant national resource and have been systematically inventoried by the National Forestry Bureau (NFB) and managed for forest products in the more productive regions. Historic fire statistical data are produced by the NFB, which records most significant wildfire events occurring in China. However, the official burned-area statistic is a rough data source because of personal and impersonal reasons, such as limited monitoring and communication techniques in past several decades. The NFB has reported information regarding significant wildfires across China since 1950, including the number of fires, burned

area, forest loss and human death. In 1987, the inventory was updated to cover more detailed wildfire information, and the accuracy has greatly improved since then.

2.2.3 Data preprocessing

Burned areas are characterized by deposits of charcoal and ash, removal of vegetation, and alteration of the landscape structure. Therefore, fires can be detected by using a contextual algorithm that takes advantage of these spectral, temporal and structural changes. The MODIS algorithm uses the bidirectional reflectance model-based change detection approach to detect the approximate date of burning at 500 m by locating the occurrence of rapid changes in the daily surface reflectance time series data at multiple wave bands. The burned area detection rate was evaluated according to fire size and land cover using the University of Maryland modification of the International Geosphere-Biosphere Program (IGBP) land cover type classification scheme of the MODIS Level 3 Land Cover Product. A fire event was considered detected if the incident fire perimeter polygon was within 1 km of any MODIS-DB fire event buffer. The evaluation of the fire detection rate by land cover type used the UMD cover type scheme aggregated to 6 cover types (forest, savanna, shrub, grassland, crop, and barren). The MODIS Land Cover Product was converted to polygons and intersected with the incident polygons. The dominant cover type by area for each fire event was taken as that event's cover type for the analysis (Urbanski et al., 2009).

A user-friendly geotiff version of the MCD45 product is derived from the standard MCD45A1 hdf version by the University of Maryland. The geotiffs cover a set of sub-continental windows (Figure2-1). In this study, sub-continental windows of

15,16,18 and 19 were selected to cover the entire region of China. Burning detected in the middle month plus and minus eight days (the detection precision) is reported. For each gridded land pixel, the following information is described: the approximate Julian day of burning; a code indicating unburned, or no burning detected but snow detected, or no burning detected but water detected, or an insufficient number of MODIS observations to make a detection decision (usually due to cloud or missing data) and ancillary processing path and quality information (Roy *et al.*, 2008).

2.3 RESULTS AND DISCUSSION

2.3.1 Wildfire variability and trend based on historic fire statistical data of china

China is a country that lacks forestry resources and suffers from numerous wildfire attacks every year. Losses due to forest fires in China from 1950 to 2010 are shown in Table 2-1. The total forest area and stock volume are estimated to be only 0.134 billion ha and 11.78 billion m^3, respectively, and the forest cover rate is 13.92% (Zhong *et al.*, 2003). Analyses using official fire statistical data showed there were 788,683 fires between 1950 and 2010, with an average of 5.7×10^5 ha/yr.

Table 2-1 Loss due to wildfires in China from 1950 to 2010

Period	Amount (10^4)	Burned forest (10^4 ha)	Burned forest for per fire (ha)	Injuries	Deaths
1950–1960	20.9022	1371.56	65.62	7759	1126
1961–1970	15.3471	764.81	49.83	4980	895
1971–1980	14.5928	1074.45	73.63	7166	1111
1981–1990	13.0685	403.00	30.84	5853	1091
1991-2000	5.3489	53.81	10.06	1699	469
2001-2010	9.6087	134.28	13.97	624	666
Total	78.87	3802		28081	5358

Table 2-1 shows the fire-induced losses, including ecological damage and social loses. From 1950 to 2010, there were a total of 78.87×10^4 fire events, and 3802×10^4 hectares of forest was burned. The total human deaths and injuries attributed to wildfires were 5358 and 28081, respectively, during the past 60 years (Figure2-3). Wildfire number and burned area shifts exhibit an evident periodicity before 1987. In terms of fire numbers, the peak values (1955, 1962, 1979 and 1986) always occurs in every 7 or 10 years, as can be seen in Figure 2-2. In terms of statistical data, the amount of burnt area fluctuated largely year by year, as indicated in Figure2-2. The burnt areas were over 1×10^6 ha in the following years: 1951, 1955, 1956, 1961, 1962, 1972, 1977, 1987, 1996, 2004 and 2006. For burned area, there is a similar periodic trend with fire number change before 1987.

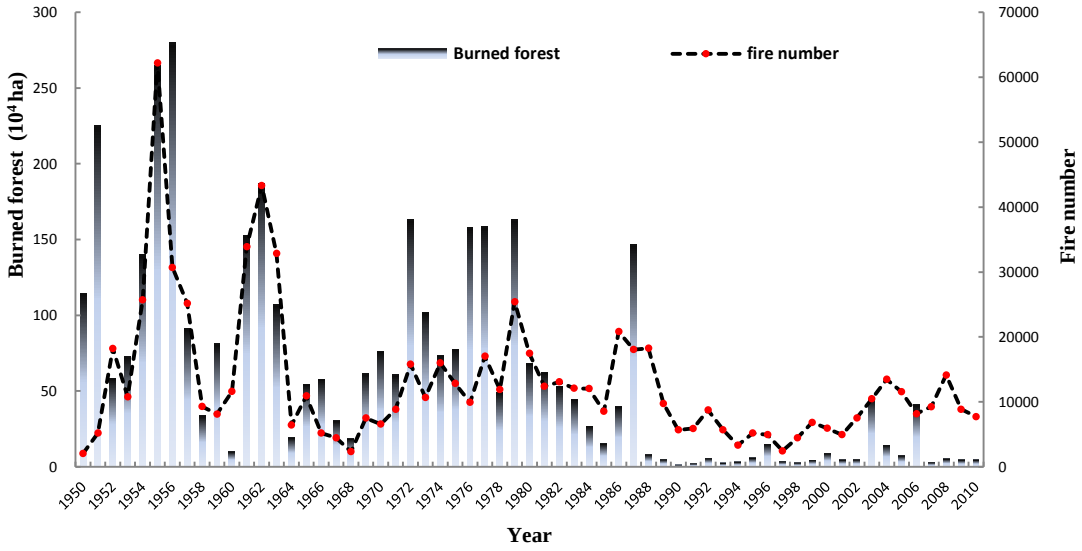

Figure 2- 2 Total wildfire numbers and burned forest in china from 1990 to 2010

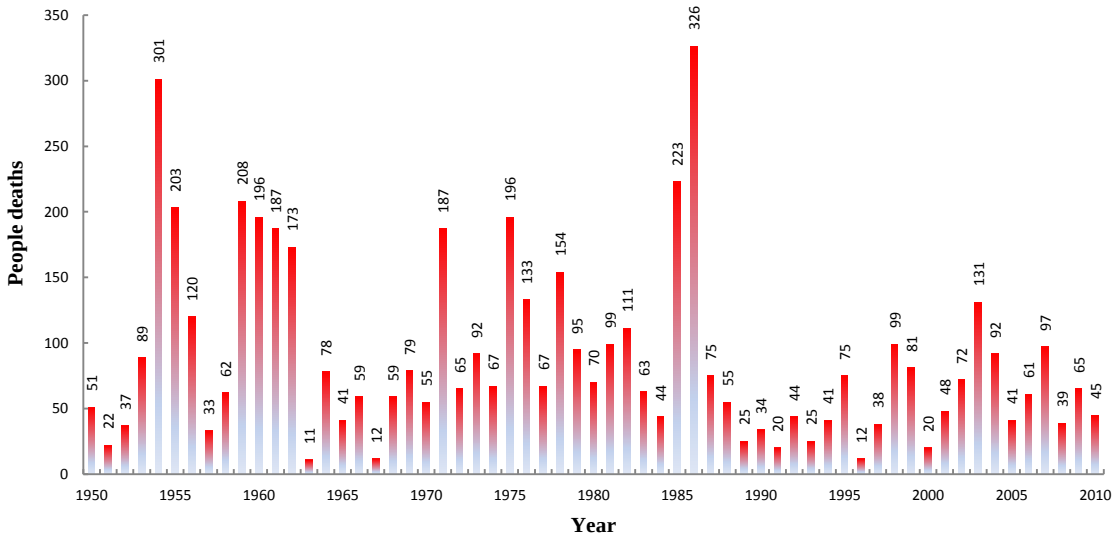

Figure 2-3 Deaths due to forest fires from 1950 to 2010

Fortunately, the general trend of wildfires in China has markedly decreased over time. On May 6, 1987, a catastrophic fire occurred on the northern slopes of the Great Hing'an Mountains, burning a total area of 1.3×10^6 ha. Since this catastrophe, the Chinese government has paid special attention to protection from wildfires. Many effective actions were taken in the subsequent years, such as the establishment of professional fire prevention forces and the organization of a series of fire protection agencies from central to local governments. Thus, the tide of wildfires in China has turned significantly in recent years. Figure 2-4 shows the general trend of wildfires in China over the past 60 years. The total burned area declined from 1371.56×10^4 ha in the first 10 years (1950-1960) to 134.28×10^4 ha in the last 10 years (2001-2010) (Figure 2-4 a). The average burned area for single fires also decreased dramatically, from 65.62 ha for 1950-1960 to 13.97 ha for 2001-2010 (Figures 2-4 b and 2-5).

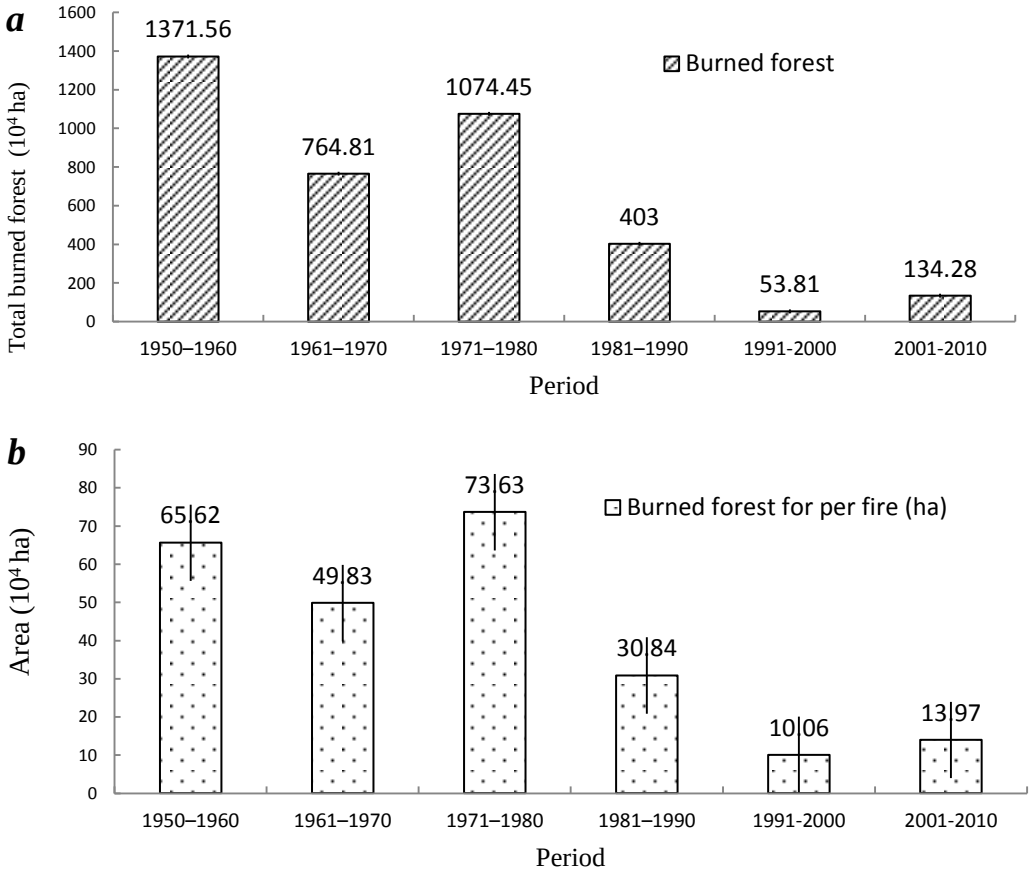

Figure 2- 4 Burned area shift in every 10 years period, Total burned forest area (a); average burned forest area for single fire (b)

Chinese records indicate that the number of fatalities due to forest fires has increased in recent years, most likely due to the increased emphasis on the expedient suppression of wildfires. Local residents participate in suppression activities organized by town/village authorities and report fires to the town/village fire management office. If a fire becomes a Class 3 fire (> 100 hectares), the county fire control center reports it to the provincial fire control center, and the provincial fire control officer assumes responsibility for controlling the fire (PRC, 2000). These procedures for reporting and assuming control are well established and are displayed in each fire control center. Generally, each county, municipality, province and

national level of the organization has a fire management committee comprising representatives of various agencies, such as civic administration, police, army, urban fire service, finance department and meteorology bureaus (PRC, 2000).

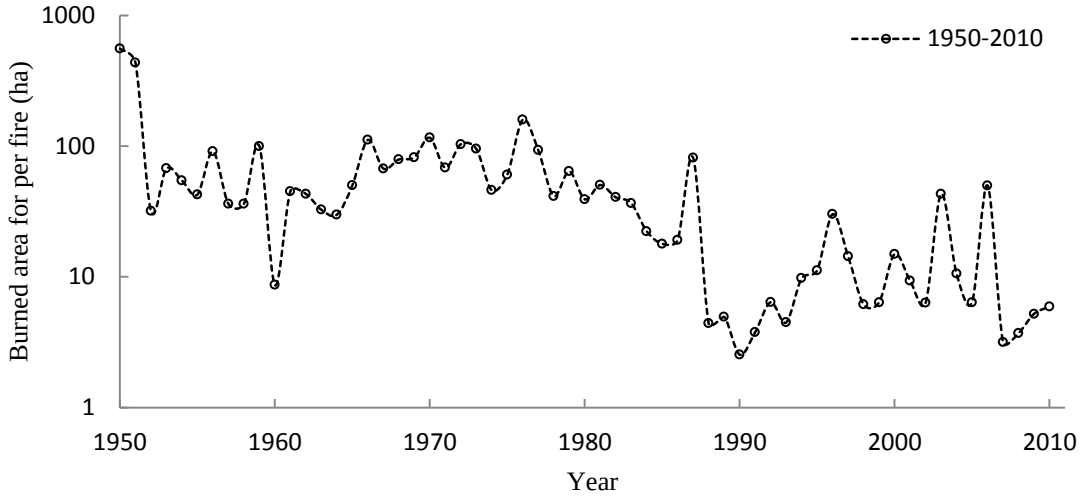

Figure 2-5 The average burned area for per wildfire from 1950 to 2010

Nevertheless, the number of fires has been underestimated due to fires occurring in remote and sparsely populated regions, where they are seldom recorded. In these regions, local government agencies only report severe fires they cannot control by local forces. Thus, because of personal and impersonal reasons, the official statistical data could represent only the lower limit of the estimated area affected by fire (Song *et al.*, 2009a). Therefore, there is a strong impetus for long term burned area datasets with high spatial and temporal resolution.

2.3.2 Wildfire variability and trend based on MODIS burned area product

2.3.2.1 Spatial distribution of fire in China

Mapping the timing and extent of fires is important, as fire is a prominent agent of change that affects ecosystem structure and the cycling of carbon and nutrients and is

a globally significant cause of greenhouse gas emissions (Roy *et al.*, 2005). Satellite data have been used to monitor biomass burning at the regional and global scales for more than two decades using algorithms that detect the locations of active fires at the time of satellite overpass and, in the last decade, using burned area algorithms that directly map the spatial extent of the area affected by fires (Floyd *et al.*, 2006; Roy *et al.*, 2008).

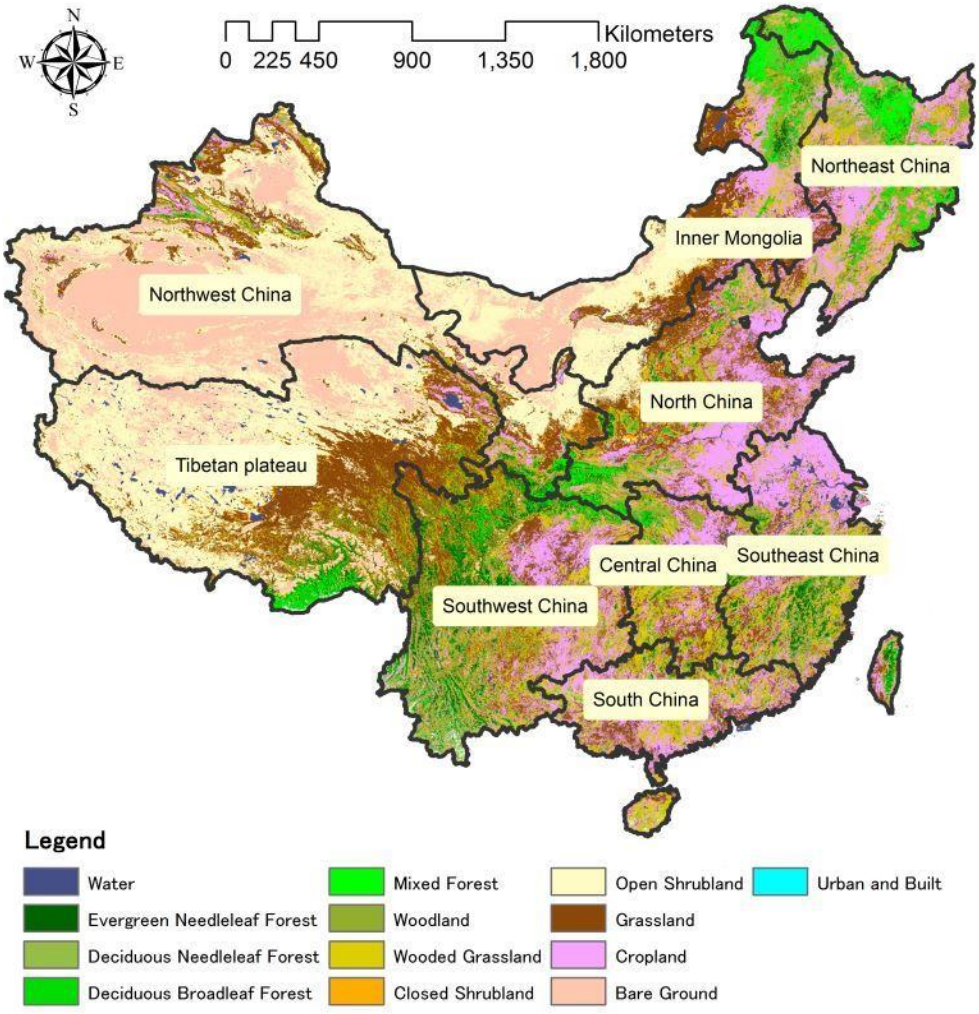

Figure 2-6 Sub-regions division and land cover characteristics in China. a, northeast China; b, inner Mongolia; c, northwest China; d, north China; e, central China; f, south China; g, southwest China; h, Tibetan plateau; i, southeast China

As mentioned above, MDCD45 was used to estimate the burned areas in this study. The MODIS burned area product covers March 2000 to the present. We selected the 12 years 2001–2012 to ensure inter-annual comparability. The burned area detection results undergo a series of quality assessments (Roy *et al.*, 2008). We divided the entire China region into 9 sub-regions to analyze the spatial variations of fire (Figure 2-6). Figures 2-7 and 2-8 show the burned area distribution across the entirety of China from 2001 to 2012. The colors in Figures 2-7 and 2-8 represent the confidence of burned area detection, where blue represents the least confidence and red the most confidence. Fire activity was not evenly distributed throughout China, with the locations of fires varying by year. As shown in Figure 2-6, the majority of the woodlands are located in the southwest and northeast regions. An analysis of the fire products showed that, during the period 2001–20012, an average of 3.2×10^6 ha (32,000 km^2) yr^{-1} of fires occurred in China. Figures 2-7 and 2-8 present the spatial distributions of annual burned areas over China from 2001 to 2012. Most of the forest fires occurred in a only few excessive-fire regions. From 2001 to 2012, four regions accounted for 90% of the area burned: (a) Northeast China, consisting of the three provinces Heilongjiang, Jilin and Liaoning (45%); (b) Inner Mongolia (15%); (c) Southwest China, consisting of the four provinces Sichuan, Chongqing, Guizhou and Yunnan (20%); and (d) Southeast China, consisting of the four provinces Jiangsu, Shanghai, Zhejiang and Fujian (10%). The majority of fires occurred in northeast China and in the southwest provinces. Southwest China is characterized by many small fires and more casualties, but the northeast has fewer and larger fires and more serious damage. Comparing the burned area maps (Figures 2-7 and 2-8) with the land

cover map (Figures 2-6), most of burned area detected by satellite between 30 ℕ and 40 ℕ is overlaid with croplands, representing agriculture fires that had never been taken into account in the official fire statistical data.

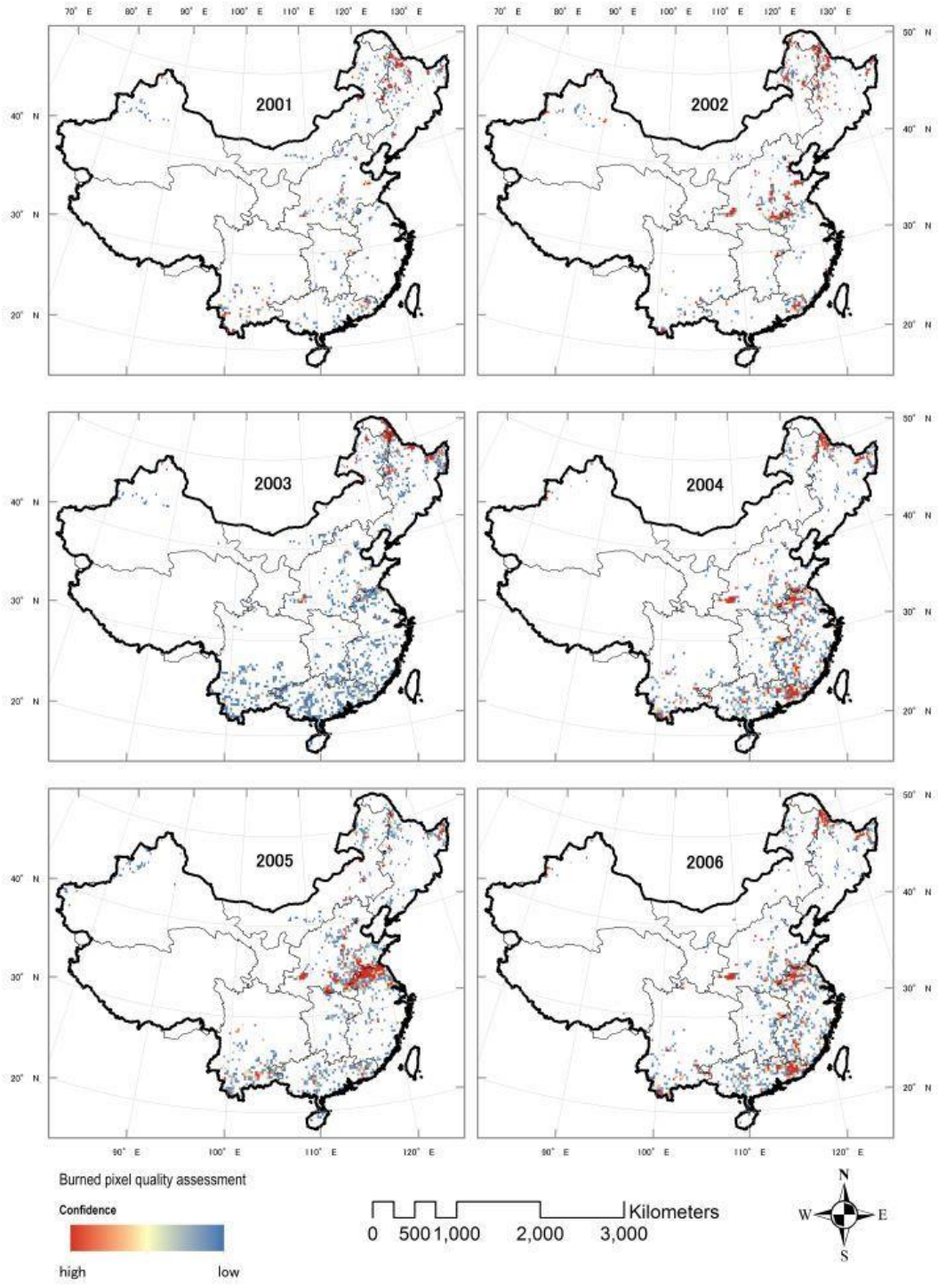

Figure 2-7 Annual burned area measured by MODIS from 2001 to 2012. Note that the size of the burn scars increases slightly for the display purpose

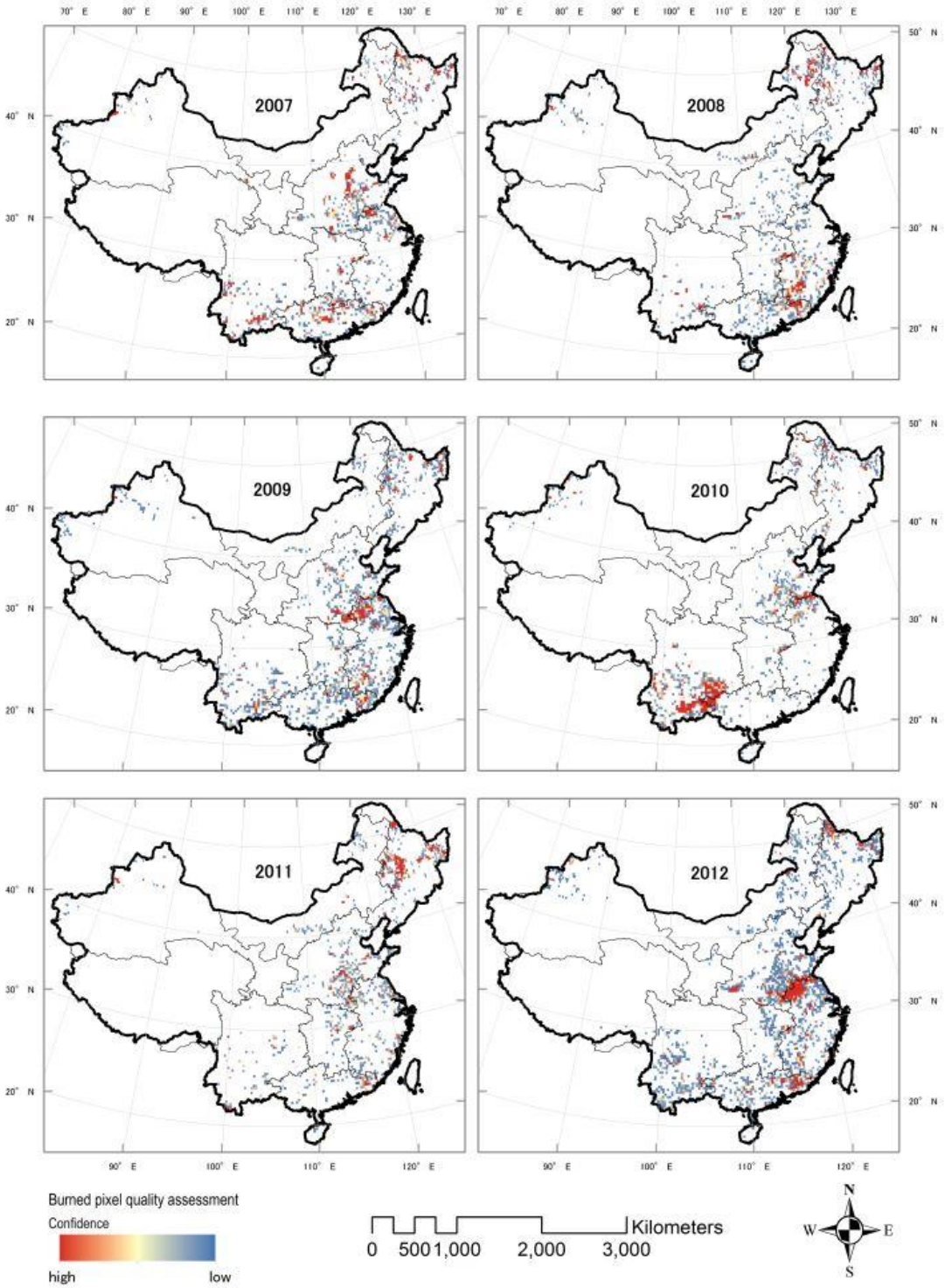

Figure 2-8 Figure 7 continued

2.3.2.2 Temporal trend of fire from MODIS detection in China

Figure 2-9 presents the temporal trend of monthly burned area from 2001 to 2012. The peak fire years during this period occurred in 2002, 2003 and 2008. The profile of monthly burned area exhibits a distinctive seasonality. From this figure, we find that there are two peak fire seasons, i.e., spring and autumn, every year for the entirety of China. The two seasonal peaks pattern is much more obvious in severer fire years. In addition, spring (March, April and May) exhibits a much severer fire situation than autumn in most years, except 2002 (Figure 2-9).

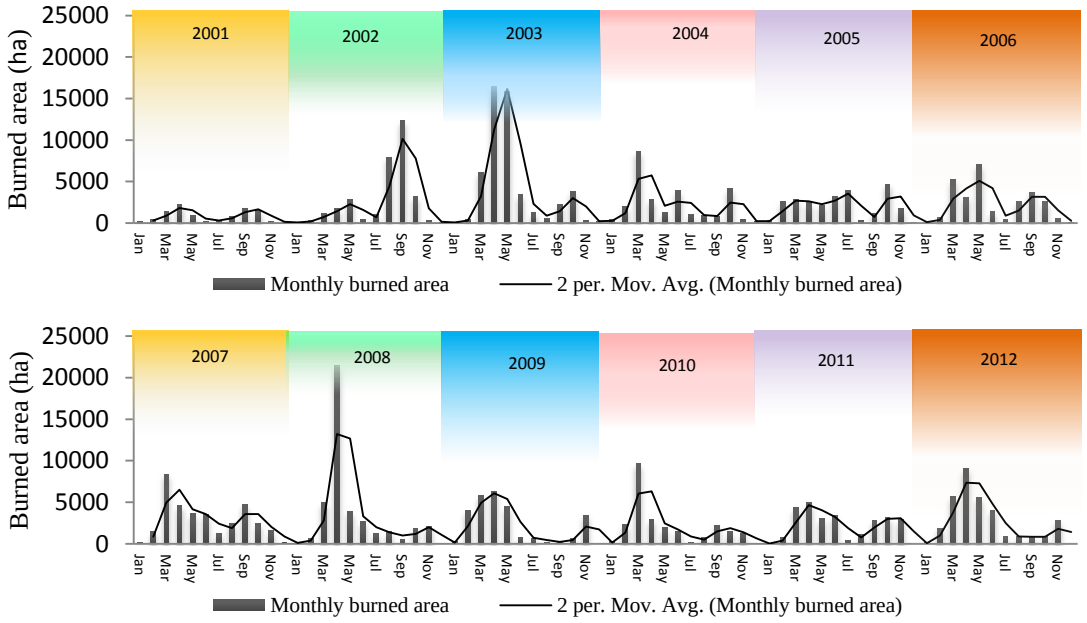

Figure 2- 9 Monthly burned areas for the MODIS detection in China from 2001 to 2012

Fire exhibits a large regional variation in China due to the differences of solar radiation between the north and south and the differences of precipitation between the east and west. Therefore, in this study we divide the whole of China into 9 sub-regions (Figure 2-6). The fire seasonality variables in these nine sub-regions are shown in figure 2-10, which indicates difference in fire seasonality for different

regions. The majority of fires occur in northeast China and in the southwest provinces. Southwest China is characterized by many small fires and more casualties, but the northeast has fewer and larger fires and more serious damage. South China has potentially the most volatile fire risk because of the rapid increase in fuel load and because of the cyclic variations in rainfall patterns caused by the El Niño effect (PRC, 2000).

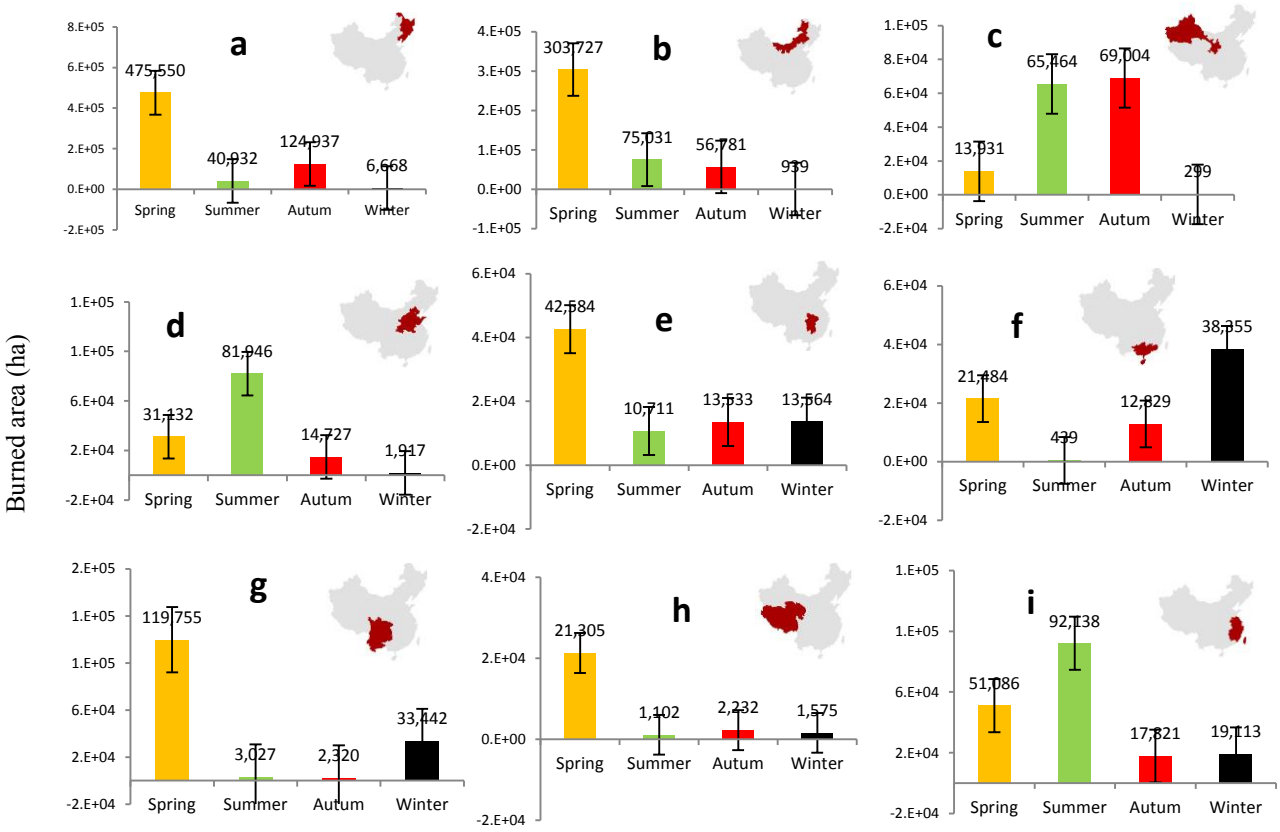

Figure 2-10 Fire seasonality variables in nine sub-regions of China

China has different fire seasons in different sub-regions, with the net effect that its overall fire season extends virtually throughout the year. Figure 2-10 shows the fire season patterns for each of the 9 sub-regions. For each region, the width and length of the blue shape indicates the fire season duration and the amount of burned area,

respectively. The northeastern region of China exhibits the most burned areas (including Heilongjiang, Jilin and Liaoning provinces), contributing an average of 49% to the total burned area, especially in spring and autumn each year (Figure 2-10.a). This region experiences a typical monsoon climate, i.e., dry weather and strong winds in spring, which increases the probability and duration of fire occurrences. The relative humidity is also very low in autumn. Inner Mongolia and Northwest China also account for a large portion of burned area in the MODIS fire product (11, and 4%, respectively). Fires are also frequent in summer in the Shaanxi and Shanxi provinces (Figures 2-10.c and 2-11.c). Northwest China experiences relatively dry weather and contains large areas of forest in the southern regions. The southwest accounts for 7% of the total burned area. In the Southwest, fires often occur in autumn (September to November, spatially in October) (Figure 2-12.h). Located in the subtropical region of southwestern China, the Southwest has dense vegetative cover, which facilitates fire events in dry weather.

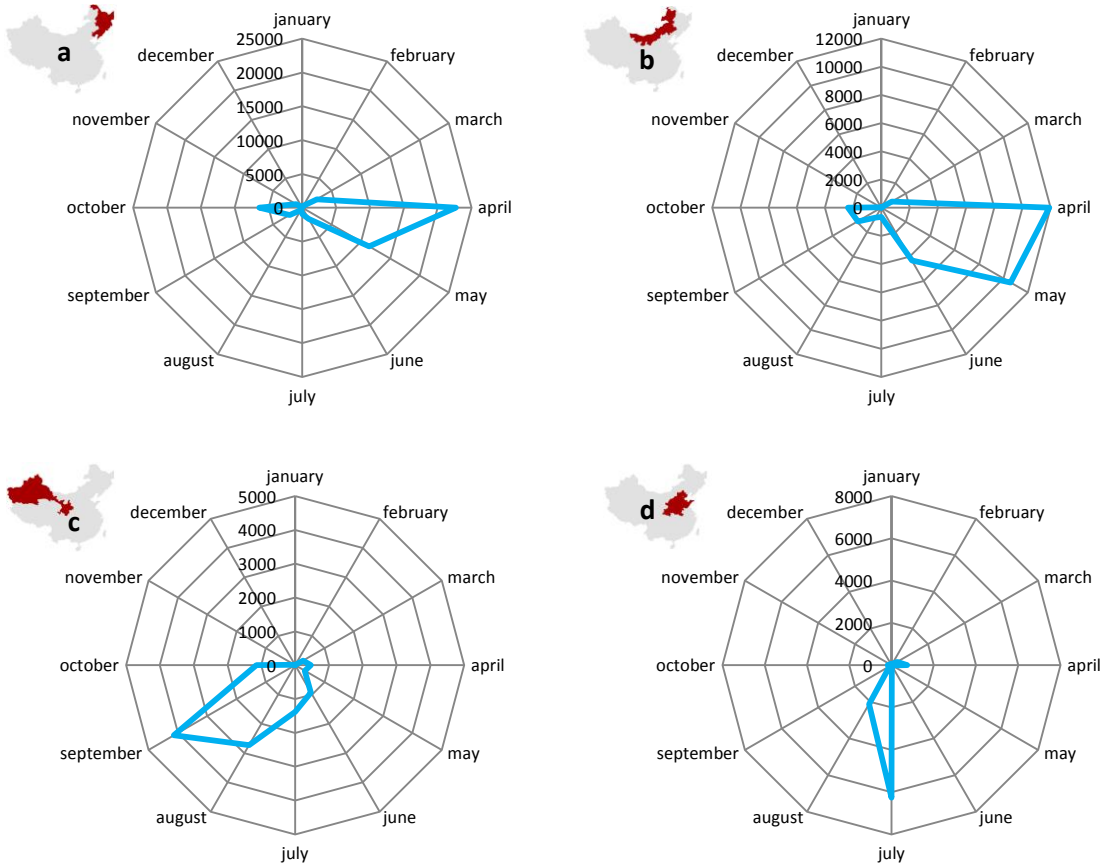

Figure 2- 11 Fire season patterns of each 9 sub-regions in China. For each region, width and length of the blue shape indicate the fire season duration and the amount of burned area, respectively.

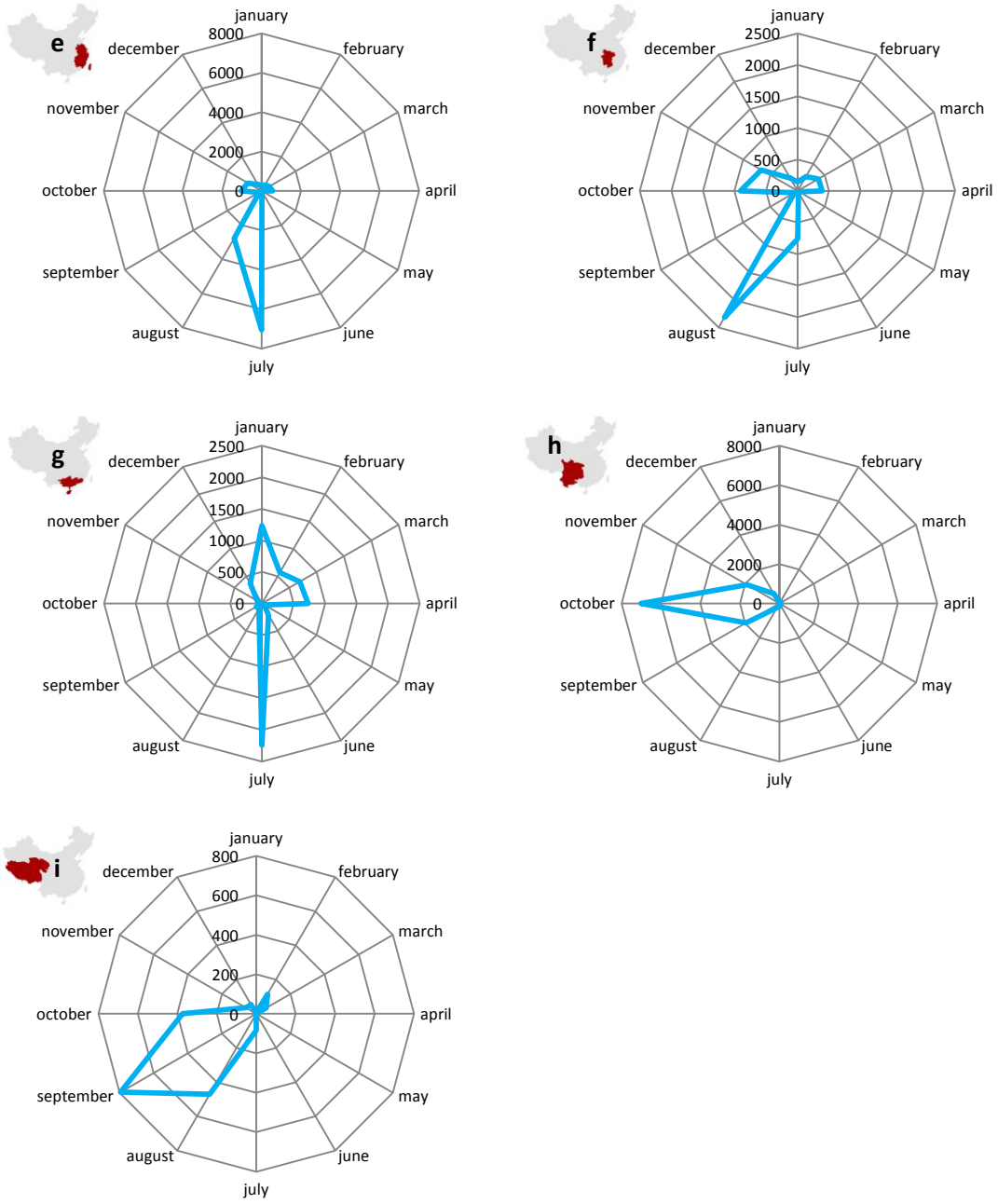

Figure 2- 12 Figure 11 continued

The number and extent of active fires are driven by natural factors such as fuel availability, temperature, precipitation and wind as well as anthropogenic factors. It is widely known that climate fluctuations significantly affect these natural factors and, thus, the severity of the fire season at a variety of temporal and spatial scales (Westerling *et al.*, 2003). Although many of the fires included in this analysis are human-caused rather than "natural" in origin, such as crop residue burning, fires in wildlands are still largely governed by climatic factors, especially temperature and precipitation. Therefore, we reveal regional climate characteristics by calculating the mean annual temperature and precipitation of nine sub-regions. Monthly meteorological data at 130 stations in China were used to examine regional climate characteristics over a 50-year period (1952-2013) (Figure 2-13). The monthly meteorological data, monthly mean temperature and monthly total precipitation used in this study were obtained from NOAA NCDC (National Oceanic and Atmospheric Administration, National Climate Data Center).

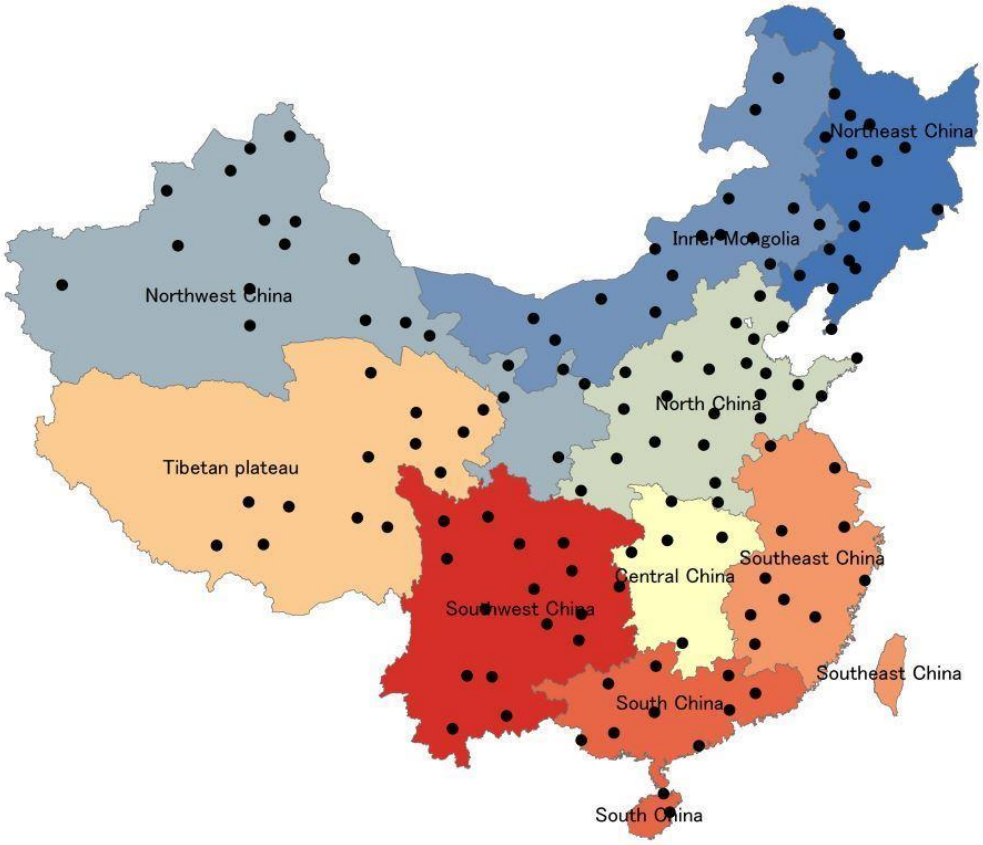

Figure 2- 13 Locations of 130 climate stations in China used to calculate the regional climate characteristics of each 9 sub-regions in China. Mean annual temperature and precipitation of stations within each region were applied to calculate the regional climate characteristics

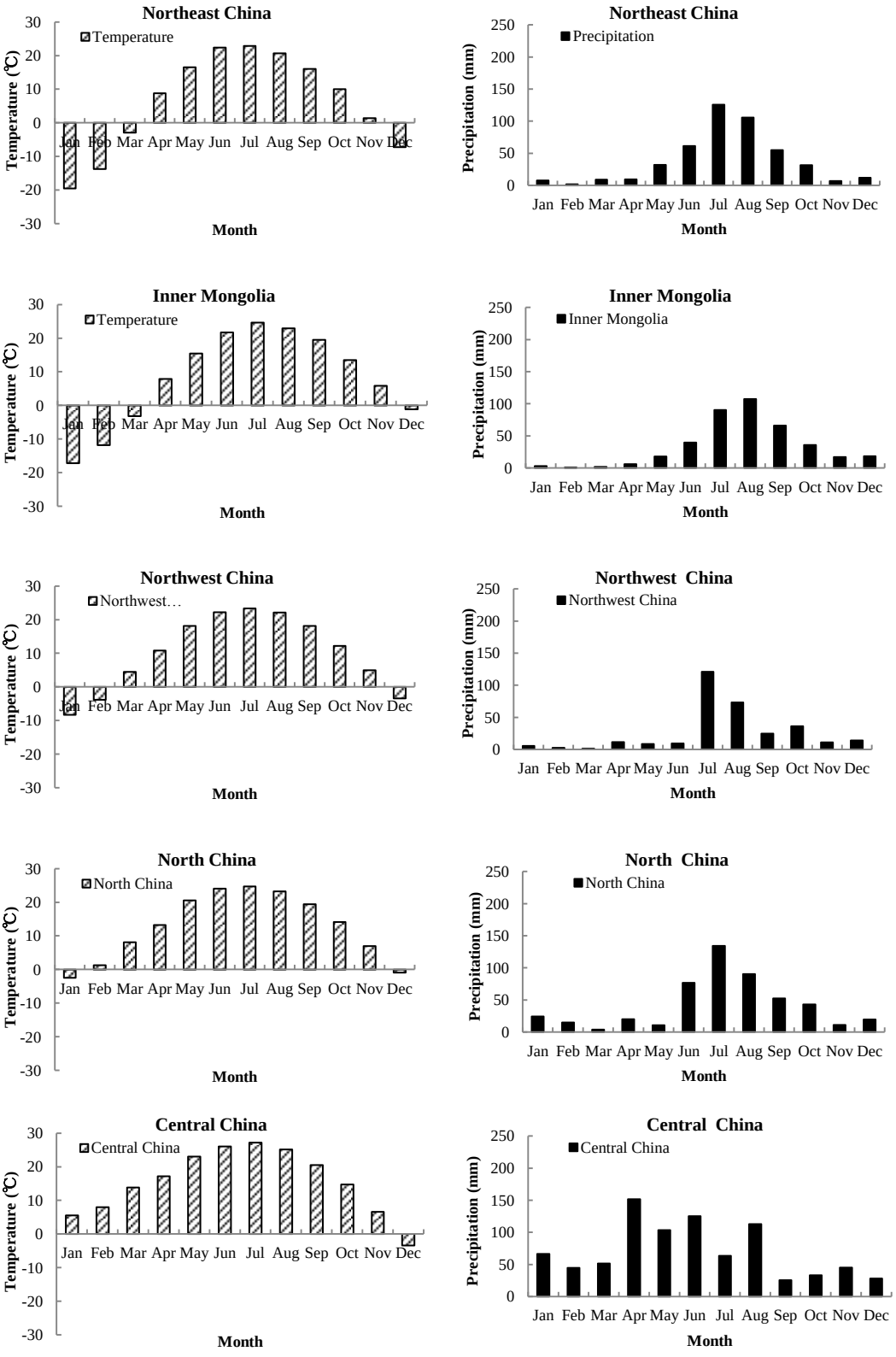

Figure 2- 14 Climate characteristics of each 9 sub-regions in China

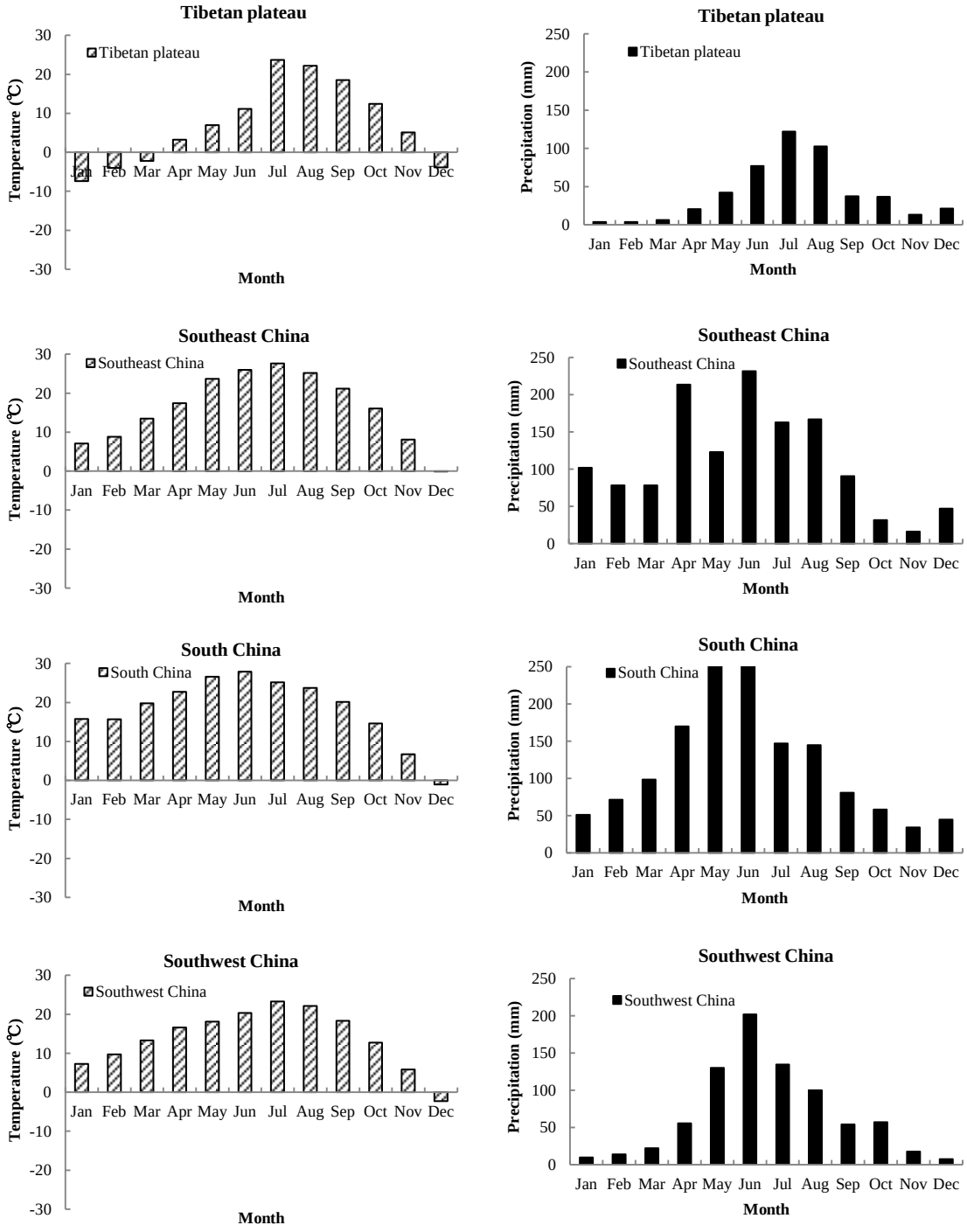

Figure 2- 15 Figure 14 continued

Temperature and precipitation are two important factors that affect climate, and they are naturally the factors of greatest concern for spatial and temporal fire pattern analyses. Figures 2-14 and 2-15 show the climate scenarios in the 9 sub-regions of China. The fire activities in the northeast region and Inner Mongolia are strongly seasonal. The climate scenarios in Inner Mongolia and the northeast are similar, with low temperatures and long-term snow cover in winter from November to early March. Therefore, there are almost no fire events in this season. Spring, from March to May, is the driest season and is characterized by strong wind and low precipitation. This results in the highest fire danger in spring, especially in April and May, yielding a peak in fires and acres burned when the snow melts, with 70% of area burned occurring in this season. Therefore, it is not surprising that the peak of the fire season occurs during the relatively drier seasons (spring and autumn) of the climatological annual cycle in the Northeast and Inner Mongolia regions. The peak temperature and precipitation comes in the same season from June to August. Thus, summer is a relatively humid season with low fire danger. Fires still occur in some extreme drought years, but these fires do not turn into severe events due to the high fuel moisture in summer. After late August, the next significant fire season arrives in Autumn, from September to October, with the decrease of precipitation.

The Southwest, consisting of the four provinces Sichuan, Chongqing, Guizhou and Yunnan, is another significant fire prone region in China, accounting for nearly 20% of the burned area, following the Northeast and Inner Mongolia regions, as shown in Figure 2-10. The climate in the Southwest is subtropical monsoon, which is completely different from the climate of Northeast China (Figures 2-10 and 2-12).

There are no large differences of temperature across the whole year compared with Northeast China. Winter and spring are crucial fire danger seasons due to the relatively drier conditions (Figure 2-11). The duration of the fire season is much longer than in Northeast China due to the lack of snow cover there. This is why the fire frequency is higher but the severity lower in the Southern areas compared with the Northeast and Inner Mongolia regions.

The open fires in southeast and north China are concentrated in the middle and lower Yangtze River and the North China plains, which are also the largest agricultural zones in China. Crop residue burning plays an important role in these regions. Agricultural crop residue burning is a common practice, as it is the most cost effective way of disposing of residues from farms, especially in China. Therefore, the fire activities in southeast and north China are dominantly governed by agricultural activities. Burning is primarily performed in rural China, where large amounts of agricultural residues are produced and are disposed of by burning in open fields. The biomass burning in these regions are typical human-induced fires, which are hardly affected by regional climate characteristics.

Biomass burning is also a common phenomenon in Central China, South China and the Tibetan plateau region. Although the fire frequency may be very high in certain years, the fires in these regions account for only a very small portion of the total acres burned in China. However, fire prevention is also an important task in these regions; as the saying goes, “How small a spark it takes to set fire to a vast forest.”

2.4 CONCLUSION

This paper presented a national analysis of fire characteristics by combining National historic records (1950-2010) and a set a metrics derived from Earth observation sensors (Terra MODIS) (2000-2010). Our study is the first to consider the larger picture of open fires for the entirety of China, analyzing fire spatial patterns and temporal trends from nine sub-regions whose territories span a diverse array of ecosystems. To analyze the spatial variations of fire, we divided the entire China region into 9 sub-regions: a, northeast China; b, Inner Mongolia; c, northwest China; d, north China; e, central China; f, south China; g, southwest China; h, the Tibetan plateau; i, and southeast China (Figure 2-13). This scale is commensurate with that of some important climate variations, yet still allows us to make comparisons across diverse ecosystems. While the spatial patterns of fire occurrence have been previously described, this paper has emphasized the importance of characterizing fire activity by also considering the fire season duration and the extent of acres burned. An analysis of the fire products showed that, during the period 2001–20012, an average of 3.2×10^6 ha (32,000 km^2) $yr^{-1}$of fires occurred in China.

In addition, we identified several regional climate characteristic that help explain the spatial distribution and fire season duration of these fire groups, most remarkably the extent of the dry–warm season, which primarily affects fire density and seasonality. The majority of fires occur in northeast China and in the southwest provinces. Southwest China is characterized by many small fires and more casualties, but the northeast has fewer and larger fires and more serious damage. The inter- and intra-annual fire trends and variations of nine sub-regions were reported by analyzing

regional climate characteristics. Monthly meteorological data at 130 stations in China were used over a 50-year period (1952-2013). The monthly burned area profiles of each sub-region exhibit a distinctive seasonality. Spring and autumn are the two peak fire seasons every year for the entirety of China. Fire season duration and severity are closely related to modes of regional climate variability in the Northeast, Southwest and Inner Mongolia. Crop residue burning plays an important role in southeast and north China, especially concentrated in the middle and lower Yangtze River and the North China plains. Therefore, the fire activities are dominantly governed by agricultural activities and are less affected by the regional climate in southeast and north China.

Future efforts should be made to explore the spatial variations of specific fire metrics and to analyze the relations between human and biophysical variables at regional scales. Additionally, an analysis should be performed of the different ecological and social implications of the different fire groups.

Chapter 3. Analyzing forest fire disturbances from satellite-sensed and meteorological parameters in Northeast China

ABSTRACT

In this chapter, a Fire Disturbance Index (FDI) algorithm is designed to capture long-term variations in the ratio of Land Surface Temperature (LST) to Enhanced Vegetation Index (EVI) on a pixel-by-pixel basis. There is a dramatic difference in the LST-EVI relationship between pre-fire and post-fire values in the case of a fire that occurred in 2003. The algorithm was tested using data from a Moderate Resolution Imaging Spectroradiometer (MODIS) to explore continuous spatiotemporal patterns of fire disturbances. The findings suggest that the FDI can be used to detect pixels corresponding to burned regions. However, it often overestimates the fire-affected area with a large amount of noises. The fire disturbance patterns are also analyzed using meteorological parameters in Northeast China.

KEYWORDS:

Land Surface Temperature (LST), Enhanced Vegetation Index (EVI), meteorological parameters, fire disturbance

3.1 INTRODUCTION

The prevalence of large-scale natural disturbances across diverse ecosystems are becoming a major concern for scientists and decision makers because of their amplitudes and implications for overall resource management(Sousa, 1984; Schelhaas *et al.*, 2003; Schmiegelow *et al.*, 2006; Kurz *et al.*, 2008; Raffa *et al.*, 2008). Wildfire is a drastic natural disturbance that can result in a significantly different surface coverage. The effects of fire disturbances are controlled in large part by their severity, duration, frequency, timing, and spatial impacts(Mildrexler *et al.*, 2009). A wildfire

impacts the forest age structure, as fires in the boreal region are typically large, intense, and stand replacing. In the era of climate change, understanding the past and predicting fire disturbances are scientific challenges that are central to the development of sustainable forest management practices and policies (Girardin *et al.*). In addition to the unpredictability of wildfire behavior, uncertainty also stems from inaccurate/missing data, limited resources and measures to guide prioritization across fire disturbances (Thompson and Calkin, 2011). Understanding the role that fire disturbance plays in the signals measured by satellite sensors could aid and improve the modeling of the effects of climate, CO_2, and fire, as well as their impact on vegetation phenology (Peckham *et al.*, 2008).

Fuel moisture content (FMC) is a the critical factor that affects fire ignition and fire propagation. Therefore, FMC is widely regarded as one of the most important variables in fire risk modeling, and it is incorporated in most fire danger rating systems worldwide (Chuvieco *et al.*, 2002; Verbesselt *et al.*, 2007; Yebra *et al.*, 2008; Brewer *et al.*, 2013). In the wildfire risk literature, the water content of plants is commonly expressed as the fuel moisture content (FMC). The FMC is defined as the ratio between the quantity of water in vegetation and either the fresh or dry weight of the vegetation (Trowbridge and Feller, 1988; Renkin and Despain, 1992):

$$\mathrm{FMC} = \frac{\mathrm{FW} - \mathrm{DW}}{\mathrm{FW}} \times 100\%$$

where FW is the fresh weight of vegetation measured in the field and DW is the weight of the same sample of vegetation after it has been oven-dried. When FMC assessment is applied to the prediction of forest fires, however, it requires frequent laboratory and field experiments of water deficits over a large area. Remotely sensed data possess significant potential for monitoring the FMC, given the synoptic

coverage and repeated temporal sampling of satellite observations. Satellite data-derived indices make use of remote sensing data to estimate vegetation conditions in relation to photosynthetic activity or drought conditions (Gabban *et al.*, 2008).

Fire causes substantial spectral changes by consuming vegetation, destroying leaf chlorophyll, exposing soil, charring stems, and altering both aboveground and belowground moisture. Chlorophyll-related indices are based on the hypothesis that when vegetation dries out, the chlorophyll content of the leaves decreases in a manner that is proportional to the moisture content. Chlorophyll-related indices, such as the enhanced vegetation index (EVI), can be used in regions where the relationship between chlorophyll content, degree of curing, and water content has been established. A reduction of chlorophyll absorption leads to increased reflectance in the visible electromagnetic region, along with leaf tissue damage leading to a decreased reflectance in the near-infrared (NIR) region (Veraverbeke *et al.*). In contrast, with a decrease in crown shadow and a decrease in canopy moisture, mid-infrared (MIR) reflectance typically increases following a fire (Eck *et al.*). Therefore, changes in the NIR and MIR regions have been effectively exploited for studying fire disturbance traits in plants.

Radiometric Land Surface Temperature (LST) is another key parameter that has been used to detect fire-induced changes in plants. It is closely related to surface–atmosphere interactions and the energy flux between the atmosphere and the land surface. Many previous studies have observed a strong negative relationship between LST and attributed the negative correlation to changes in vegetation cover and fuel moisture (Julien *et al.*, 2006; Han *et al.*, 2010; Karnieli *et al.*, 2010; Veraverbeke *et al.*, 2012b; Zhou *et al.*, 2012). As a metric for land cover change detection,

LST/NDVI ratio metrics were statistically better at detecting changes than the NDVI metric alone, confirming the importance of LST data as a complementary source of information to NDVI data (Lambin and Ehrlich, 1995, 1996; Borak *et al.*, 2000). However, several studies have noted the shortcomings of the NDVI as a vegetation index, especially due to the saturation effect that it presents for dense vegetation covers(Galti é, 2006; Lyons *et al.*, 2008; Anaya *et al.*, 2009). Other vegetation indexes, such as EVI and LAI, have been designed to correct this drawback (Sobrino and Julien, 2013).

Northeast China, especially the Great Xing'an Mountain range is the largest natural forest area of China. This is also a significantly fire-prone area (Chen *et al.*, 2011; Liu *et al.*, 2012). Hence, in this paper, we aim (i) To analyze the feature space changes between LST and EVI over pre-fire and post-fire periods in Northeast China. (ii) To evaluate the potential of satellite data derived LST and EVI as fire disturbance indicators for mapping/assessing fire disturbances from 2000 to 2010. (iii) To analyze fire disturbance patterns with meteorological parameters in Northeast China.

3.2 DATA AND METHOD

3.2.1 Study area

This paper focuses on wildfire and agricultural drought events in Northeastern China (38.72°N−53.56°N, 115.53°E−135.08°E) including Heilongjiang, Jilin, and Liaoning provinces, and eastern Inner Mongolia. The landscape of northeast China can be characterized by three major mountain systems surrounded on three sides with a plain in the middle: the Great Xing'an Mountains, Lesser Xing'an Mountains, Changbai Mountains and the Northeast plain (Figure 3-1.a). The average altitude of

the mountainous areas is 1000 m, while the central plains average 200 m. Northeast China experiences of a monsoon system that characterizes the medium latitudinal zone of China where the climate changes from warm temperate, temperate, to cool temperate and the longitudinal zone where climate alters from humid, semi humid, to semi-arid. There is a large difference in the temperatures from north to south, and precipitation declines from east to west. In spring (March−May) the temperatures increase rapidly with strong winds and drought. The annual precipitation is 400−700 mm in most of the region, and up to 1000 mm in the southeast at Changbai Mountain. Approximately 70% of the precipitation occurs in concentrated in the summer. The long-term annual air temperature varies spatially from -4.7 °C to 10.7°C, and the annual range of air temperature can reach up to 40 °C. The length of time over which snow covers the ground can last as long as half a year in certain regions(Liang *et al.*, 2011).

The main forest type in the region is the temperate coniferous-deciduous broad-leaved mixed forest (Figure 3-1.b). There is a total of 45.33 million hectares of forest area in the region, accounting for 37% of the total forest area in China. The Great Xing'an Range, located in the northwestern Heilongjiang Province and Northeastern Inner Mongolia, has *Larix gmelinii, Pinus sylvestris, Pinus koraiensis, Betula platyphylla, Quercus mongolicus, Populus davidiana, Tilia tuan, Juglans mandshurica,* and Fraxinus mandshuricaas the main forest species. Larch forest covers 86.1% of the forest area in The Great Xing'an Range. The Lesser Xing'an Range is located in the northern part of the Heilongjiang Province, an area about four million hectares, with tree species similar to those in The Great Xing'an Range, but with more Korean pine forest and less larch forest(Tian *et al.*, 2011).

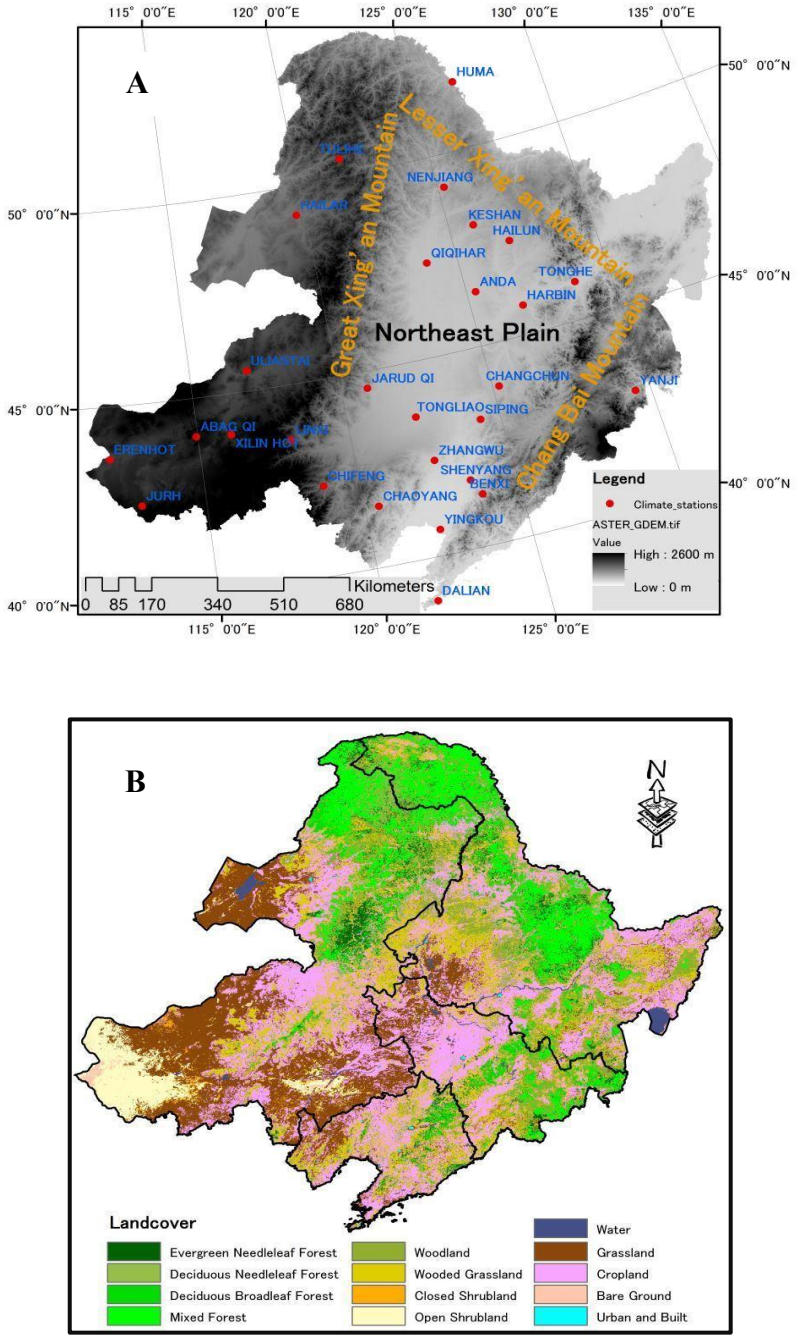

Figure 3- 1 Overview of the study region. Terrain (A) and Land-cover types (B) of Northeast China

3.2.2 MODIS LST and EVI products

We obtained the 8-day maximum LST (MOD11A2) and 16-day EVI (MOD13A2) level 3 MODIS products (collection 5) from 2000 to 2010 from the MODIS archive. Terra, launched in late 1999, has a morning (AM) overpass, whereas Aqua, launched in early 2002, has an afternoon (PM) overpass. In general, LST is expected, under cloudless conditions, to be warmer in the early afternoon than in the morning due to the link between the maximum skin temperature and the solar isolation peak time. Therefore, the Aqua PM LST is likely to be closer to the maximum daily LST than Terra. To utilize the full MODIS archive from 2000 to 2010. We applied a published adjustment to the Terra AM LST estimates, to approximate a "synthetic" Aqua PM LST product from 2000 to mid-2002 thereby providing a seamless afternoon MODIS LST product from 2000 to 2010(Coops *et al.*, 2009).

3.2.3 Method

3.2.3.1 Remotely sensed indicator of vegetation conditions

The relationship between LST and vegetation indices (VIs), such as NDVI and EVI, has been extensively documented in the literatures. The combination of LST and NDVI by a scatterplot results in a triangular shape (Carlson *et al.*, 1995; Gillies *et al.*, 1997). The slope of the LST–NDVI curve has been related to vegetation moisture conditions, and the evapotranspiration of the surface (Gillies and Carlson, 1995; Owen *et al.*, 1998; Gottschalck *et al.*, 2001). As the fractional vegetation cover increases, the surface temperature decreases, leading to a negative LST–NDVI relationship (Nemani and Running, 1989; Nemani *et al.*, 1993). The increase in evapotranspiration caused by higher temperature results in a decrease in soil moisture

and a decline of NDVI, while dense vegetation induces lowers the LST or the transpiring canopy is cooler (Nishida *et al.*, 2003; Yang *et al.*, 2006).

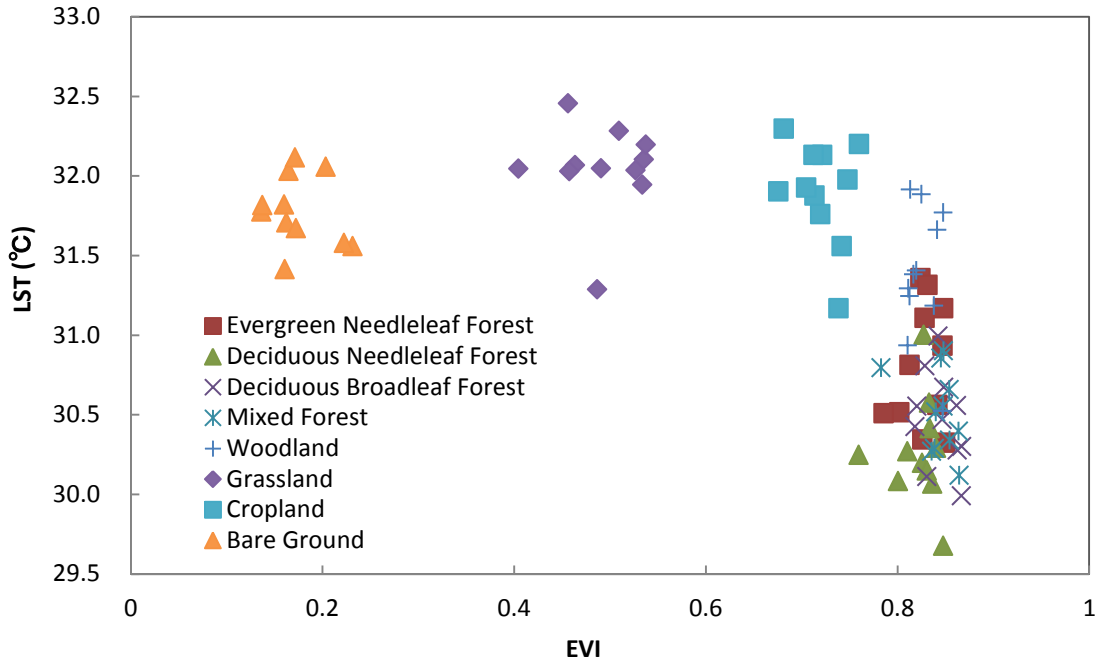

Figure 3- 2 Characteristics of various land-cover types in LST-EVI space in Northeast China

The LST–EVI space contains information about the inherent relationships between vegetation canopy and energy exchange and describes exchange of energy and water between vegetation and the atmosphere (Coops *et al.*, 2009; Tang *et al.*, 2011; Tang *et al.*, 2012). Figure 3-2 shows the characteristics of various land-cover types in the LST-EVI space in Northeast China region. Disturbance trajectories of different land-cover types can be characterized by deviations from their natural status in this space.

3.2.3.2 Fire Disturbance Index (FDI) calculation

A Global Disturbance Index algorithm is designed to capture long-term variations in the LST/EVI ratio on a pixel-by-pixel basis, with an annual time step (Mildrexler *et*

al., 2009). In subsequent years the annual maximum LST/EVI is then compared to this long-term record. Pixels that are significantly different from the long-term mean are deemed to have undergone a subtle yet critical change with respect to concerning the LST and EVI data (Mildrexler *et al.*, 2007). The basis of the index is the development of a "long-term" annual maximum LST/EVI ratio for all of the pixels in an image to detect natural disturbances, such as wildfire and hurricane events. In this study, we named this index the fire disturbance index (FDI) because we are only concerned with fire events and not with other disturbances. FDI is computed as the ratio of the annual maximum composite LST and EVI, such that:

$$FDI_{(k,y)} = \frac{LST_{\max(k,y)}/EVI_{\max(k,y)}}{(LST_{\max}/EVI_{max})_{(k,y-1)}}$$

where $FDI_{(k,y)}$ is the Fire Disturbance Index (FDI) value for pixel k of year y, $LST_{\max(k,y)}$ is the annual maximum eight-day composite LST for pixel k of year y, $EVI_{\max(k,y)}$ is the annual maximum 16-day EVI for pixel k of year y, the ratio of $(LST_{\max}/EVI_{max})_{(k,y-1)}$ is the multiyear mean value for pixel k of the study period but not including the current year y. The annual LSTmax and EVImax values were computed for each of the 12years and the LSTmax for each year then divided by the corresponding EVI max value based on the pixel scale, resulting in a ratio of LST max to EVI max from 2000 to 2010. These annual values were then divided by the long-term average of the index for that pixel, averaged over all previous years. For example, the annual 2003 ratio is divided by the long-term average of the index from 2000 to 2002.

The index was developed to reveal both positive and negative changes in the land surface energy partitioning while avoiding the natural synoptic variability associated

with LST. Fire disturbances that result in decreased vegetation density would lead to an increase in LST as sensible the heat flux that can be sensed increases. Pixels that fall within ±1 standard deviation of the long-term mean are considered to be within the natural variability defined for that individual pixel. Pixels that depart significantly (N±1sd) from the long-term mean LST/EVI ratio are flagged as areas of potential fire disturbance events (Mildrexler *et al.*, 2007; Mildrexler *et al.*, 2009).

3.2.3.3 Fire data

To obtain information about the location of fires, fire hotspot thermal information was collected using the satellite MODIS MCD45 Burned Area Level 3 product, which provides the most comprehensive data concerning fire-affected areas in remote boreal regions. MCD45A1 is a monthly product at 500m resolution and is now available online (since April 2000); MCD45A1 reporting the approximate day of burning with an 8-day precision. Data from this sensor are combined to estimate the annual area that has been burned from 2000 to 2010. The data regarding fire-impacted areas for three severe years (2003, 2005 and 2010) formed the basis of this comparison. The area estimated by MODIS to have been burned on an annual basis within the forest cover in Northeast China was compared to the number of FDI pixels that were flagged as being disturbed for the corresponding years. As with most remote sensing-based change detection approaches the particular cause of a disturbance is not provided by the index. As such we do not expect a 1:1 relationship between the area of flagged FDI pixels and the fire extent over all forests. Therefore to increase the reliability of the comparison, we constrained the fire area comparison to areas where fire is known to be the dominant cause of disturbance.

3.3 RESULTS

The Northeast region is a typical fire-prone ecosystem in China Historically, fire regimes in this region were characterized by frequent, low intensity surface fires mixed with sparse stand-replacing fires over relatively small areas (Wu *et al.*, 2011). The fires have been particularly severe due to the 2003, 2005 and 2010 Northeast China drought. Rapid desertification, the unusual convergence of strong winds and unseasonably warm temperatures have exacerbated the problem. Figure 3-3 shows a case of wildfire disturbance that occurred on May 5th 2003 in the Jinhe forestry bureau in Inner Mongolia of Northeast China.

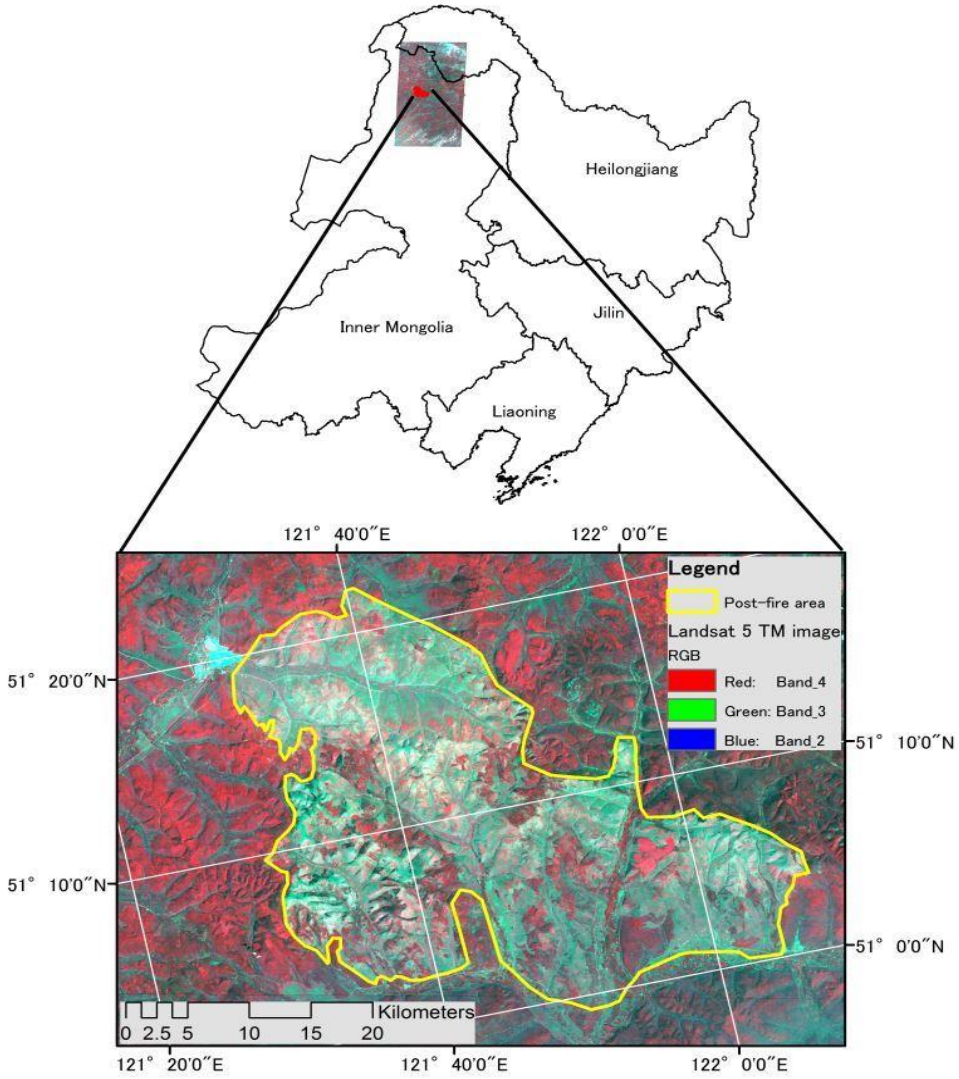

Figure 3- 3 Location of fire event in Inner Mongolia May, 2003

This fire burned approximately 79000 hectares including 62740 hectares of forest. The fire caused substantial spectral changes by consuming vegetation and altering both aboveground and belowground moisture. Figure 3-4 shows the LST-EVI feature space changes induced by the wildfire disturbance. Each plot position in this figure represents one pixel value of LST and EVI. There is a dramatic difference in the LST-EVI relationship between pre-fire and post-fire periods.

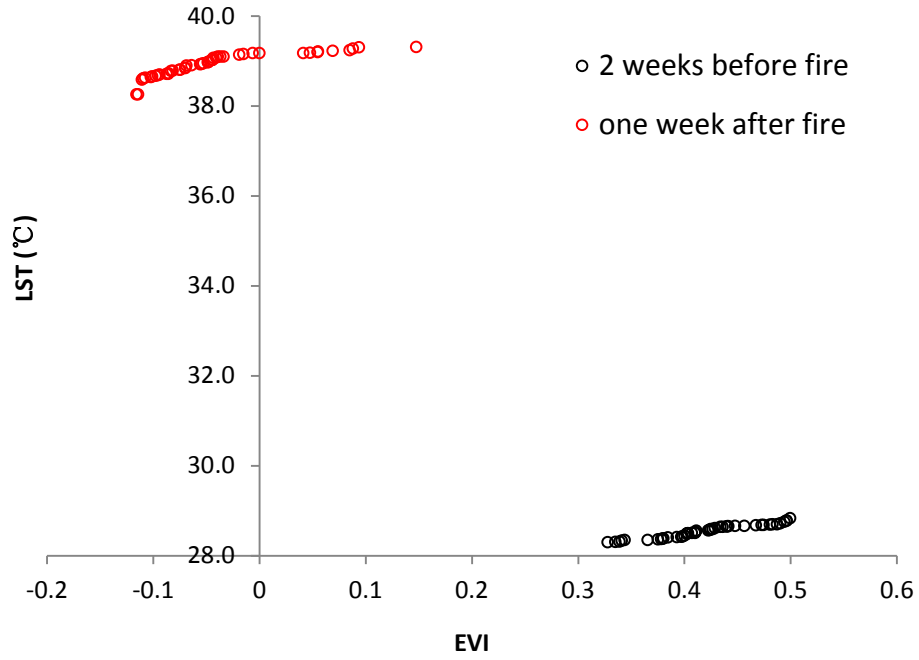

Figure 3-4 Fire-induced LST-EVI space changes in May, 2003

The mean LST/EVI ratio reflects the undisturbed energy balance of the land surface and provides a solid baseline to assess any departures from the range of natural variability. It is important to have several years of data so that the pixel mean can the normalized to reflect the natural variability associated with fluctuations between wet and dry years(Mildrexler et al., 2009). Figure 3-5 shows the powerful effect of the FDI in magnifying the disturbance signal through the LST/EVI rationing approach. The FDI values of pixels within the fire affected area shows a significant increase when comparing pre-fire and post fire FDI raster images (Figure 3-5). There are also several pixels that show high values that are probably associate with logging or other human disturbances. The FDI image exhibits good spatial consistence with the fire affected area. There is a dramatic increase within the burned area while there are negligible changes in pixels outside the burned region (Figure 3-5).

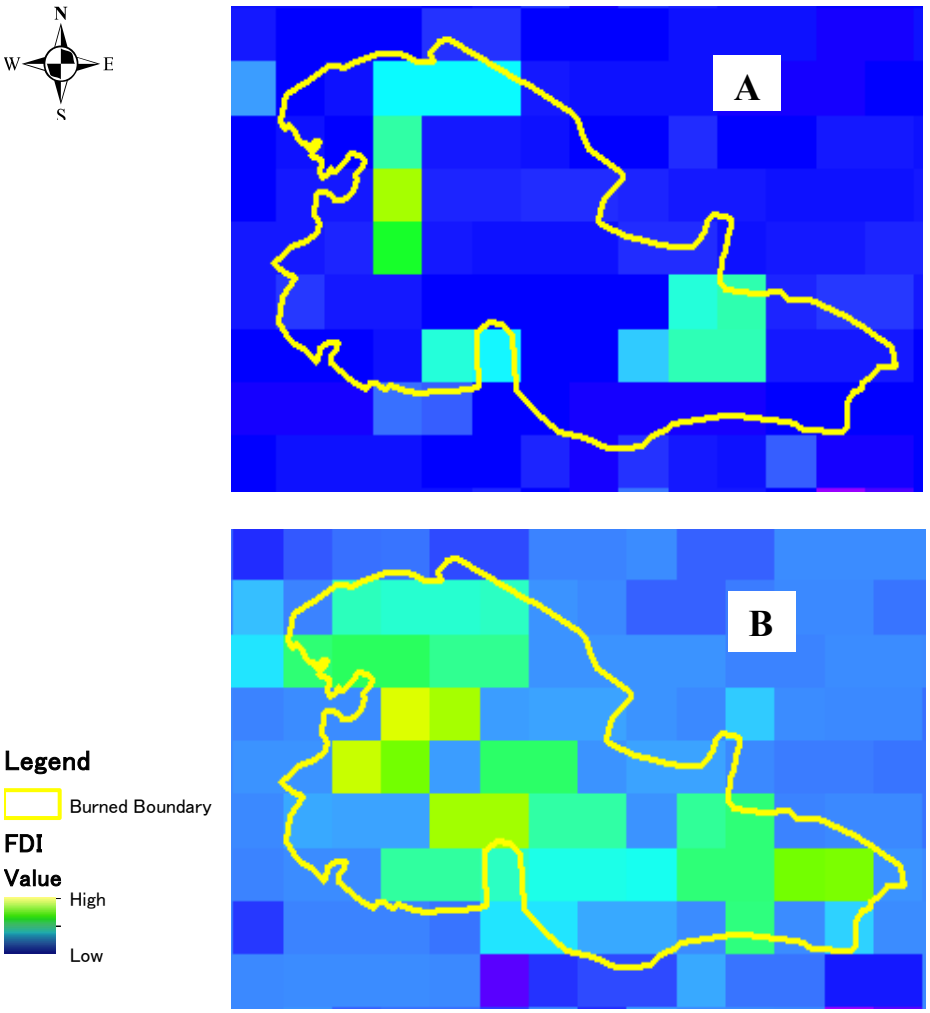

Figure 3-5 Fire Disturbance Index (FDI): 2 week before the fire (up), and one week after the fire (down). This illustrates that the abrupt impact that wildfire has on the landscape can be detected by FDI

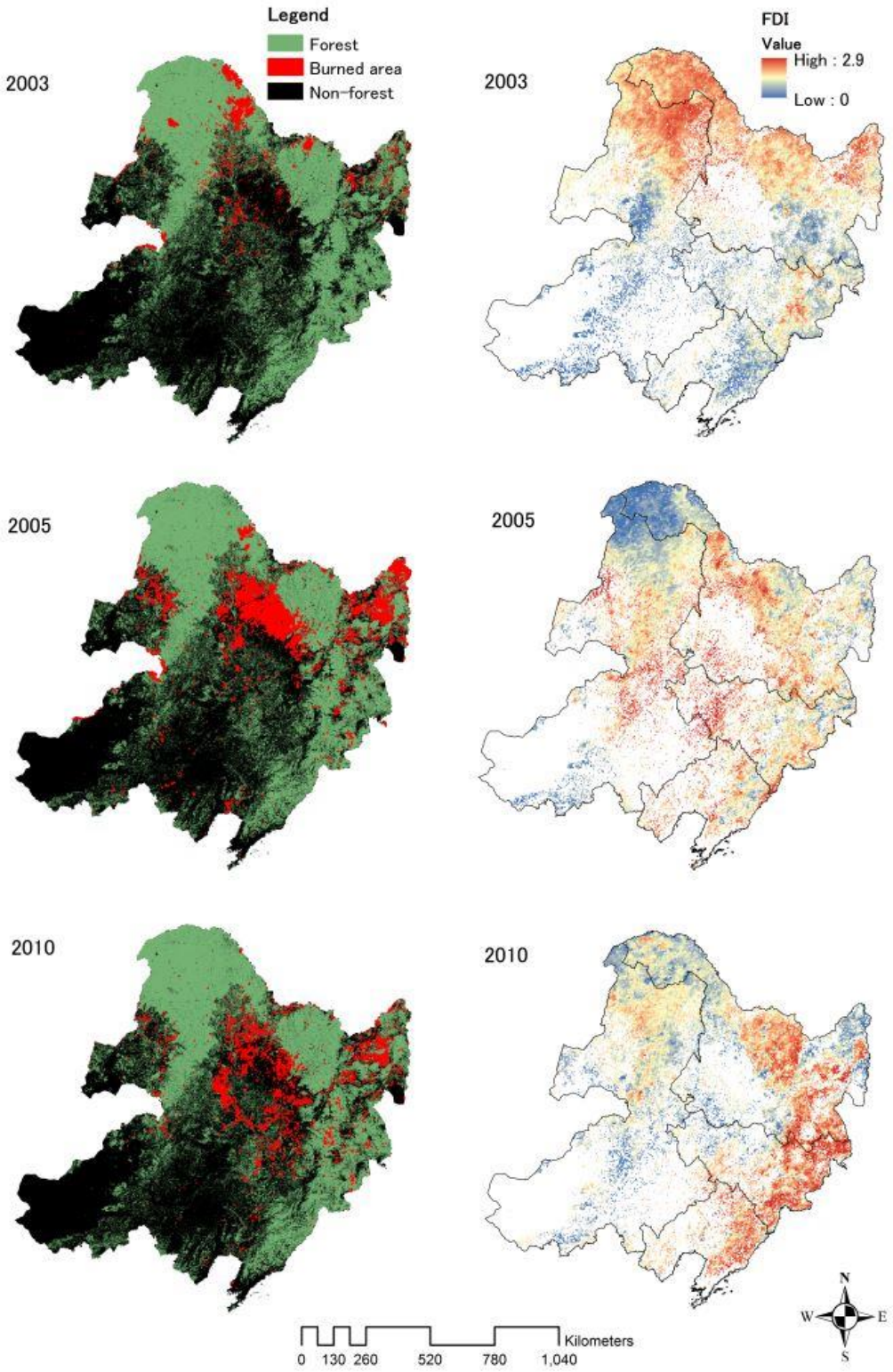

Figure 3-6 Validating the FDI algorithm (right) with MODIS burned area data (left) of three typical fire years in 2003, 2005 and 2010

In the northeastern forest ecosystem, wildfire is the dominant cause of disturbance. From 2000 to 2010 there were three years, 2003, 2005 and 2010, with large burned areas per fire event. Therefore, for those three years, we compared the burned areas and FDI images to validate the sensitivity and ability of FDI to detect fire disturbances (Figure 3-6). As shown in figure 3-6, a high FDI value in the pixels corresponded to burned regions. However, there were much higher FDI-value pixels than we expected. This may be caused by other disturbances, such as drought or human activity. Therefore, these results indicate that FDI can be used to detect the burned regions. However, FDI often overestimates the fire-affected areas, with a significant amount of noise.

The investigated area has historically been affected by large and frequent forest fires. From 2000−2010 there were 372×10^4 ha of area that were burned according to MODIS results, accounting for over 70% of the total burned area in the country. The fire-affected area was the highest in 2003, followed by the fire-affected areas in 2005,

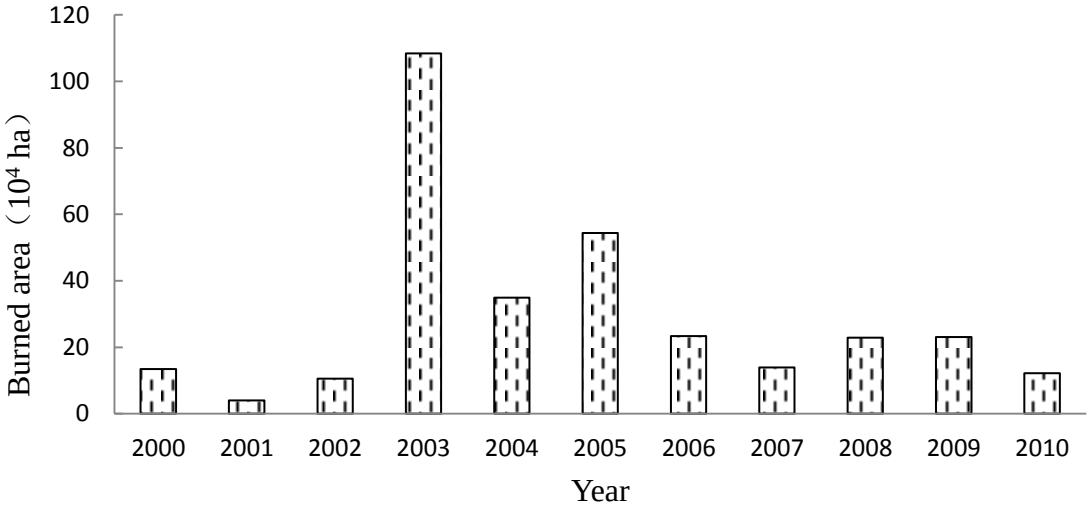

Figure 3-7 Total fire area in Northeast China from 2000 to 2010 according to MODIS data

2004 and 2009 (Figure 3-7).

The major causes of fire in the area are lightning and human activity. However, it strongly depends on fire weather conditions whether a fire will develop into a large one or not. The seasonality of the fire patterns is shown in figure 3-8, which indicates two seasonal peaks in the numbers of fires in Northeast China. The number of fires in the spring is lower than in the autumn. However, the spring fires are harder to control and are much easier to develop into large fire events than the autumn fires.

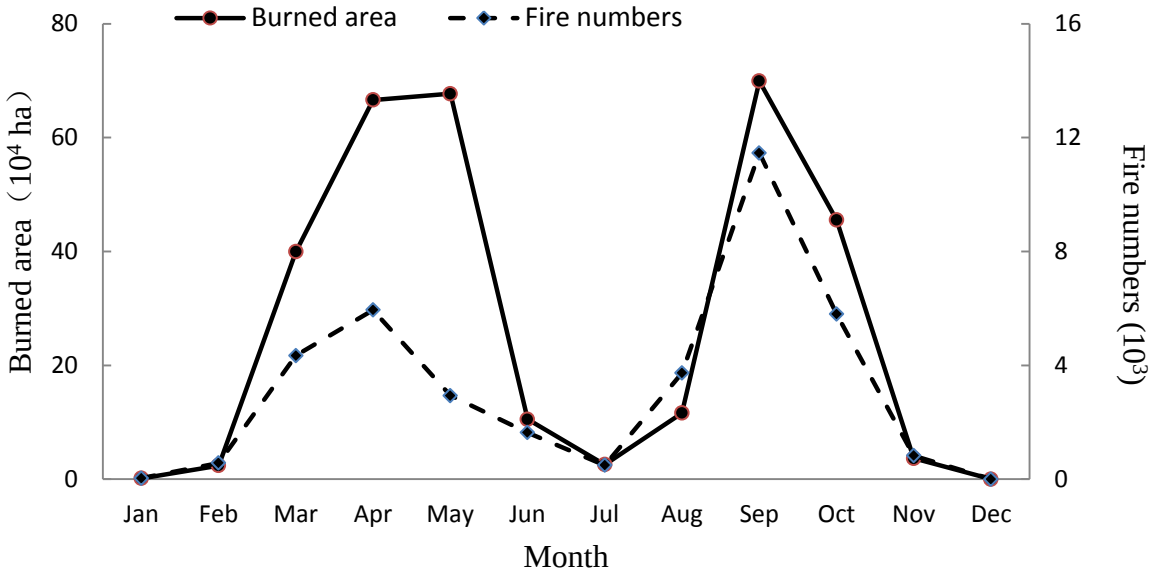

Figure 3-8 Seasonality of fire patterns in Northeast China. Here, the fire number is not the number of fire events but the number of fire patches in the MODIS image

Temperature and precipitation are two important factors that affect climate, and they are naturally the factors of the greatest concern for the analysis of the spatial and temporal patterns of fire disturbances. Climate gradients can influence fire occurrence, with drier environments in otherwise metric biomes typically displaying greater fire activity than wetter ones (Mitchener and Parker, 2005). Figure 3-9 shows the climate scenario in Northeast China, with great spatial differences between the

Changbai Mountains and the Great Xing'an Mountains. The climate at the Changbai Mountains is a temperate continental monsoon climate with a total annual precipitation of 600 mm to 1000 mm. It is wetter than other regions in Northeast china. Therefore, there are no large fires, even though there are large amounts of forests in the Changbai Mountains. In contrast, the climate at the Great Xing'an Mountains is a cold temperate continental monsoon climate with low precipitation (less than 400 mm) and strong winds in the spring and autumn. Therefore, there are large and frequent forest fires in the Great Xing'an Mountains.

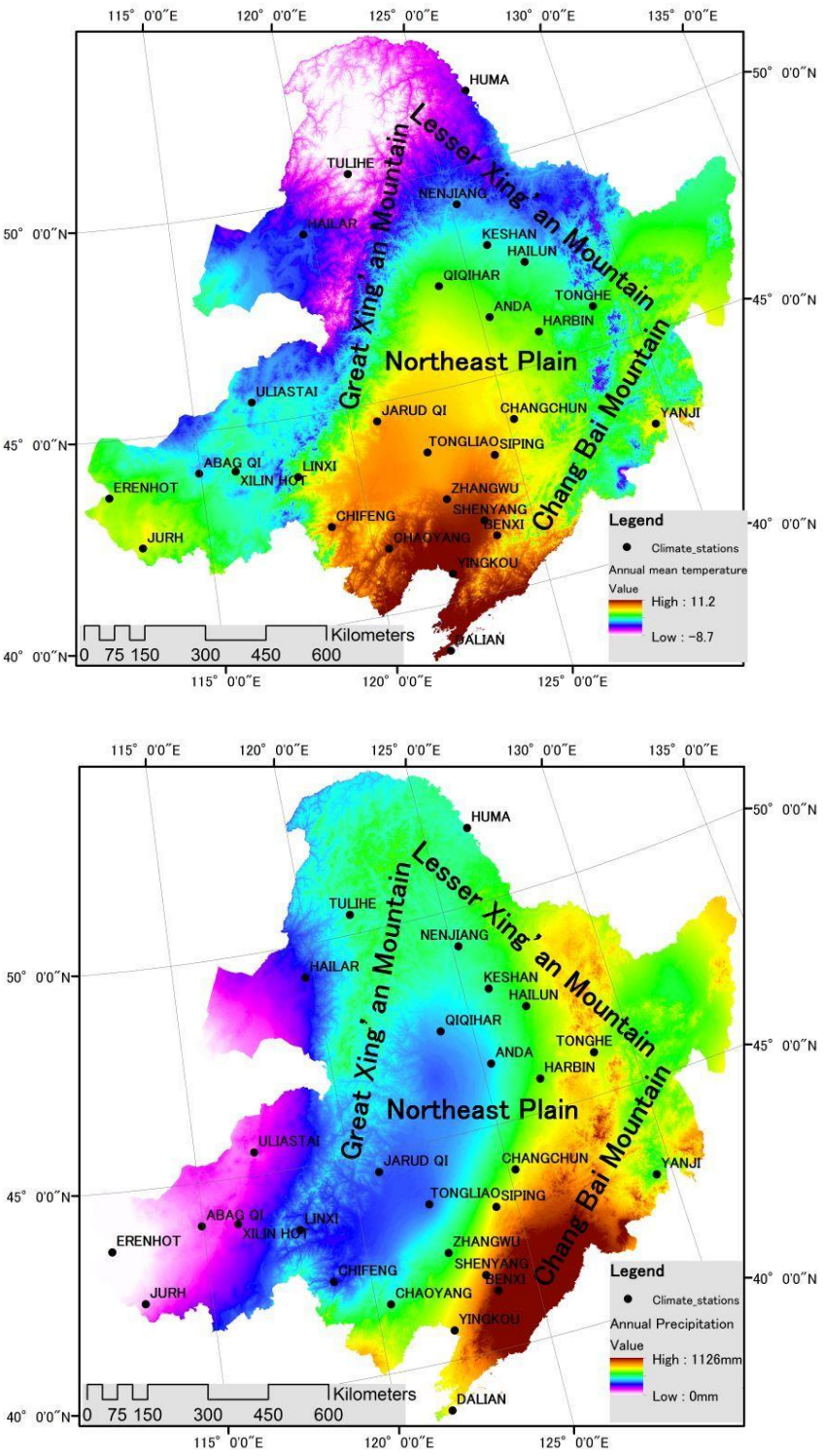

Figure 3-9 Meteorological parameters in Northeast China

In general, fire activities are strongly seasonal due to the continental monsoon climate in the northeastern region. The climate is characterized by low temperatures and long-term snow cover in the winter, from November to early March. Therefore, there are almost no fire events during this season. Spring, from March to May, is the driest season and is characterized by strong winds and low precipitation. This results in the highest fire risk in the spring, especially in April and May, yielding a peak in the number of fires that start and the acres burned as the snow is melting. Seventy percent of the areas that are burned are burned during this season. Therefore, it is not surprising that the peak of the fire season occurs during the relatively drier seasons, in the spring and autumn of the climatological annual cycle in the Northeastern region. The peak of temperature and precipitation occurs in the same season, from June to August. Therefore, summer is a relatively humid season with low fire danger. Fires still occur in some extreme drought years, but these fires do not grow into severe events due to the high fuel moisture in the summer. After late August, another significant fire season arrives in autumn, from September to October, with a decrease in precipitation.

3.4 CONCLUSION

A Fire Disturbance Index (FDI) algorithm is designed to capture long-term variations in the ratio of Land Surface Temperature (LST) to Enhanced Vegetation Index (EVI) on a pixel-by-pixel basis. There is a dramatic difference in the LST-EVI relationship between pre-fire and post-fire periods in the cases of fires that occurred in 2003. The algorithm was tested by using Moderate Resolution Imaging Spectroradiometer (MODIS) fire-product data to explore continuous spatiotemporal patterns of fire disturbance. The findings suggest that FDI can be used to detect the

burned areas but often overestimates the fire-affected area with a large amount of noise. The spatial and temporal patterns of the fire disturbances are also analyzed using meteorological parameters in Northeast China. The climate in Northeast China shows great spatial differences from the Changbai mountains to the Great Xing'an mountains. The climate at the Changbai mountains is a temperate continental monsoon climate, with a total annual precipitation of 600 mm to 1000 mm. It is wetter than other regions in Northeast China. Therefore, there are no large fires even though there are large amounts of forests at the Changbai mountains. In contrast, the climate at the Great Xing'an mountains is a cold temperate continental monsoon climate with low precipitation (less than 400 mm) and with strong winds in the spring and autumn. Therefore, large and frequent forest fires occur in the Great Xing'an mountains. The peak of the fire season occurs during the relatively drier seasons in the spring and the autumn of the climatological annual cycle in the Northeastern region.

Chapter 4. Estimates of biomass burning emissions in the Great Xing'an Mountains of China from 1986 to 2010

ABSTRACT

Biomass burning emissions in the boreal region yield an important contribution to the chemical budget of the troposphere. To assess the contribution of biomass burning to the emissions of atmospheric trace species in the Great Xing'an Mountains (GXM), which is also the most severe fire-prone area in China, we estimated various biomass burning activities by combining explicit spatio-temporal remote sensing data with fire-induced emission models. We derived 9998 fire scars with 46,096 km^2 in the Great Xing'an Mountains between the years 1986 and 2010. The years 1987 and 2003 contributed 33.2% and 22.9%, respectively, in burned area during the 25 years. Fire activity is the strongest in May. Most large fires occurred in the north region of GXM between 50ºN and 54ºN latitude due to much drier weather and higher fire danger in the northern region than in the southern region of the study domain. Evergreen and deciduous needleleaf forest and deciduous broadleaf forest are main sources of emissions, accounting for 84%, 81%, 84%, 87%, 89%, 86%, 85% and 74% of the total annual CO_2, CH_4, CO, PM_{10}, $PM_{2.5}$, SO_2, BC and NOx emissions, respectively. Fire emissions from shrubland, grassland and cropland only account for a small fraction of the total emissions level (approximately 4%-11%). Comparisons of our results with other published estimates of biomass burning emissions show reasonable agreement; however, substantial uncertainties remain concerning the modeling parameters.

KEYWORDS:

Emissions, biomass burning, MCD45, trace gas, particulate matter

4.1 INTRODUCTION

Biomass burning is the act of burning living, or once living, biological material. Biomass burning acts as a double-edged sword in the natural context. On the one hand, fire is traditionally used as a tool to aid in many land use and related changes, including the clearing of forests for agriculture and for shifting agricultural practices. Biomass burning is an important part of ecosystem services, providing nutrients and recycling material. On the other hand, biomass burning always provides some emissions of gases and aerosols to the atmosphere (Keywood et al. 2013). Fire was considered as a major source of aerosol that affect air quality, atmospheric composition and the Earth's radiation budget (Marshall et al. 1996; Jacobson et al. 2009). Smoke emissions emitted by fires are composed of aerosol particulate matter (PM) and numerous trace gases, including carbon monoxide (CO), carbon dioxide (CO_2), methane (CH_4) and nitrogen oxides (Knox and Clarke). Globally, biomass burning contributes approximately 50% of the total direct CO emissions and approximately 15% of surface NO_X emissions (Ito and Penner 2004; Levine et al. 1995). Most of these particular matters and trace gases can have significant effects not only on air quality and on human health but also some (e.g., PM and the greenhouse gases) affect the climate, with potential feedback on air quality. As we know, the increase in trace gas concentrations are closely linked to acid precipitation, the greenhouse effect and the photochemical production of ozone in the troposphere (Palacios-Orueta et al. 2005). Some species have significant and far-reaching consequences due to their long lifetime (N_2O:150 years, CO_2:100 years CH_4:10 years) and to the reduction of the carbon storage capacity in vegetation ecosystems. In addition, smoke PM influences precipitation processes, resulting in delayed,

suppressed or invigorated rainfall, which changes cloud albedo and scatters and absorbs solar radiation, affecting atmospheric warming or cooling and contributing to climate change (Liu, L. Goodrick, and A. Stanturf; Crimmins 2004; Aldersley, Murray, and Cornell 2011). With increasing scientific and political concern regarding the carbon cycle, there is a strong impetus to better understand biomass burning carbon emissions on both a global and regional scale.

There is a strong requirement for information concerning the global and regional distribution of biomass burning emissions. For several decades, researchers have made great efforts to estimate burned biomass emissions from ground-based and in situ measurements. However, the spatial and temporal coverage of these studies is severely limited (Simoneit 2002; Randerson et al. 2012; Zhang and Kondragunta 2008). During the past two decades, major advances have occurred in the detection of atmospheric pollution from space. The generation of satellite instruments launched since 1995 has proven to be capable of observing a wide range of chemical species at increasingly high spatial and temporal resolutions. In addition, the transformation of raw satellite retrievals to user-friendly, archived products has considerably progressed, such that the application of satellite observations to a wide range of atmospheric problems is no longer a daunting prospect (Stephens and Collins 2004). Space-based observations, such as the Along-Track Scanning Radiometer (ATSR) and the Moderate Resolution Imaging Spectroradiometer (MODIS), provide information concerning global burning hotspots at a spatial resolution of 1 km, which have allowed a better identification of biomass burning and emissions.

Previous studies have attempted to estimate the amount of burned biomass and the fire-induced emissions in China (Qin and Xie 2011; Huang et al. 2011; Lu et al. 2006;

Song et al. 2009b). The total amount of carbon emitted per year via the burning of terrestrial biomass in China has been estimated at 11.31 Tg from 1950 to 2000 (Lu et al. 2006). This amount of carbon emissions has resulted from the atmospheric emissions of four trace gases: 40.6 Tg yr^{-1} CO_2, 27.1 Tg yr^{-1} CO, 0.112 Tg yr^{-1} CH_4 and 0.113 Tg yr^{-1} NMHC (Lu et al. 2006). Black carbon (BC) emissions have increased at an average annual rate of 25.54%, from 0.014 Tg in 1990 to 0.067 Tg in 2005 (Qin and Xie 2011). Nevertheless, current approaches depend on factors such as scale, accuracy requirements and information availability, among others. Therefore, a longer-term, higher-resolution study into the emissions from biomass burning on both a global and regional scale is required.

Local estimates are necessary to understand micro-scale emission mechanisms, whereas regional and global modeling is essential to assess the net effects of emissions on the atmosphere and on global climate change (Palacios-Orueta et al. 2005). Many articles argue that China should take more responsibility for climate change mitigation than other counties due to much CO_2 emissions by fossil fuel consumption and by biomass burning (Oberheitmann 2012, 2010; Hasanbeigi et al. 2013). In China, the most severe fire-prone area is the northeastern region, particularly the Great Xing'an Mountains (GXM) region. Wildfire is inevitable and is ecologically important in forests throughout much of the GXM because of the fuels, ignition sources and variable climatic conditions. It has been roughly estimated that 1.2×10^4 Mg carbon emissions were released from forest fires, with approximately 1.0×10^6 hm^2 of forest burned in the GXM during the period from 1980 to 2005 (Zhang, Hu, and Wang 2011). However, for China's forests, there is a lack of comparable data even for recent years, and this lack of data may well be the largest

source of error in providing estimates of direct carbon release from the boreal region (Cheng et al. 2010; Tan et al. 2007). The purpose of this work is to provide estimates of total direct emissions from biomass burning by combining explicit spatio-temporal remote-sensing data with fire-induced emission models. Another major objective of this investigation is to estimate the potential range and spatial-temporal patterns of wildfire events in the GXM area. We also attempt to identify gaps and limitations in existing data and methods that must be studied in the future to improve our understanding of the role of biomass burning in regional carbon dynamics.

4.2 METHODS AND DATA

4.2.1 Study area

The Great Xing'an Mountains (GXM), which lie on China's northern border frontier and neighbor Russia in the north and Mongolia in the west, are commonly defined as stretching from the Heilongjiang (or Amur) River in the north to the Silas Moron River in the south. This study focuses on the Hulun Buir Plateau and the majority of the Great Xing'an Mountains (GXM) (Figure 4-1). This region is primarily a hilly mountainous region that ranges from 450 to 1500 m in elevation. The climate is terrestrial monsoon, with long, severe winters (mean January temperature -28.5℃) and short, mild summers (mean July temperature 17℃). Precipitation, which peaks in summer, is 420 mm annually and is unevenly distributed throughout the year, with more than 60% of precipitation occurring between June and August. Vegetation in this region falls within the cool temperate coniferous forests, which occur at the southern extension of the eastern Siberian light coniferous forest (Li et al. 2013).

The species composition is relatively simple, and the forest area covers over 75% of the study area. The most dominant tree species is larch (*Larix gmelini*), which

accounts for 80% of the study area. The second most dominant species is birch (*Betula Platy Plylla*), which covers 10% of the study area. Other species, including pine (*Pinus sylvestris var. mongolica*), spruce (*Picea Koraiensis*), two species of aspen (*Populus davidiana*, *Populus suaveolens*) and willow (*Chosenia arbutifolia*) cover approximately 10% of the study area. Figure 4-1 shows the land cover distribution in the study area, which was acquired from the AVHRR Global Land Cover Map (AVHRR GLC-2000).

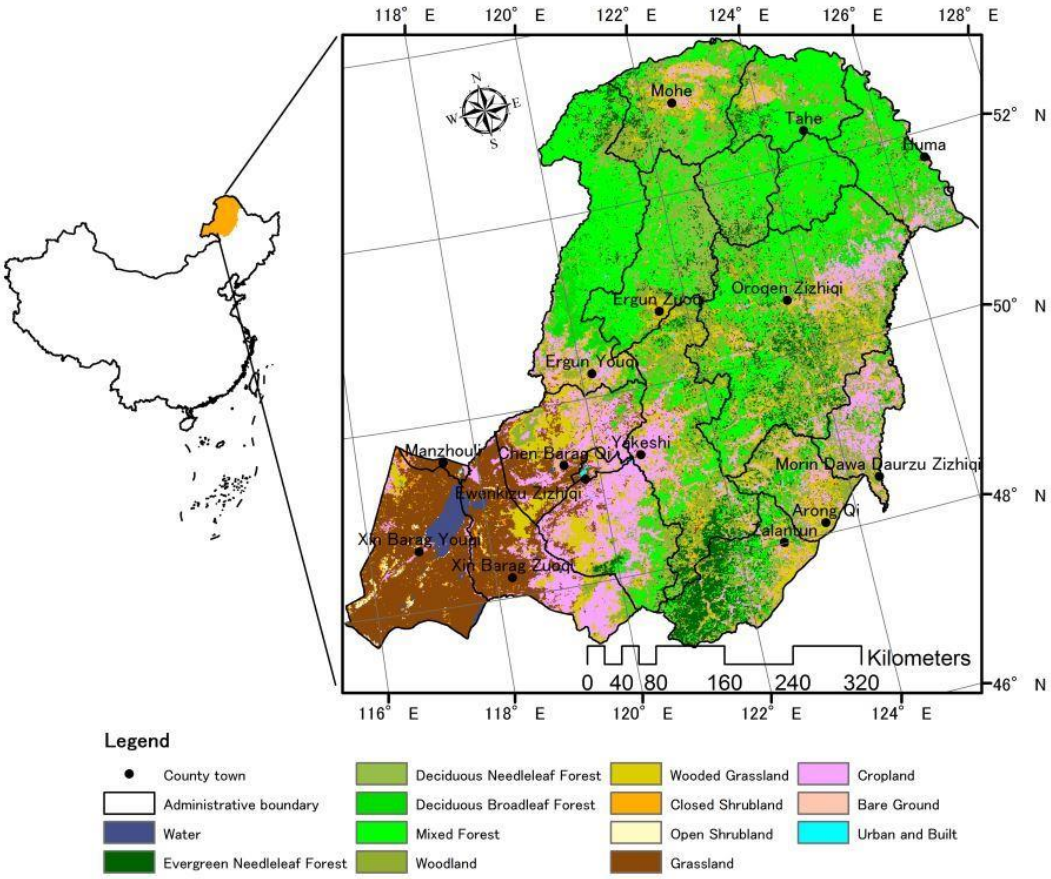

Figure 4- 1 Land cover distribution in the Great Xing'an Mountain. It is derived from University of Maryland global land cover map (UMD-GLC)

4.2.2 Methodology: Carbon emission calculations

Over the past several decades, substantial efforts have been devoted to evaluate fire-induced carbon emissions, primarily by use of models. There are many estimation approaches and methodologies involved in biomass burning emissions. Specifically, remote-sensing technologies are assessed as a feasible way to estimate emissions from both a direct approach (i.e., smoke measurements) and an indirect approach (i.e., model emissions critical factors, such as fuel availability and combustion efficiency) (Palacios-Orueta et al. 2005).

Generally, the amount of carbonaceous aerosols and trace gases of interest is derived as follows:

$$M_x = MB_{consumed} \times EF_x \quad (1)$$

where M_x is the mass of species x emitted from fire; EF_x is the mass of species x released per kilogram of the biomass burned (emission factor); and $MB_{consumed}$ is the mass of the dry biomass burned. $MB_{consumed}$ can be estimated using the following equation (Stephens 2005):

$$MB_{consumed} = BA \times BD \times BE \quad (2)$$

where BA (ha) is the area burned by fire; BD (kg ha^{-1}) is the density of the dry biomass in the area; and BE (%) is the burn efficiency or combustion completeness, i.e., the fraction of biomass consumed by fire. In this study, we presume that biomass below ground does not burn, although fires can burn deep into the ground under certain conditions, such as peat fire. This model integrates a series of biophysical variables that can be estimated based on various sources from remote sensing imagery and from the literature.

4.2.3 Determination of variables

4.2.3.1 Burned area (BA)

The Great Xing'an Mountains are typical of fire-prone ecosystems, in which many species have a recognized ability to regenerate after fire. Fire has been a primary disturbance in most forests of this region and has shaped their plant communities for millions of years. Historically, fire regimes in this region have been characterized by frequent, low intensity surface fires mixed with sparse stand-replacing fires in relatively small areas (Wu et al. 2011). The historical burned areas used in this study were derived from NOAA-AVHRR from 1986-2000. For the period from 2000 to 2010, the burned area was estimated using the satellite MODIS MCD45 Burned Area Level 3 product, which provides the most comprehensive data concerning fire-affected areas in remote boreal regions. The MCD45 algorithm maps the approximate day and the extent of burning by locating the occurrence of rapid changes in multi-spectral daily surface reflectance time series data (Roy et al. 2005).

4.2.3.2 Biomass density (BD) and Burning Efficiency (BE)

Biomass density and burning efficiency are two uncertain parameters in biomass burning estimates due to the high-spatial variability of the burning process and of fuel availability, which are related not only to general ecosystem characteristics but also to the micro-scale environmental conditions. Trace gas emissions are directly related to biomass and land cover through the amount and composition of the burned fuel. Simply stated, the higher the biomass density is, the higher the amount available for burning and, therefore, the greater the total quantity of carbon that can be released as trace gases (Prasad et al. 2002). In areas of low precipitation and in regions with dry periods of high temperature, biomass consumption is higher than in more humid

climates, with a linear relation between the annual area burned and the fraction of biomass consumed. Thus, in warmer years, when a higher number of fires occur, the burning efficiency is also higher (Palacios-Orueta et al. 2005). However, thousands of fire events occurred during such a long period (1986-2000). Thus, it is infeasible to identify the specific meteorological conditions of each fire event. Phytogeography tells us that the geographic distribution of plant species is primarily decided by those regional climate characteristics. In this sense, the land cover map can also commendably reflect the site climate characteristics. Therefore, in this study, the biomass densities (BD) and burning efficiencies (BE) were derived from values published in (Song et al. 2009b) using the AVHRR Global Land Cover Map (AVHRR GLC-2000) at a 1 km resolution. Table 4-1 shows the determination of biomass densities (BD) and burning efficiencies (BE), whose values are derived from published literature based on specific sites across the globe and from laboratory experiments (Wiedinmyer et al. 2006), (Wang, Fang, and Zhu 2008) and (Vasileva and Moiseenko 2013). By combining table 4-1 and fuel type (Figure 4-1), biomass densities (BD) and burning efficiencies (BE) raster image were produced on a pixel-by-pixel basis (Figure 4-2).

Table 4-1 Determination of emission model parameters for each bioclimatic zone against the AVHRR-GLC classification

NN	Description	BD (Mg/ha)	(BE %)
1, 3	Evergreen and deciduous needle leaf forest	140	40
4	Deciduous broadleaf forest	95	40
5	Mixed forest	12	40
6	Woodland	95	40
7	Wooded grassland	11	90
8, 9	Shrub land	43	50
10	Grassland	11	90
11	Cropland	5	90
0, 12-14	Water bodies, barren, built-up, undefined	0	0

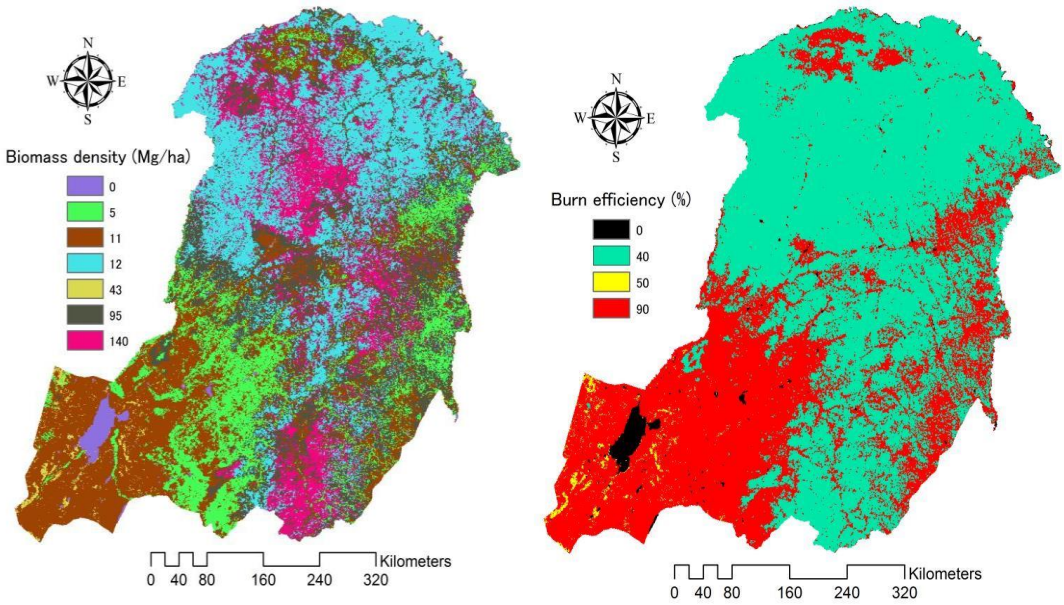

Figure 4-2 Biomass density (left) and burned efficiency (right) distribution in Great Xing'an Mountain

4.2.3.3 Determination of emission factors (EF)

Emission factors are defined as the amount of certain trace gas species released per amount of fuel consumed, which are expressed in grams of a gas compound per kilogram of dry matter (kg species emitted Mg^{-1} biomass burned). Emission factors are based on the correlation between the concentration of a certain gas species and the

concentration of the reference species emitted and are estimated from experiments for specific conditions (Palacios-Orueta et al. 2005). Emission factors for various ecosystems and environmental conditions have been derived either in natural conditions or in controlled laboratory experiments (Wiedinmyer et al. 2006), (Wang, Fang, and Zhu 2008) and (Vasileva and Moiseenko 2013) where the rest of the variables were known (i.e., the amount of the compound released, the amount of fuel burned and the concentration of the element in the fuel) (Palacios-Orueta et al. 2005). In the present study, emission factors were also assigned for each land cover classification in the AVHRR GLC-2000 data. These emission factors for each emitted species, which are given in Table 4-2, were based on previously published studies (Wiedinmyer et al. 2006), (Wang, Fang, and Zhu 2008) and (Vasileva and Moiseenko 2013). The average of relevant emission factors for each gaseous or particulate species was applied when more than one emission factor was available in the literature. Therefore, emission factors raster images were produced by combining table 4-2 and land cover classes in AVHRR GLC-2000 on a pixel-by-pixel basis (Figure 4-3).

Table 4-2 Emission factor assigned to fires in each of the vegetation types of the AVHRR GLC-2000 land cover classes

Description	CO_2	CH_4	CO	PM_{10}	$PM_{2.5}$	SO_2	BC	NOx
Evergreen and deciduous need leaf forest	1700	4.8	89	13.1	12.7	0.6	0.77	3.1
Deciduous broadleaf forest	1750	4.5	94	15	12.3	0.5	0.82	2.5
Mixed forest	1670	4.5	84	12.5	7.9	0.6	0.8	3
Woodland	1652	4.5	90	8.5	7.3	0.5	0.5	6.5
Wooded grassland	1642	3.1	80	8.5	7	0.5	0.52	3.2
Shrub land	1632	3.1	85	8.5	7	0.5	0.52	6.5
Grassland	1588	3.1	80	9.9	6.3	0.5	0.48	4
Cropland	1353	2.2	80	9.9	6.3	0.4	0.63	2.9
Water bodies, barren, urban**	0	0	0	0	0	0	0	0

* Unites are gram species per kilogram of dry biomass burned (g/kg). values given in this table are derived from published literatures (Wiedinmyer *et al.*, 2006),(Andreae and Merlet, 2001),(Cao *et al.*, 2008) and (Song *et al.*, 2009b)**.**

** Emission factors for water bodies, barren area and urban area were are assigned a value of zero.

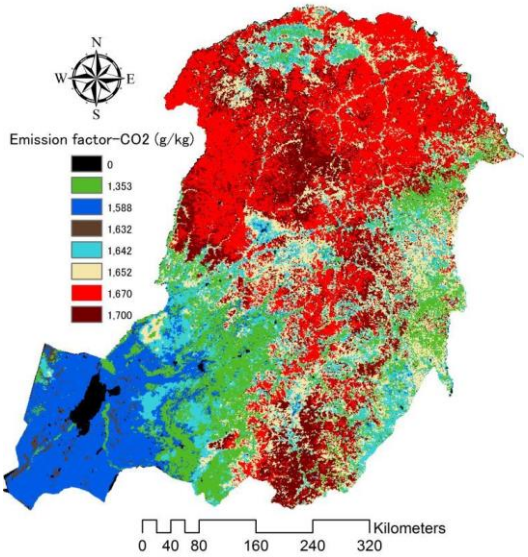

Figure 4-3 The determination of CO_2 emission factor in china. The emission factors of other emitted species (CH_4, CO, PM_{10},$PM_{2.5}$,SO_2, BC and NO_x) were also determined in the same way

4.3 RESULTS AND DISCUSSION

4.3.1 Wildfire distribution in the Great Xing'an Mountain

Figure 4-4 shows the historical burned area distribution by month from the years 1986 to 2010. In total, 9998 fire scars were found in the GXM between the years 1986 and 2010. Particularly during the spring fire season, there are always serious large forest fire events. For example, on May 6, 1987, a catastrophic fire occurred on the northern slopes of the Great Xing'an Mountains, which burned a total area of 1.3×10^6 ha, with disastrous effects on the forest composition and structure, ecosystem processes and the landscape pattern (Cahoon et al. 1994). The wildfire that broke out in Jinhe and Genhe counties on May 5, 2003 burned 7.9×10^4 hectares, including 6.3×10^4 hectares of forest areas, with an economic loss of more than 198 million (Lin and Wang 2007).

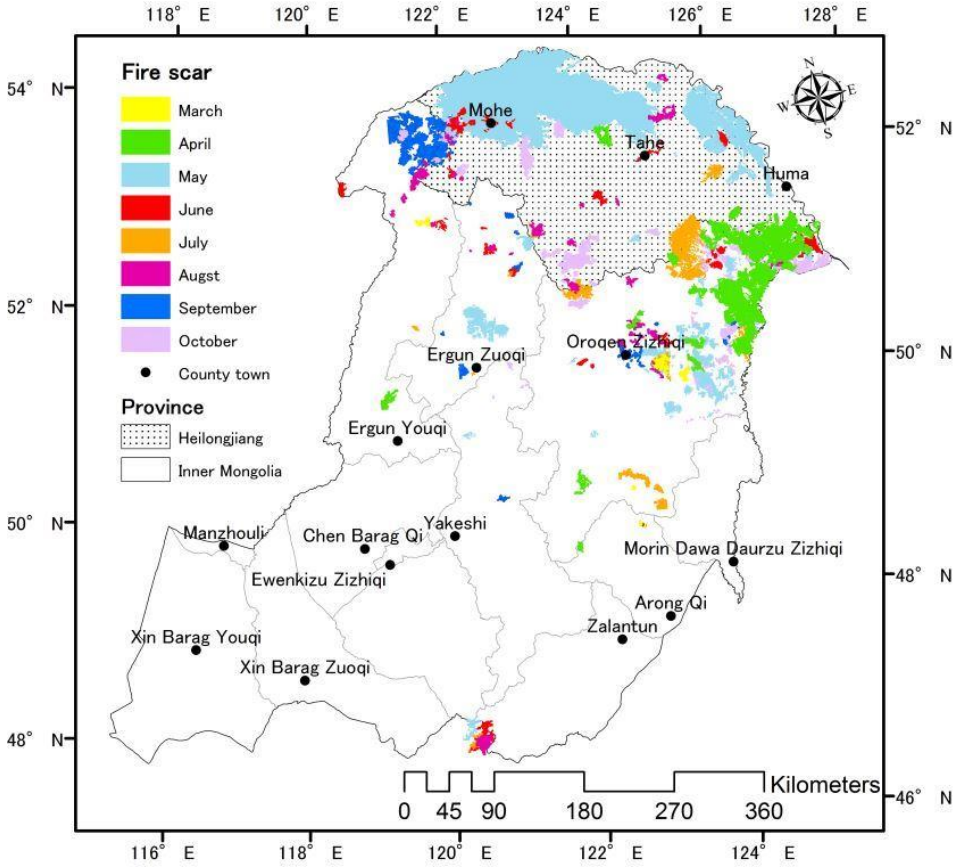

Figure 4-4 Burned areas distribution by month from 1986 to 2010. Only the fire scars which larger than 100 ha were showed in this figure. Note that the size of the burn scars increases slightly for the display purpose

In the Great Xing'an Mountains, two primary peak seasons of forest fires were recorded in spring and in autumn, particularly in May and in October. Normally, there are no large fire events due to high precipitation and high fuel moisture in summer (July and August) and to low temperatures accompanied by the accumulation of snow and frozen land in winter (late November to February) (Figure 4-5). Thus, fire events always occur in spring from mid-March to mid-June and from mid-September to mid-November in fall. Most large fires occurred in the northern region of the GXM between 50 ℕ and 54 ℕ latitude due to much drier weather and higher fire danger in the northern region (part of Heilongjiang Province) than in the southern region (part

of Inner Mongolia Province) (Figure 4-4). The vegetation in this region is a cold-temperature mixed coniferous forest, in which fire is likely to occur. Burn scars and the associated vegetation succession lead to a mosaic of landscape patches. These spatial patterns of regenerating vegetation in various successional stages are important considerations for carbon budget studies in boreal forests (Balzter et al. 2007).

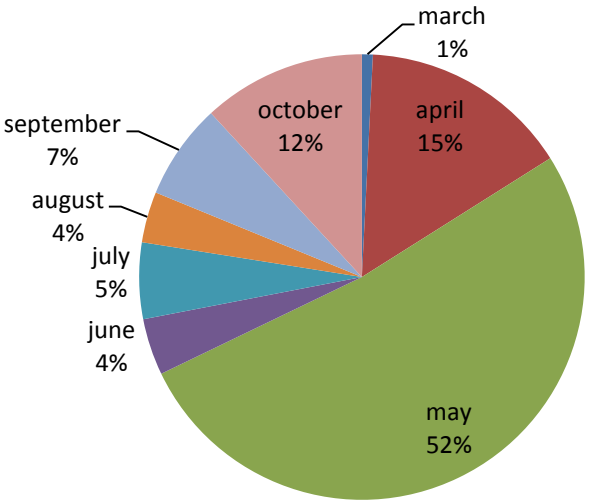

Month	Burned area (ha)
March	36512
April	703243
May	2388044
June	189394
July	255307
August	170299
September	320805
October	546072
Total	4609675

Figure 4-5 Monthly pattern of wildfire in Great Xing'an Mountain

Table 4-3 and Figure 4-6 show the burned area shift in Great Xing'an Mountains from 1986 to 2010. The years 1987 and 2003 contributed 33.2% and 22.9%, respectively, in burned area during the 25 years. In total, 1.53 million hectares have been charred by fires in 1987, which was the most destructive fire year in China's history, with a specific larger fire in May that burned 1.33 million hectares alone. Extreme meteorological conditions, in combination with the lack of accessibility, has resulted in large, high-intensity crown fires throughout China's boreal forests in 1987 (Cahoon et al. 1994). Another severe fire year in the history of the Great Xing'an Mountains is 2003, during which approximately 1.1 million hectares was burned. Dozens of fires attacked the entire GXM region from Inner Mongolia to Heilongjiang

Province in May 2003. As the neighbor of the Great Xing'an Mountains, West Siberia's largest forest fires on record also occurred during the same period in 2003, claiming approximately 20 million hectares of land and emitting heat-trapping emissions equal to the total cuts in emissions that the European Union pledged under the Kyoto Protocol (Frey and Smith 2005). Higher temperatures and thawing permafrost are most likely contributing to the rising frequency and severity of forest fires in West Siberia (Sheng et al. 2004).

Table 4-3 Yearly burned area (ha) in Great Xing'an Mountain

Year	Burned area (ha)	Year	Burned area (ha)
1986	30976	1999	118459
1987	1531597	2000	170731
1988	41261	2001	113731
1989	195052	2002	79262.5
1990	35773	2003	1056814
1991	88451	2004	70516.49
1992	66836	2005	17577.23
1993	76956	2006	136875
1994	71632	2007	41973.39
1995	176864	2008	36570.98
1996	264207	2009	17193
1997	117434	2010	18325
1998	34606	Total	4609675

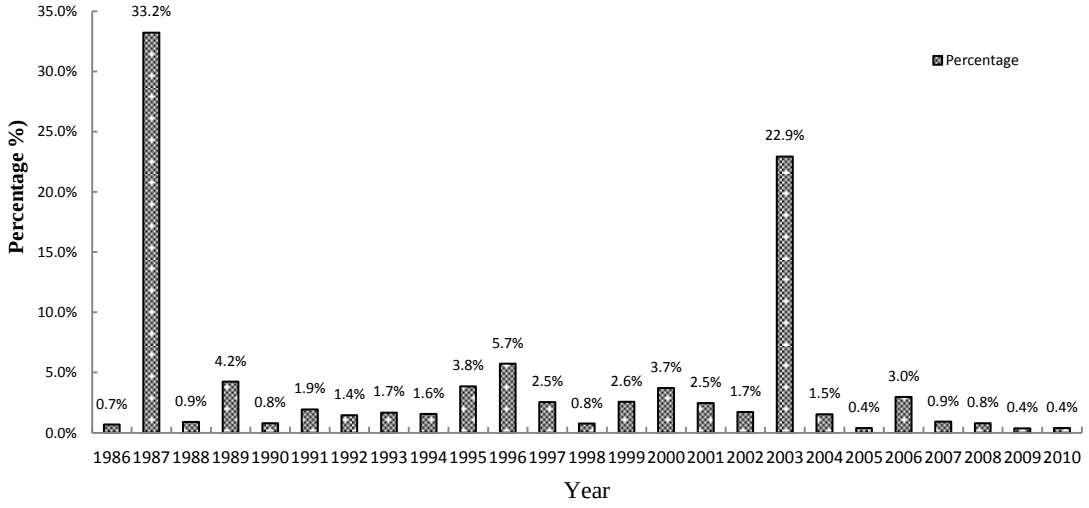

Figure 4-6 Yearly burned area shift in Great Xing'an Mountain

4.3.2 Trends in biomass burning emissions

Yearly and monthly emissions of CH_4, CO, PM_{10}, $PM_{2.5}$, SO_2, BC and NO_x from biomass burning in the Great Xing'an Mountains have been estimated from 1986 to 2010. The spatial and temporal distribution of fire emissions is similar to that of the burned area because the burned pixels were defined as 1, whereas unburned pixels were defined as 0. Table 4-4 summarizes the average annual emissions of trace gases and particulate matter for different land cover types. Evergreen and deciduous needleleaf forest and deciduous broadleaf forest are the main sources of emissions, accounting for 84%, 81%, 84%, 87%, 89%, 86%, 85% and 74% of the total annual CO_2, CH_4, CO, PM_{10}, $PM_{2.5}$, SO_2, BC and NOx emissions, respectively. Fire emissions from shrubland, grassland and cropland only account for a small fraction of the total emissions level (approximately 4%-11%). The two extreme fire years of 1987 and 2003 contributed approximately 60% of total biomass burning emission, according to this study from 1986 to 2010. Cahoon et al. estimated that 14.5 million ha burned and that approximately 36 Tg CO were emitted during the Great China Fire by using AVHRR burn scars (Cahoon et al. 1994). This result suggests that the

inclusion of fire emissions that are specific to a particular period and region is essential for realistically simulating air quality (Wiedinmyer et al. 2006).

Table 4-4 Emissions of estimated trace gases and particulate matter (Tg/year) from fires for the average annual value of the period from 1986 to 2010

Description	CO_2	CH_4	CO	PM_{10}	$PM_{2.5}$	SO_2	BC	NOx
Evergreen and deciduous needleaf forest	52.66	0.15	27.57	0.41	0.39	0.02	0.02	0.10
Deciduous broadleaf forest	30.65	0.08	16.47	0.26	0.22	0.01	0.01	0.04
Mixed forest	2.22	0.01	1.12	0.02	0.01	7.97E-04	1.06E-03	3.98E-03
Woodland	5.79	0.02	3.15	0.03	0.03	1.75E-03	1.75E-03	0.02
Wooded grassland	1.50	2.83E-03	0.73	0.01	0.01	4.56E-04	4.75E-04	0.00
Shrubland	3.23	0.01	1.68	0.02	0.01	9.91E-04	1.03E-03	1.29E-02
Grassland	2.90	0.01	1.46	0.02	0.01	9.13E-04	8.76E-04	0.01
Cropland	0.56	9.13E-04	0.33	4.11E-03	2.61E-03	1.66E-04	2.61E-04	1.20E-03
Total	99.51	0.26	52.51	0.76	0.68	0.03	0.04	0.19

Several published papers have also estimated the biomass burning emissions in different regions for recent years (Yan, Ohara, and Akimoto 2006; Wiedinmyer et al. 2006; Song et al. 2009a; Lu et al. 2006). The emissions from bio-fuel in our study are compared with four other previous study results (Table 4-5) because our study period includes two extreme fire years, 1987 and 2003, which play an important role in the final average annual result from 1986-2010. Thus, we calculated another average annual emission result for a normal period (2005-2010) without any extreme fire events. The areas of these study domains differ from our study area. Thus, we list all estimated regions and their area ratios in table 4-5 for comparison (United States – 962.9×10^4 km^2; Canada – 998.5×10^4 km^2; China – 962.9×10^4 km^2; Our study area – 32.7×10^4 km^2). Wiedinmyer et al. (2006) estimated the entire fire-induced emissions across North America and Central America for the calendar year 2004. These authors

estimated 356 Tg and 227 Tg yearly total CO_2 emissions for the United States and Canada, respectively. The yearly total CO_2 emissions for the United States is only 3.6 times and 14.7 times our resulting annual CO_2 emissions of the Great Xing'an Mountains for 1986-2010 and for 2005-2010, respectively. However, the area of the United States is 29.4 times that of our study domain. Table 4-5 indicates that the yearly total CO_2 emissions in the United States is much higher than in China by approximately 3-9-fold, according to different estimates (Yan, Ohara, and Akimoto 2006; Song et al. 2009a; Lu et al. 2006). Other emission species in the United States also show a similar relation with China. Estimating trace gas emissions from biomass burning is a complex issue due to the many variables that are involved in the process. The level of uncertainty includes several factors directly related to the working scale and to each of the variables involved in the models (Palacios-Orueta et al. 2005). Notably, there was a significant difference in the emissions results among different studies, even within the same study domain (Yan, Ohara, and Akimoto 2006; Song et al. 2009a; Lu et al. 2006). Compared with the CO_2 emission for all of China's, the average annual CO_2 emission (2005-2010) accounts for 24%, according to Song et al. (2009b), 30.3%, according to Yan et al. (2006) and 59.3%, according to Lu et al. (2006).

Table 4-5 Comparison of our biomass burning estimations with sever other published estimations (Tg/year)

Literatures	Regions	Area ratio[1]	CO_2	CH_4	CO	PM_{10}	$PM_{2.5}$	SO_2	BC	NOx
(Wiedinmyer *et al.*, 2006)[2]	United states	29.4:1	356	1.0	19.8	2.7	2.4	0.16	-	0.68
	Canada	30.5:1	227	0.64	12.7	1.8	1.6	0.11	-	0.43
(Yan *et al.*, 2006)[3]	China	29.5:1	79.7	0.24	5.4	-	0.66	0.05	0.03	0.2
(Lu *et al.*, 2006)[4]	China	29.5:1	40.7	0.11	2.7	-	-	-	-	-
(Song *et al.*, 2009b)[5]	China	29.5:1	102	0.27	6.8	-	0.69	0.05	0.06	0.2
This study[6]	GXM	1:1	99.51	0.26	52.51	0.76	0.68	0.03	0.04	0.19
This study[7]	GXM	1:1	24.15	0.06	1.27	0.18	0.16	0.05	0.02	0.05

[1]The area ratio of other study domain and Great Xing'an Mountain (GXM).

[2]Calendar year 2004 estimated by (Wiedinmyer *et al.*, 2006).

[3]Calendar year 2000 estimated by(Yan *et al.*, 2006).

[4]Average from calendar years 1950 to 2000, estimated by (Lu *et al.*, 2006).

[5]Fire year 2000 (April 2000 to March 2001) estimated by (Song *et al.*, 2009b).

[6]Average annual value of the period from 1986 to 2010.

[7]Average annual value of the period from 2005 to 2010.

4.4 UNCERTAINTY

Thus far, modeling methodologies are the most realistic way to accomplish emissions estimations, and remote-sensing data acquisition seems to be a feasible way to estimate those parameters required for the models. These approaches depend on factors such as the scale, accuracy requirements and information availability, among others. The variables involved in most of the models are the burned area, fuel availability, burning efficiency, emission factors and ratios. Detecting the burned area over large scales from satellite has been proven a difficult task. The historical monthly and yearly burned area used in this study were derived from NOAA-AVHRR (1986-2000) and from the MODIS fire product (2000-2010). The Global Land Cover Map

(AVHRR GLC-2000) from the AVHRR satellite product was used to determine biomass density (BD) and burning efficiency (BE) values in this study. The numbers and types of ecosystem classes used varied substantially. Many authors have noted that although land-cover data sets often show reasonable broad agreement at a global level in terms of total area and general spatial patterns, there is disagreement in the individual land classes and in the spatial distribution of land-cover classes. In addition, burning efficiency (BE) is also affected by instantaneous meteorological conditions on the burning days, such as wind and precipitation. Concerning the emission factors, data are available only for specific sites across the globe or for laboratory experiments. Although remote sensing may provide helpful insight into their temporal and spatial evolution, further developments are required to consistently relate spectral data and vegetation properties. The use of common emission factors for highly diverse environmental conditions introduces a high level of uncertainty into the calculations. In this sense, uncertainty is highly associated with the land cover inside class variability; areas with high variability show higher levels of uncertainty due to the difficulty in applying precise coefficients (Palacios-Orueta et al. 2005).

4.5 CONCLUSIONS AND RECOMMENDATIONS

This study improves strategies that optimize input information by combining explicit spatio-temporal remote-sensing data with models to obtain reliable emissions information. Biomass burning emissions in the boreal region yield an important contribution to the chemical budget of the troposphere. To assess the contribution of biomass burning to the emissions of atmospheric trace species in the Great Xing'an Mountains (GXM), which is the most severe fire-prone area in China, we estimated various fire activities by combining explicit spatio-temporal remote sensing data with

models. We derived 9998 fire scars with a total area of 4,6096 km^2 in the Great Xing'an Mountains between the years 1986 and 2010. The years 1987 and 2003 contributed 33.2% and 22.9%, respectively, in burned area during the 25 years. Fire activity is the strongest in May. Most large fires occurred in the northern region of the Great Xing'an Mountains between 50ºN and 54ºN latitude due to much drier weather and higher fire danger in the northern region than in the southern region. Evergreen and deciduous needleleaf forest and deciduous broadleaf forest are the main sources of emissions, accounting for 84%, 81%, 84%, 87%, 89%, 86%, 85% and 74% of the total annual CO_2, CH_4, CO, PM_{10}, $PM_{2.5}$, SO_2, BC and NOx emissions, respectively. Fire emissions from shrubland, grassland and cropland only account for a small fraction of the total emissions level (approximately 4%-11%). Comparisons of our results with other published estimates of biomass burning emissions show reasonable agreement; however, substantial uncertainties remain concerning the modeling parameters. The variability in emission factors greatly contributed to the uncertainty. There is an urgent requirement to obtain more accurate biomass burning estimates because of its considerable contribution to the regional and global carbon balance and to the atmosphere.

Chapter 5. Long-term satellite detection of post-fire vegetation trends in boreal forests of China

ABSTRACT

This paper describes the long-term effects on vegetation following the catastrophic fire in 1987 on the northern Great Xing'an Mountain by analyzing the AVHRR GIMMS 15-day composite normalized difference vegetation index dataset. Both temporal and spatial characteristics were analyzed for natural regeneration and tree planting scenarios from 1984 to 2006. Regressing post-fire NDVI values on the pre-fire values helped identify the NDVI for burnt pixels in vegetation stands. Stand differences in fire damage were classified into five levels: Very High (VH), High (H), Moderate (M), Low (L) and Slight (S). Furthermore, intra-annual and inter-annual post-fire vegetation recovery trajectories were analyzed by deriving a time series of NDVI and relative regrowth index (RRI) values for the entire burned area. Finally, spatial pattern and trend analyses were conducted using the pixel-based post-fire annual stands regrowth index (SRI) with a nonparametric Mann-Kendall (MK) statistics method. The results show that October was a better period compared to other months for distinguishing the post- and pre-fire vegetation conditions using the NDVI signals because colored leaves on grasses and shrubs fall down, while the leaves on healthy trees remain green in October. The Mann-Kendall (MK) statistics method is robustly capable of detecting vegetation trends in a relatively long time series. Because tree planting primarily occurred in the severely burned area (approximately equal to the Medium, High and Very High fire damage areas) following the 1987 fire, the severely burned area exhibited a better recovery trend than the lightly burned

regions. Reasonable tree planting can substantially quicken the recovery and shorten the restoration time of the target species. This research involves a large area (1.33×10^6 ha) and a long time span (1984-2006). Therefore, it is unfeasible to perform actual field validation for such a study. More detailed satellite analyses and field data will be required in the future for a more convincing validation of the results.

KEYWORDS:

Wildfire, remote sensing, vegetation recovery, Mann-Kendall, boreal forest

5.1 INTRODUCTION

Wildfire is an important process in regulating vegetation succession, plant regeneration, and species composition in boreal forest ecosystems (Kang et al., 2006; Wulder et al., 2009; Beck et al., 2011). Large areas of the boreal forest zone, which natural fires have shaped over several millennia, are burned annually. Industrial and recreational use of boreal forests and forest fire suppression capabilities have dramatically increased over the past century (Cahoon et al., 1994). Northeast China maintains abundant forest resources, with a forest area of ~47.0 ×104 km2, occupying 31% of China's total forest area (Tan et al., 2007a). This region stores 1.0-1.5 Pg C and contributes to approximately 24–31% of the total carbon storage in China (Fang et al., 2001). Most carbon is stored in living trees. For thousands of years, wildfires have been the predominant disturbances in this region, which has been strongly modified by humans during the recent half century. Historically, fire regimes in these systems were characterized by frequent, low intensity surface fires mixed with sparse stand-replacing fires over relatively small areas. From 1950 to 1995, the annual average burned area in the northeast region accounted for 55% of the national total

(Zhong et al., 2003). Wildfires play a dominant role in boreal ecosystems, altering the forest succession, biogeochemical cycling and carbon sequestration (Goetz et al., 2006). During pre-fire periods, forests are believed to be a net carbon sink. When wood is burned, carbon is emitted in decomposition, and wildfires are believed to represent a globally significant source of terrestrial carbon to the atmosphere. Following a wildfire, more carbon is absorbed in younger trees during the faster regrowth phases. Therefore, a better observational base for understanding post-fire vegetation dynamics in the boreal forests will contribute to predicting the effects of the increasing number of wildfires caused by climate change in these ecosystems and subsequently forecasting the future role of boreal forests as a carbon sink or source (Cuevas-GonzÁLez et al., 2009).

Wildfires create profound changes in ecosystems, causing variations in vegetation reflectance, moisture and temperature, which can be detected by means of satellite imagery (Segah et al., 2010; Matthews et al., 2012). Fire disturbance causes substantial spectral changes by consuming vegetation, destroying the leaf chlorophyll, exposing soil, charring stems and altering vegetation moisture. These effects of a fire on vegetative ecosystem properties are often defined as burn severity, which is restricted to the loss of organic matter in or on the soil surface, and in this respect represents what BAER assessments term ‘soil burn severity’ (Parsons, 2003). The post-fire re-growth process is of great importance because while fire releases carbon into the atmosphere, carbon sequestration through post-fire regeneration of plants and woody vegetation may help to reduce the amount of carbon in the atmosphere (Balzter et al., 2007). Numerous studies have focused on the use of the Normalized Difference

Vegetation Index to analyze seasonal and inter-annual vegetation dynamics and trends following wildfire disturbances (Telesca and Lasaponara, 2006; Leon et al., 2012). The NDVI data capture the contrast between red and near-infrared reflectance of vegetation, which signals the abundance and energy absorption of leaf pigments, e.g., chlorophyll.

NDVI can be used as a proxy for the vegetation response to wildfire disturbances because it is well correlated with vegetation regrowth and the fraction of photosynthetically active radiation absorbed by plant canopies and thus leaf area and biomass (Zhou et al., 2001). In the present paper, NDVI derived from and the Advanced Very High-Resolution Radiometer (AVHRR) satellite measurements is exploited to investigate post-fire regeneration and temporal dynamics in the boreal forest. Because of an unusually prolonged drought and high winds in northeastern China, the Great Xing'an Mountains exploded in a catastrophic wildfire in May 1987. The success of fire suppression in this region, coupled with a warmer, drier climate due to global warming, has led to fuel buildup and resulted in fires of greater intensity and extent than those that occurred historically in the region (Wang et al., 2007). This fire created a mosaic of burn severities across the landscape and provided an ideal opportunity to study post-fire vegetation patterns in a Chinese boreal forest. The main goals of the present work are (i) to assess the fire damage of the entire fire-affected areas in the Great Xing'an Mountains from the 1987 fire event, (ii) to better understand how vegetation responds to fire disturbances by analyzing intra- and inter-annual variability in satellite observations and (iii) to characterize the spatial pattern

of post-fire vegetation trends using the AVHRR GIMMS NDVI record over the period 1986-2006.

5.2 DATA AND METHOD

5.2.1 Study area

The Great Xing'an Mountain is a typical fire-prone ecosystem in which many species have a recognized ability to regenerate after fire. Historically, fire regimes in this region were characterized by frequent, low intensity surface fires mixed with sparse stand-replacing fires over relatively small areas (Wu et al., 2011). The 1987 fire occurred on May 6th and was located on the north slope of Great Xing'an Mountain (52°15'N−53°33'N, 121°51'E−125°05'E) in northeastern China (Figure 4-1). It is primarily a hilly mountainous region ranging from 450 to 1500 m in elevation. The 1987 fire burned more than 1.33 million hectares of forest resulting in the loss of over 200 lives and 50000 homes. Fires of this magnitude are a major but infrequent disturbance to this landscape, occurring at 100- to 300-yr intervals (Turner et al., 1997). The 1987 fires produced a strikingly heterogeneous mosaic of burn severities (effects of fire on the ecosystem) and islands of unburned vegetation across the landscape. The spatial extent and heterogeneity of the 1987 fires provide an ideal opportunity to study the effects of fire size and pattern on post-fire succession. The climate in this region is terrestrial monsoon with long, severe winters (mean January temperature -28.5℃) and short, mild summers (mean July temperature 17℃). The precipitation, which peaks in summer, is 420 mm annually and is unevenly distributed throughout the year, i.e., more than 60% occurs between June and August. Vegetation in this region falls within the cool temperate coniferous forests occurring at the southern extension of the eastern Siberian light coniferous forest (Li et al., 2013). The species composition is relatively simple and the forest covers more than 75% of the

study area. The most dominant tree species is larch (Larix gmelini), accounting for 80% of the study area, followed by birch (Betula Platy Plylla), which covers 10% of the study area. Other species, including pine (Pinus sylvestris var. mongolica), spruce (Picea Kor-aiensis), two species of aspen (Populus davidiana, Populus suaveolens), and willow (Chosenia arbutifolia) cover approximately 10% of the study area.

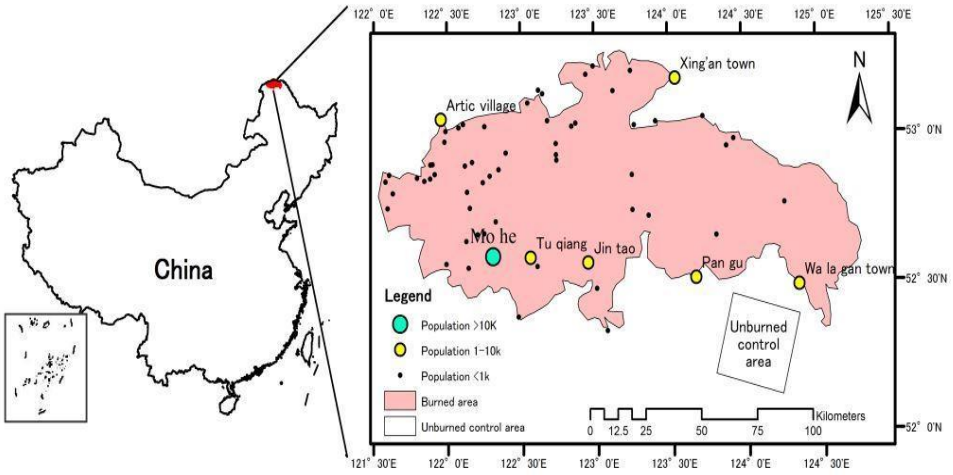

Figure 5- 1 Location of the study area

5.2.2 AVHRR GIMMS 15-day composite NDVI dataset

We used the continental NDVI dataset at 8 km resolution for the period 1984-2006 produced by the Global Inventory Monitoring and Modeling Studies (GIMMS). The dataset was derived from imagery obtained from the AVHRR instrument onboard the NOAA satellite series 7, 9, 11, 14, 16 and 17. It contains channel 1 (0.58- 0.68 μm) and channel 2 (0.73-1.1 μm) reflectance, channel 4 (10.3-11.3 μm) and channel 5 (11.5-12.5 μm) brightness temperatures, solar and view zenith angles, and the day of compositing. These channels and associated data correspond to the maximum NDVI value during a 15-day compositing period. The NDVI is expressed on a scale between -1 and +1. GIMMS NDVI values range between -0.2 and 0.1 for snow, inland water bodies, deserts, and exposed soils, and increases from approximately 0.1 to 0.7 for increasing amounts of vegetation. The GIMMS dataset includes calibration using

desert targets, atmospheric correction for stratospheric aerosol, and normalization for temporal changes in solar zenith angle (Pouliot et al., 2009).

5.2.3 Method

5.2.3.1 Mapping fire damage

In the present study, the difference in vegetation activity obtained from the NDVI between the pre- and post-fire periods was used to estimate fire damage. Fire damage represents the reflectance changes between the pre-fire vegetation and post-fire burn scar that can be interpreted as the extent of degradation of the pre-fire vegetation community. Therefore, fire damage (D) can be measured as a difference between pre- and post-fire NDVI values, as given by

$$\mathrm{D} = \mathrm{NDVI}_{\mathrm{pre-fire}} - \mathrm{NDVI}_{0}, \quad (1)$$

where $\mathrm{NDVI}_{\mathrm{pre-fire}}$ is the average NDVI value in the pre-fire period, i.e., from 1984 to 1986, while NDVI_{0} is the NDVI value in the fire year, i.e., 1987. In this paper, we prefer fire damage to burn severity because the latter definition is often associated with numerous factors that include the effects on soil composition, the amount of organic material consumed by the fire, the effects on vegetation, e.g., amount of char on shrubs, scorch height and crown scorch, tree mortality or the presence of colonizers (Bastos et al., 2011).

5.2.3.2 Modeling of vegetation recovery

Fire disturbances cause abrupt changes in the trend and seasonality of vegetation growth trajectories. Several studies concerning the regeneration of vegetation have proven that the NDVI is particularly useful for monitoring plant regrowth after fire disturbances (Viedma et al., 1997; van Leeuwen, 2008; Kennedy et al., 2012). To ascertain how long it takes burnt vegetation stands to return to their pre-fire average NDVI conditions, a relationship between pre- and post-fire NDVI values for a control

scenario is necessary. The post-fire recovery also relies on the so-called healthy state (Gouveia et al., 2010). Here, the healthy state is considered the theoretical potential vegetation attainable ($\mathrm{NDVI}_{\mathrm{potential}}$) by an ideal healthy state without any disturbance. Therefore, we define the stand regrowth index (SRI) at time t after the fire as:

$$\mathrm{SRI}_{\mathrm{t}} = \frac{\mathrm{NDVI}_{\mathrm{post,t}}}{\mathrm{NDVI}_{\mathrm{potential}}} \times 100\% , \qquad (2)$$

where t is the elapsed year since the fire and $\mathrm{NDVI}_{\mathrm{post,t}}$ is the stand average annual NDVI at time t. Moreover, $\mathrm{NDVI}_{\mathrm{potential}}$ is the NDVI value of the healthy state, which is defined by the maximum NDVI value of the pre-fire period (1984-1986). Actually, it is very difficult or even impossible for all post-fire pixels to reach the healthy state. Therefore, stand regrowth index approaches 100% as time progresses following a fire disturbance. However, the rate never attains this value. Therefore, the growth rate can be used as a proxy for the vegetation recovery trend.

Furthermore, inter-annual NDVI signals are also greatly influenced by climate changes, e.g., temperature and precipitation anomalies. With the goal of separating the inter-annual variations caused by climate from changes in NDVI and highlighting fire-induced effects on vegetation, another similar index using a control stand NDVI instead of the pre-fire NDVI has been used in numerous fire recovery studies (Lampainen et al., 2004; Cuevas-GonzÁLez et al., 2009; Hope et al., 2012). This relative regrowth index (RRI) at time t can be expressed as follows:

$$\mathrm{RRI}_{\mathrm{t}} = \mathrm{NDVI}_{\mathrm{B,t}} - \mathrm{NDVI}_{\mathrm{C,t}} \qquad (3)$$

where $\mathrm{NDVI}_{\mathrm{B,t}}$ and $\mathrm{NDVI}_{\mathrm{C,t}}$ are the average NDVI values of the burned area and unburned control plot, respectively, derived from the GIMMS NDVI.

The advantage of using SRI to evaluate post-fire recovery is that it relates all post-fire NDVI values to the actual situation in the stand before the fire. However, pre-fire vegetation is specific to antecedent environmental conditions affecting

vegetation growth. Hence, by utilizing an adjacent unburned control stand NDVI to derive the RRI, changes in environmental conditions are potentially captured by the NDVI signals throughout the analysis period (Hope et al., 2012). It is very important for the calculation of the RRI that the selected control area has similar properties (e.g., vegetation type or climate) to the burnt area. The control area was required to have a long history without fire or other disturbances to ensure that it was not undergoing changes associated with vegetation recovery. To minimize differences in temperature and precipitation characteristics, the selected control area should have a similar elevation range to the burned area. In considering these premises, an adjacent area to the fire scar was chosen as the unburned control area (Figure 5-1).

5.2.3.3 Mann-Kendall trend assessment

Trend significance was evaluated using a statistical rank-based nonparametric Mann-Kendall test (Mann, 1945; Kendall, 1975), which is a commonly used method to assess the significance of monotonic trends in long-term time series. It has the advantage of not assuming any distributional form for the data and has similar capabilities as its parametric counterparts. In this study, the time series of the calculated SRIs are analyzed to identify meaningful long-term trends using the Mann-Kendall statistics. In the Mann-Kendall test, the data are ranked with reference to time; each data point is treated as the reference for the data points in successive time periods (Neeti and Eastman, 2011). The equation used to calculate the Mann Kendall correlation coefficient (S) is defined by Kendall as

$$\mathrm{S} = \sum_{\mathrm{i}=1}^{n-1} \sum_{j=\mathrm{i}+1}^{n} sign\left(SRI_i - SRI_j\right), \quad (4)$$

where

$$sign\left(SRI_i - SRI_j\right) = \begin{cases} 1 & if \quad SRI_i - SRI_j < 0 \\ 0 & if \quad SRI_i - SRI_j = 0 \\ -1 & if \quad SRI_i - SRI_j > 0 \end{cases}. \quad (5)$$

Here, n is the length of the time series dataset and SRI_i and SRI_j are the observational stand regrowth index at times i and j, respectively. According to Mann and Kendall, the statistic S is approximately normal when n≥8 with the mean and the variance as follows:

$$E(S) = 0, \quad (6)$$

$$\mathrm{Var(S)} = \frac{n(n-1)(2n+5) - \sum_{i-1}^{n} t_i(i)(i-1)(2i+5)}{18}, \quad (7)$$

where t_i denotes the number of ties of extent i.

The equation used to calculate Mann Kendall significance (U and p) is as follows:

$$U = \begin{cases} \frac{S-1}{\sqrt{\mathrm{Var(S)}}} & \text{for} \quad S > 0 \\ 0 & \text{for} \quad S = 0. \\ \frac{S+1}{\sqrt{\mathrm{Var(S)}}} & \text{for} \quad S < 0 \end{cases} \quad (8)$$

The U statistic follows the standard normal distribution with zero mean and unit variance under the null hypothesis of no trend. A positive U value indicates an upward trend; a negative value indicates a downward trend. The p value of an MK statistic S can then be determined using the normal cumulative distribution function:

$$p = 2[1 - \emptyset(|U|)], \quad (9)$$

where $\emptyset()$ denotes the cumulative distribution function of a standard normal variate.

5.3 RESULTS AND DISCUSSION

5.3.1 Fire damage assessment

The goal of this study was to examine the spatial and temporal patterns of forest regeneration and then assess the driving factors relevant to the vegetation recovery process, especially for fire damage. The differences between the immediate post-fire and pre-fire NDVI values enabled us to identify the fire-damaged areas that were likely burned. Figure 5-2 shows a spatial pattern of fire damage that was computed from the pre- to post-fire difference in GIMMS NDVI. Red pixels represent large

NDVI differences between pre- and post-fire, while blue pixels represent small NDVI

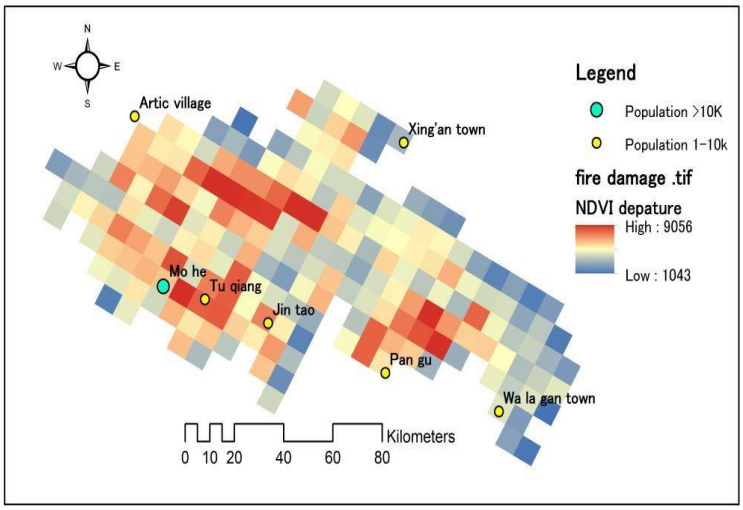

Figure 5- 2 Fire damage map of the study area for the 1987 fire event with fire damage values obtained using Equation 1

differences. Fire damage is expected to influence the spatial configuration and arrangement of forest patches, contributing to and influencing ecological processes during post-fire recovery and succession (Lee et al., 2009). Therefore, to track vegetation behavior that was affected by different fire damage extents, we classified the fire damage into five classes using the z-score (standard deviation) method (Nielsen et al., 2008).

A z-score, or standard deviation, measures the dispersion of data. A reclassification procedure was used to divide the z-scores of the simple difference images (the standardized difference between pre- and post-fire NDVI values) into five categories (Table 5-1).

Table 5-1 Fire damage classification using the z-score method

Pre-fire year (1984-1986)	Post-fire year (1987)	Standard difference	z-score	Fire damage class	Pixels	Percentage (%)
0.7708	0.6542	-2~-1	1	Slight	5	2.44
0.7764	0.5352	-1~0	2	Low	49	23.90
0.7852	0.3868	0~1	3	Medium	94	45.85
0.7884	0.2239	1~2	4	High	46	22.44
0.8165	0.0524	2~999	5	Very high	11	5.37

Figure 5-3 and Figure 5-4 illustrate the result of the fire damage classification using the z-score approach. The image is mapped in a blue-red color scale. Low z-scores are represented in blue, while a red color was assigned to high z-score pixels. The spatial pattern of the fire damage classes is clearly visible in the map with an evident differentiation between very high and slight patches.

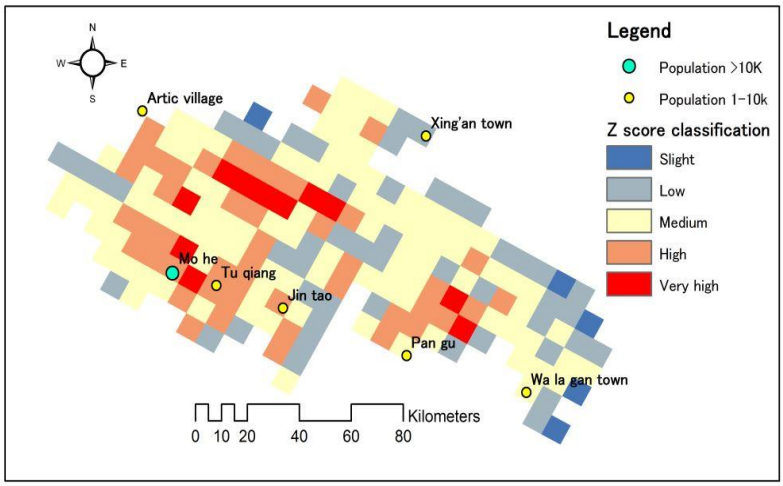

Figure 5-3 The fire damage of the entire burned area divided into five classes: Very high (VH), High (H), Moderate (M), Low (L) and Slight (S)

There were five different fire sources for this large fire event. Some burned areas joined together while others did not (Figure 5-4 and Table 5-2). Therefore, very high and high fire damage pixels were concentrated in a few disjunctive regions.

Table 5-2 Five sources of the 1987 large fire related to Figure 5-4

Fire source	Name	Longitude	Latitude	Burned area (ha)	Ignition reason
Source-1	Gulian	122°22′	52°26′	38×10^4	Electric spark
Source-2	Hewan	122°21′	53°11′	33.8×10^4	Smoking
Source-3	Pangu	123°43′	52°45′	28×10^4	Unknown
Source-4	Xingan	122°22′	122°22′	616	Smoking
Source-5	Yixi	123°25′	53°05′	587	Electric spark

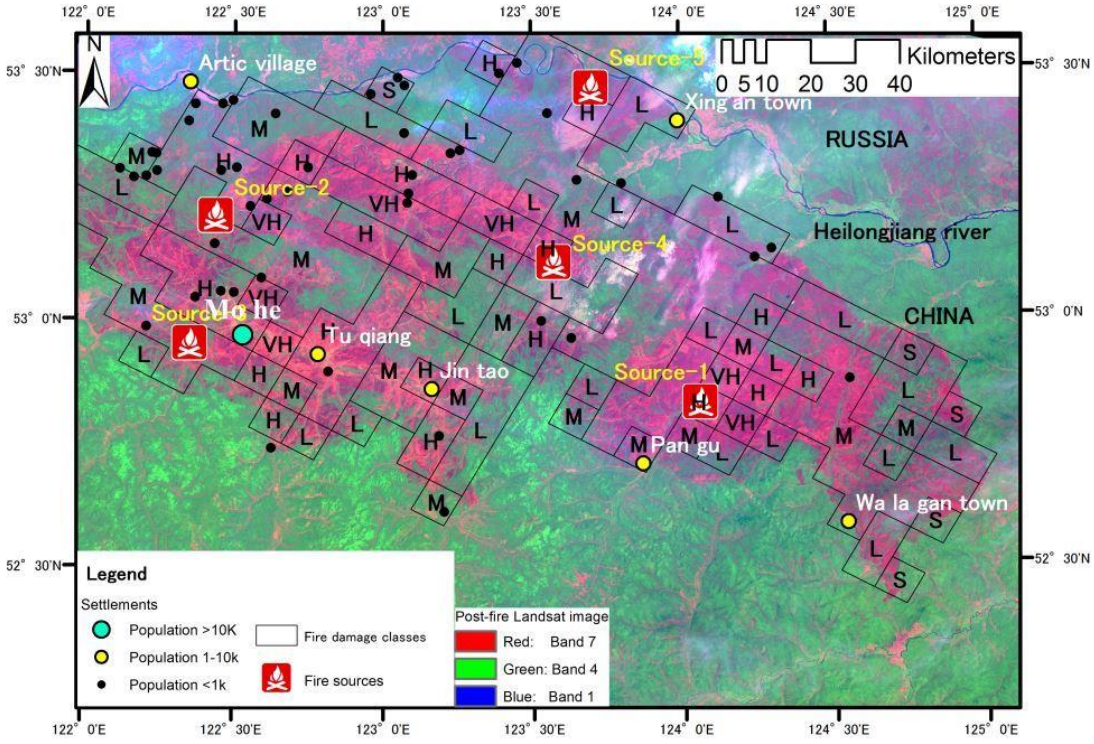

Figure 5-4 Fire sources and fire damage classes. The base map image is a composition of two Landsat 5 TM images from June 1987 (false color composite bands: red-band 7; green-band 4; blue-band 1)

5.3.2 Temporal analysis of post-fire vegetation trajectory

5.3.2.1 Monthly dynamics of post-fire vegetation trajectory

The relationship between pre-fire (1986) and fire year (1987) NDVI values is illustrated in a series of scatter plots (Figure 5-5). The location of the cloud of points shows a large shift away from the 1:1 line when the fire occurred in May and a positive recovery trend after the fire. From January to April (Figure 5-5 a to d), the cloud of points is close to the 1:1 line, which indicates the NDVI values were generally equal during periods without fire disturbances in both years. However, Figure 5-5 e shows that there was a sharp decrease when the fire occurred in May 1987. Following the fire event, there was a rapid increase from June to August (Figure 5-5 f to h), which was likely the NDVI response of the understory vegetation (e.g., herbaceous and shrubs) to temperature or precipitation variability (Pausas et al., 2004; Veraverbeke et al., 2012a). From September to November, the Great Xing'an Mountain entered autumn; NDVI values decreased in both years with the spread of colored foliage and the percentage of fallen leaves increasing. Regardless, Figure 5-5 j also shows clear NDVI departures when post- and pre-fire conditions are compared. This is because colored leaves fall from grasses and shrubs while the tree leaves remain green in October. The difference in NDVI values appeared again in this month. Therefore, October was a better than the others to distinguish post- and pre-fire vegetation conditions using NDVI signals. Thereafter, this region was covered by snow from December to the following February. During this period, it is difficult to find evidence of fire effects on vegetation from NDVI values due to the values reaching a minimum for the entire seasonal cycle.

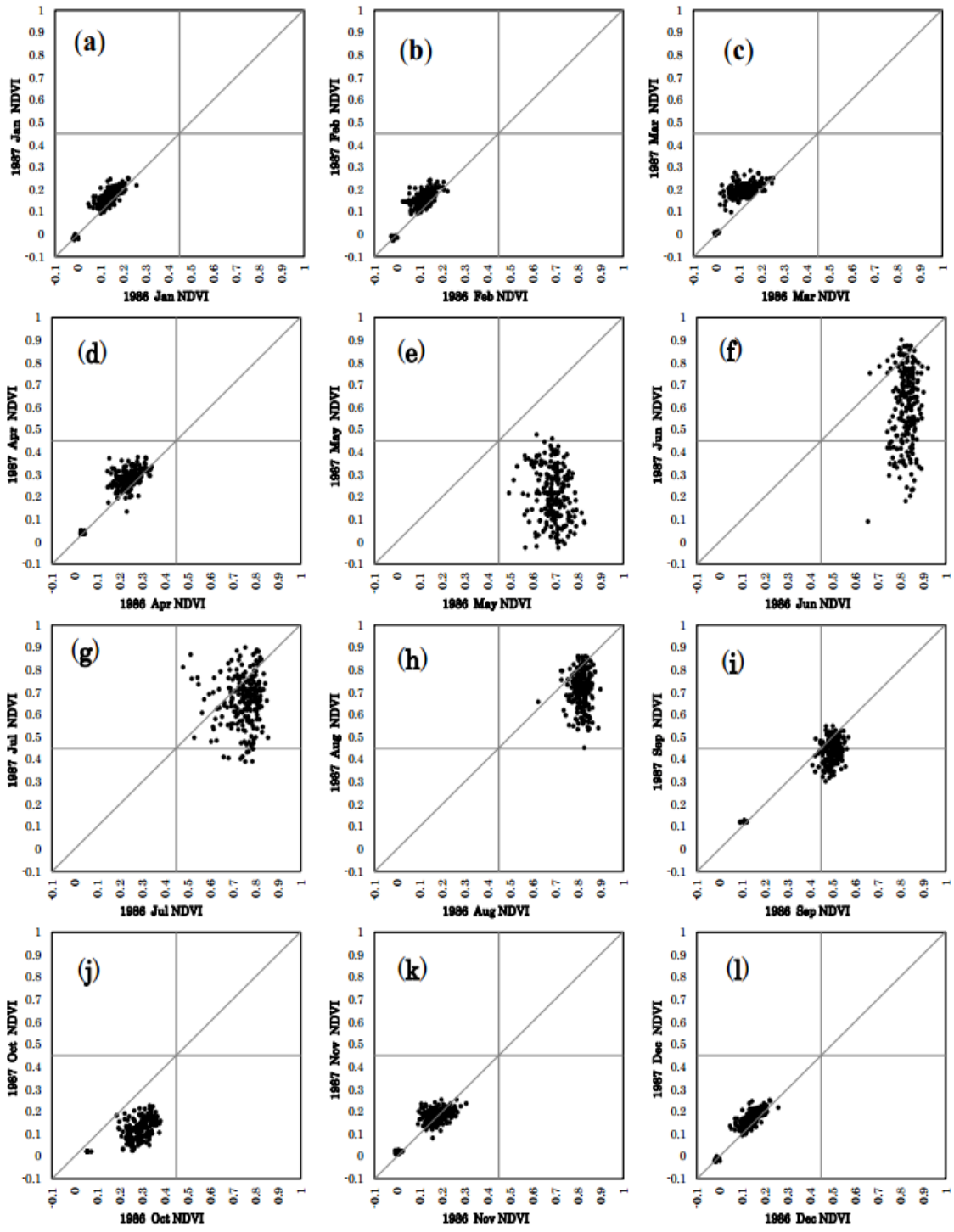

Figure 5- 5 Monthly scatterplots of post-fire NDVI (1987) versus pre-fire NDVI (1986) ((a) January, (b) February, (c) March, (d) April, (e) May, (f) June, (g) July, (h) August, (i) September, (j) October, (k) November, (l) December) for the large fire on May 1987

Shortly after the fire event, the NDVI signal should decrease significantly due to the disappearance of green grasses and shrubs before rapidly increasing again in the following months because of the re-growth of understory vegetation occurs and the phenology trajectory effect. Therefore, to avoid the phenology effect we further compared monthly NDVI trajectories of the normal year (without fire) and fire year (Figure 5-6). The trajectory of black points (average NDVI values for each month) is expected to be distributed along the 1:1 line when there is no disturbance; the monthly differences between the two normal years are very small (Figure 5-6 a). However, for the fire year, there was a large increase in the fire month (May); most points following the fire are below the 1:1 line, indicating a pronounced decrease in greenness due to the fire.

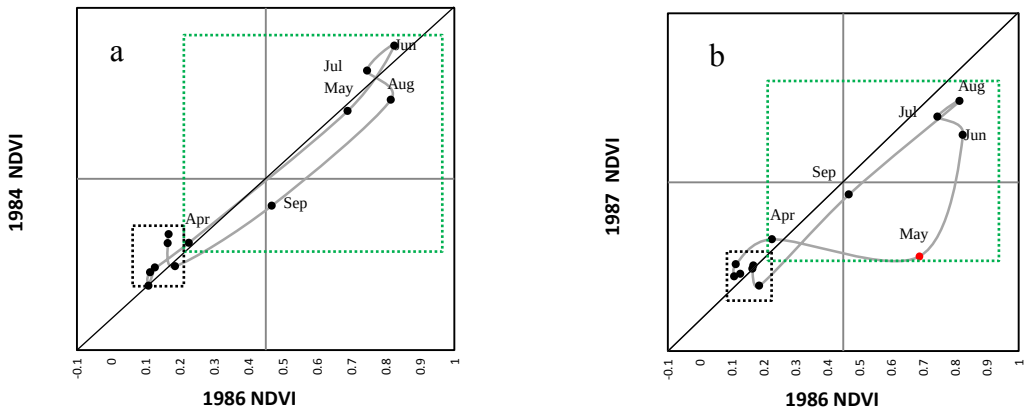

Figure 5-6 Monthly NDVI trajectories of a normal year (a) and the fire year (b). The points within the green box represent the growing season (April to October), while the points within the black box represent the snow cover season (November to March). The red point represents the month that the fire occurred

5.3.2.2 Yearly dynamics of post-fire vegetation

The entire study period (1984-2006) includes three parts: pre-fire years (1984-1986), fire event year (1987) and post-fire years (1988-2006). Figure 5-7 shows the evolution of RRI, which was calculated using NDVI differences between fire scars

and unburned control areas for the growing season average (April to October) and June (the month right after the fire in 1987) time series. Zero on the time scale represents the burn year, i.e., relative year 0 was the year of the wildfire event. Relative year -1 and +1 were years immediately before and after the fire event, respectively. In both series, there was an abrupt decrease in RRI values from 0 to -0.1 and -0.25 for the growing season average and June, respectively. Both series had low temporal variability in the pre-fire period that progressively increased in the post-fire period.

The June series RRI values decreased abruptly after the 1987 fire. This decrease was larger than for the growing season average time series. The RRI underwent a progressive increase during the first four years following the fire. Different recovery trends have been explained in relation to the species types installed and the biophysical constraints of the sites (Viedma et al., 1997). Generally, understory grass can recovery to very high RRI values within several months following a fire. Dwarf shrubs also exhibit rapid regrowth capabilities, which can reach the saturating biomass stage within a short time scale (3-5 years). Therefore, the increase in this phase was mainly the result of survived dwarf shrub and understory grass. There is a slight decrease in the relative year 5, which was mainly a consequence of post-fire logging and planning. The RRI value was less than 0 during the post-fire period. However, the recovery trend was well pronounced and the system tended to recover to pre-disturbance conditions. Figure 5-7 shows a good recovery at relative year 19 with RRI reaching zero, which indicates there was no difference between burn scar and

control plot. However, to confirm this result over a much longer period, additional observations are required.

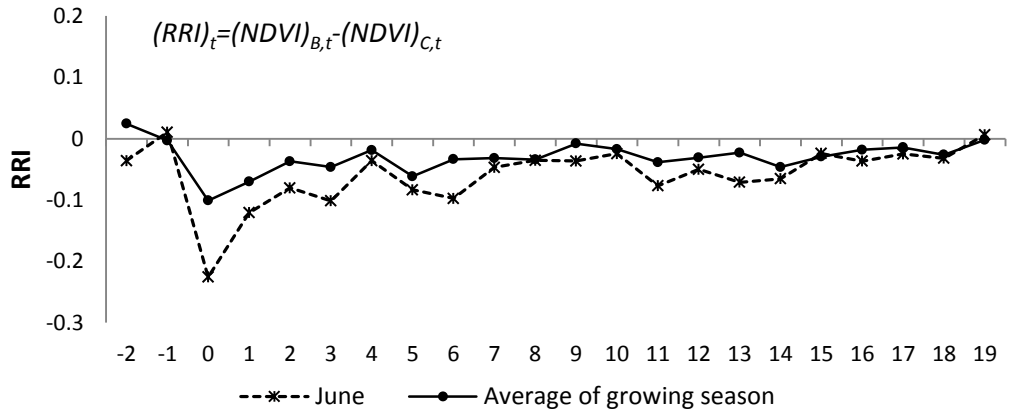

Figure 5-7 The evolution of RRI calculated using NDVI difference between fire scars and the unburned control area for the growing season average (April to October) and June (the month immediately after the fire in 1987) time series. Zero on the time scale represents the burn year, i.e., relative year 0 is the year of the wildfire event. Relative year -1 and +1 corresponds to the year before and after the fire event, respectively

5.3.3 Spatial pattern and trend analysis of post-fire stands regrowth index (SRI)

An annual stands regrowth index (SRI) series was estimated from the vegetation response after the fire. Most of the burned pixels suggest that vegetation responses follow a positive trend, increasing their annual SRI responses in subsequent years (1988-2006) after the 1987 fire event (Figure 5-8). It is evident from the figure that substantial change occurred within this region from 1988 to 2006. There was a small annual increase in SRI values during the first five years following the fire. However, there was a more robust annual increase between years 10 and 19 in the subsequent period. This change in the rate was due to intensive salvage harvesting of standing dead logs in the first two years following the fire and then coniferous trees were planted to restore the timber volume of coniferous species because lumbering was the main forest industry in this region (Li et al., 2010). Figure 5-9 presents a significance

image and degree of significance for the post-fire stands regrowth index (SRI) trend from the study area using the simple non-parametric Mann-Kendall test (single pixel-based analysis). The blue-green color shows the statistically significant positive trends. Most of the study area had significant increases in SRI, corroborating accounts of a general greening of the burned area during this period. A trend was considered statistically significant (at $P \leq 0.05$) when the Mann-Kendall (MK) statistics U was either ≥ 1.96 or ≤ -1.96 (Mann, 1945; Kendall, 1975). Therefore, the degree of significance of the post-fire stands regrowth index (SRI) trend using a non-parametric Mann-Kendall test can be divided into four categories: U<-1.96, significant downward trend; $-1.96 \leq U < 0$, downward trend, however not significant; $0 \leq U < 1.96$, upward trend, however not significant; and $1.96 \leq U$, significant upward trend (Figure 5-9 b). Table 5-3 demonstrates that all very high (VH) damage pixels had an upward trend; there was a significant upward trend (Mann-Kendal significance (U)≥ 1.96) for 18% of the pixels and a non-significant upward trend for 82% of the pixels. The results also suggest that approximately 65% and 61% of the high (H) and medium (M) fire damage pixels, respectively, underwent a non-significant upward trend. However, for the slight (S) and low (L) damage classes, this number was very low because tree planting mainly occurred in the severely burned area (approximately equal to the Medium, High and Very High fire damage areas combined). The main species planted was L. gmelinii, with a small area of P. sylvestris var. mongolica and Korean Spruce (Picea koraiensis). Therefore, the severely burned area exhibited a better recovery trend than the lightly burned regions, similar to the results of Li et al. (2010). By 1997, approximately 50% of the severely burned area had been reforested,

mostly in high accessibility areas and locations with good site conditions. In the moderately burned areas (30%–70% of trees dead), human promoted restoration was conducted with mechanical plows. However, in the lightly burned areas (less than 30% of trees dead), natural regeneration was permitted to occur (Li et al., 2010).

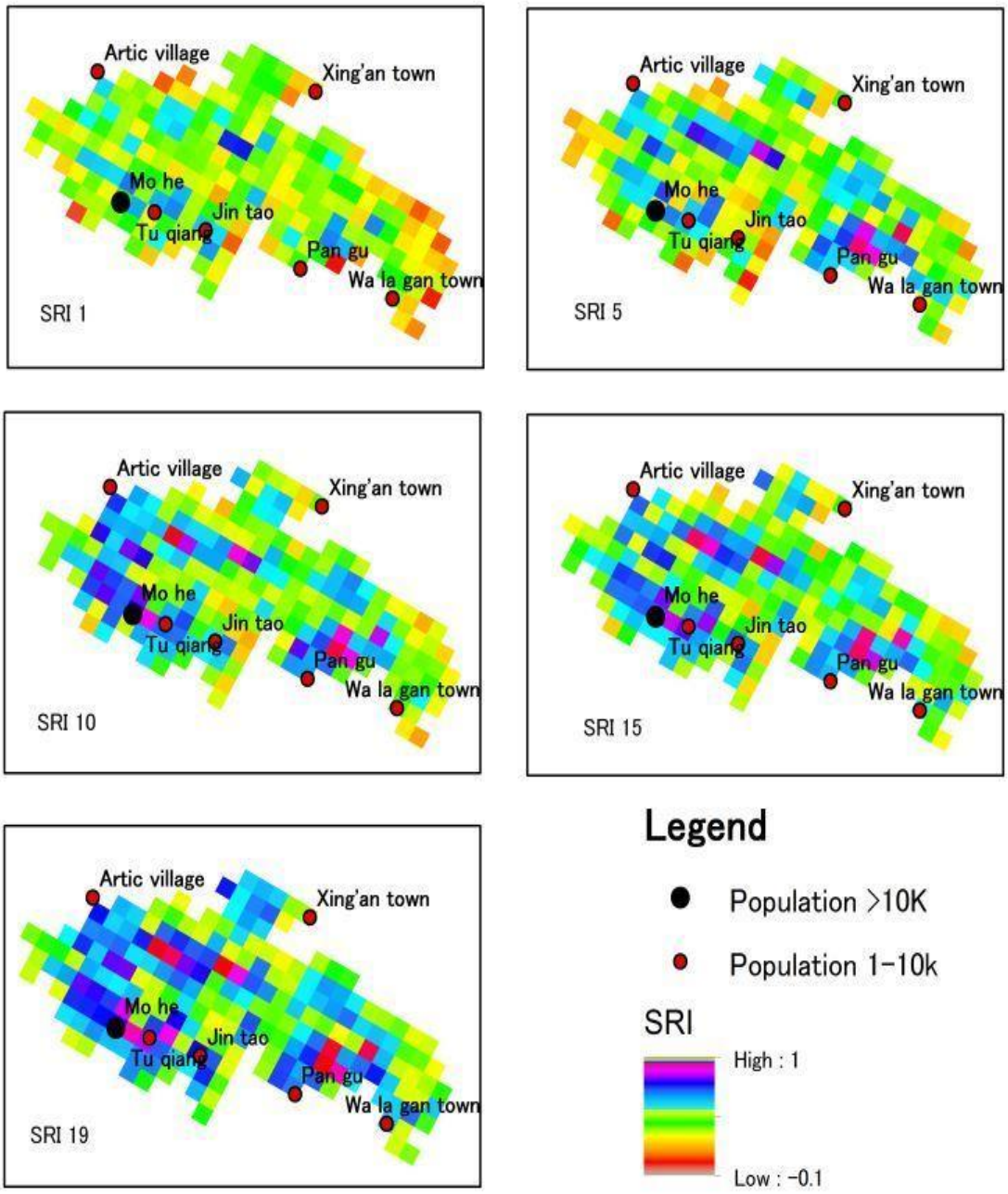

Figure 5-8 The trajectory of the post-fire stands regrowth index (SRI) for the relative year 1, 5, 10, 15 and 19

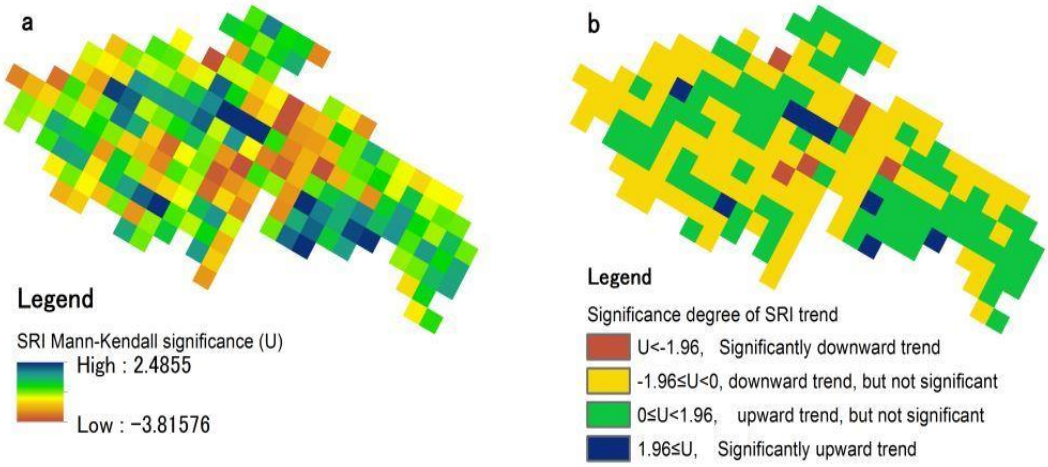

Figure 5-9 (a) The stands regrowth index (SRI) significance distribution using a non-parametric Mann-Kendall test and (b) the degree of significance degree for the post-fire stands regrowth index (SRI) trend using a non-parametric Mann-Kendall test.

Table 5-3 The degree of significance for the post-fire stands regrowth index (SRI) trends using a non-parametric Mann-Kendall test

Fire damage class		Mann-Kendal significance (U)			
		$U < -1.96$	$-1.96 \leq U < 0$	$0 \leq U < 1.96$	$1.96 \leq U$
		significant downward trend	downward trend, however not significant	upward trend, however not significant	significant upward trend
Slight	Pixel counts	0	2	3	0
(S)	Percentage(%)	0%	40%	60%	0%
Low	Pixel counts	3	33	12	1
(L)	Percentage(%)	6%	67%	24%	2%
Medium	Pixel counts	3	32	57	2
(M)	Percentage(%)	3%	34%	61%	2%
High	Pixel counts	0	13	30	3
(H)	Percentage(%)	0%	28%	65%	7%
Very high	Pixel counts	0	0	9	2
(VH)	Percentage(%)	0%	0%	82%	18%

5.3.4 Assessment against Landsat-NDVI

With higher spatial resolution than NOAA/AVHRR, enable the delineation of NDVI with a higher degree of accuracy. We attempted to assess the agreement of the GIMMS NDVI by comparing with NDVI extracted by Landsat TM/ETM+ sensors. We used Landsat TM and ETM+ data due to the relatively high spatial (30 m) and spectral resolution of the sensors. Moreover, Landsat TM data are available in the 1980s; the response of post-fire vegetation may be estimated using these data. Five 8 km × 8 km simples were acquired for the same location with GIMMS NDVI to track the detail vegetation signals in Landsat imagery (Figure 5-4). Landsat images were selected at close dates (5 June 1986, 15 June 1987, 19 June 2000 and 22 June 2004) in order to avoid the influences of phenological differences (Table 5-1 and Figure 5-10). To account for differences in the temporal resolution, GIMMS 15-day images nearest to the Landsat sample acquisition date were selected.

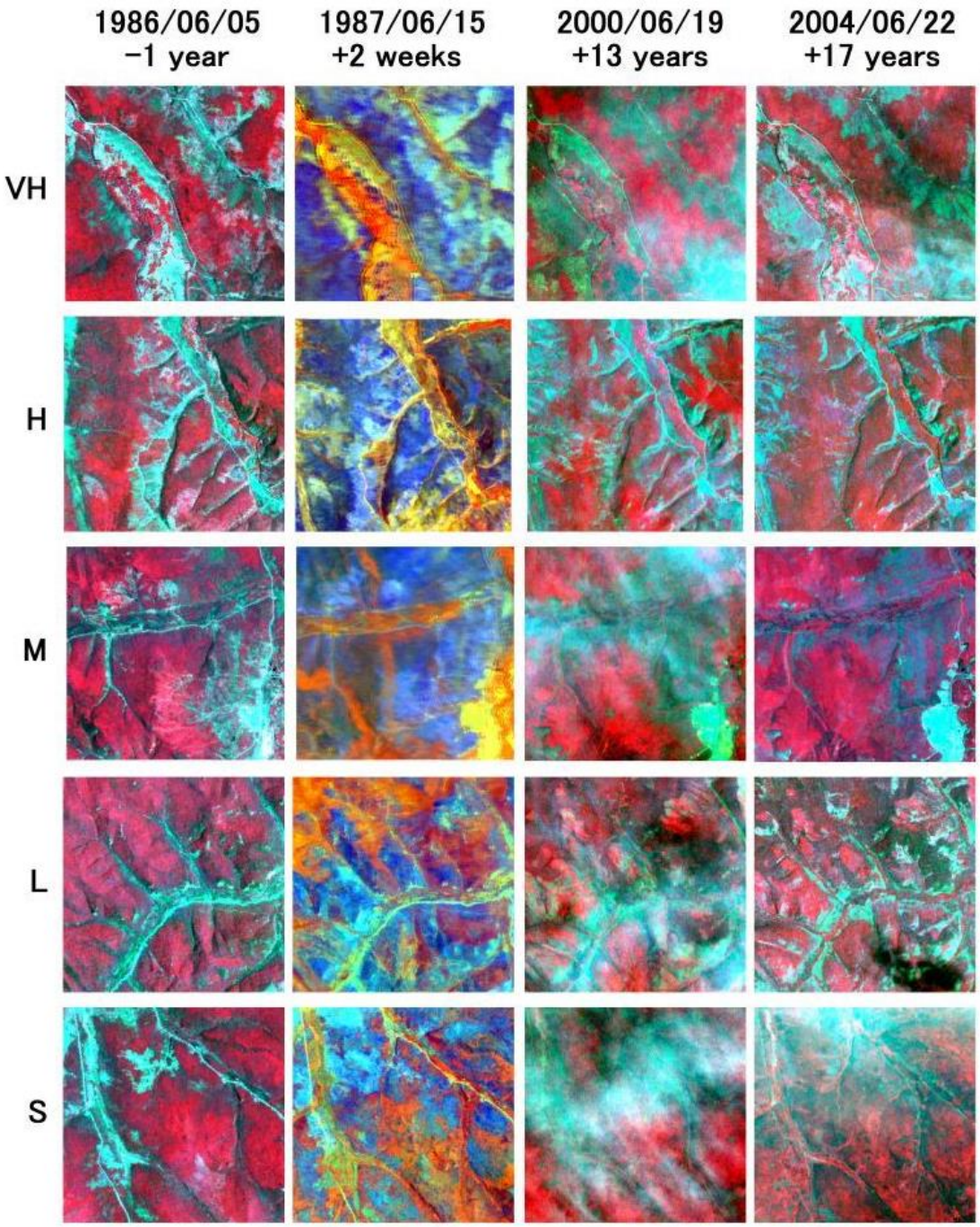

Figure 5-10 Landsat TM/ETM+ images (RGB:432) illustrating fire-caused changes on the ground vegetation. The locations of these five tracked simples can be found in Figure 5-4. Minus and plus signs represent pre-fire and post-fire period, respectively. Fire damage classes: Very High (VH); High (H); Moderate (M); Low (L); Slight (S)

Figure 5-11 shows a similar the NDVI trends of GIMMS and Landsat. GIMMS dataset appears positively biased compared to Landsat-NDVI values. Landsat-NDVI values confirm that the GIMMS dataset overestimates NDVI in this region, which is likely due to GIMMS NDVI consisting primarily of maximum acquisitions. A stronger regrowth trend of very high fire damage areas was found in both GIMMS and Landsat-NDVI. It indicates that tree planting in very high fire damage areas plays a positive role in the recovery process.

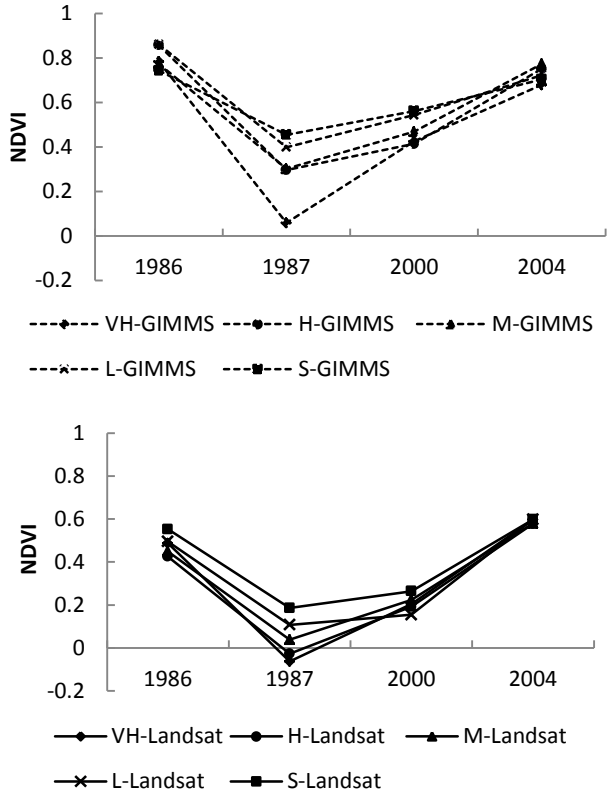

Figure 5- 11 Comparison GIMMS NDVI (up) with Landsat NDVI (down)

NDVI is an indicator of vegetation cover density and plant growth condition(Wang *et al.*, 2008a). Pixel greenness is interpreted as indicating the presence of vegetation chlorophyll. Thus, NDVI can be interpreted originally as a proxy of 'green leaf

biomass', based on experience mainly with crops, grasslands and forest. As an example of the potential usefulness of the NDVI, Tucker et al. constructed monthly greenness images for Africa in 1981 and 1982 which graphically show the advance and retreat of the tropical summer wet season and year-to-year differences in surface greenness, which they interpreted as primary production(Anyamba and Tucker, 2005; Tucker *et al.*, 2005; Fensholt *et al.*, 2006). Maxim et al. presented a simple modification to an existing empirical NDVI-based model for biomass estimation, using the ratio between the mean annual precipitation and a threshold rain level representing the transition from dwarf-shrub to shrub dominance(Shoshany and Karnibad, 2011). H. Janin et al. assessed the performance of NDVI as a proxy for plant biomass, which reinforces the idea that NDVI is most often a non-linear proxy of plant biomass(Santin-Janin *et al.*, 2009). Although, NDVI has been used to estimate vegetation biomass in many ways, it is also limited due to saturation of value in dense vegetation. Therefore, to better understand the biomass recovery in post-fire area, multiple sources remote sensing data (such as, leaf area index (LAI), GPP, NPP and SAR data) should be considered in the future study. For this study, the whole burned area was treated as a protection zone after the fire. Nobody can enter into this region without an official permission. Only helpful planting actions were taken to restore the timber volume without any other negative human disturbances during recent two decades. Thus, in this case, we believe that the NDVI signal is closely and positive correlated with forest biomass. Although, the GMMIS resolution is not high, the temporal trend of stands regrowth index (SRI) also can reflect the long-term vegetation response after the fire (Figure 5-8 and 5-9).

5.4 CONCLUSION

This paper described the long-term effects on vegetation of a catastrophic fire on the northern Great Xing'an Mountain in 1987 that were observed using a nonparametric Mann-Kendall (MK) statistics method and analyzing the AVHRR GIMMS 15-day composite NDVI dataset. Both temporal and spatial characteristics were analyzed under natural regeneration and tree planting scenarios from 1984 to 2006.

Regressing post-fire NDVI values on pre-fire values helped identify the NDVI for completely burned pixels in vegetation stands; this value was subsequently used in an index to quantify stand differences in fire damage. October was established as a better month compared with the other months to distinguish the post- and pre-fire vegetation conditions using NDVI signals because grasses and shrubs lose their colored leaves, while the leaves on healthy trees remain green. The Mann-Kendall (MK) statistics method is capable of detecting vegetation trends in relatively long time series. Normally, high fire damage area performs a slower and even harder regrowth progress than medium burned area under natural recovery conditions without tree planting. However, because tree planting primarily occurred in the severely burned areas (approximately equal to the Medium, High and Very High fire damage areas combined), this region exhibited a better recovery trend than the lightly burned locations (Table 5-3). Reasonable tree planting can substantially quicken the recovery process and shorten the restoration time of target species. We believe that it is necessary to incorporate information about spatial patterns of plantation into planting strategies. This research involves a large area (1.33×10^6 ha) and a long time span

(1984 – 2006). Therefore, it is unfeasible to perform real field validation for such a study. More detailed satellite analyses and field data are required in the future for a more convincing validation of the results.

Chapter 6. Summary and conclusions

In both global and regional scale, biomass burning events have a devastating impact on limited forest resources and atmospheric quality. As such, understanding the effects of wildfire on the environment is one of my research interests. I combine some unique methods and techniques such as quantitative analyses (e.g., time series analysis, statistical and geophysical methods) of observational and remote sensing data (e.g., MODIS, LANDSAT, NOAA-AVHRR) with physical modeling of fire-vegetation processes. I will use satellite and GIS data, in situ burned area observations information to understand fire-induced vegetation processes and interactions of fire-climate systems, and to improve our model capability to predict fire risk and to assess fire impacts and consequence on our environment, currently, and in the future.

The objective of this study was to identify spatial and temporal patterns of burned area china; to map the fire risk and danger in the northeast of China by combining remote sensing data and meteorological data; to estimate the potential range and spatial-temporal patterns of biomass burning emissions in the Great Xing'an Mountain area; To be specific, I will assess the fire damage of the entire fire-affected areas in the Great Xing'an Mountains from the 1987 fire event, (ii) to better understand how vegetation responds to fire disturbances by analyzing intra- and inter-annual variability in satellite observations and (iii) to characterize the spatial pattern of post-fire vegetation trends using the AVHRR GIMMS NDVI record over the period 1986-2006.

Chapter 2 presented a national analysis of fire characteristics by combining National historic record (1950-2010) and a set a metrics derived from Earth

observation sensors (Terra MODIS) (2000-2010). Our study is the first to consider the larger picture of open fire for the entire China, analyzing fire spatial pattern and temporal trend from nine sub-regions whose territories span a diverse array of ecosystems. In order to analyze the spatial variations of fire, we divided the entire China region into 9 sub-regions: a, northeast china; b, inner Mongolia; c, northwest china; d, north china; e, central china; f, south china; g, southwest china; h, Tibetan plateau; i, southeast china (Figure 2-8).This scale is commensurate with that of some important climate variations and still allows us to make comparisons across diverse ecosystems. While the spatial patterns of fire occurrence have been previously described, this paper has emphasized the importance of characterizing fire activity by considering fire season duration and the extent of acre burned as well. An analysis of the fire products showed that, during the period 2001–20012, an average of 3.2×10^6ha (32,000 km^2) $yr^{-1}$of fire occurred in China.

In addition, we have identified several regional climate characteristic that help to explain the spatial distribution and fire season duration of those fire groups, most remarkably the extent of the dry–warm season, which affects primarily fire density and seasonality. The majority of its fires occur in northeast China and in the southwest provinces. Southwest China is characterized by many small fires and more casualties but the northeast has fewer and larger fires and more serious damage. The inter- and intra-annual fire trends and variations of nine sub-regions were reported by analyzing regional climate characteristics. Monthly meteorological data at 130 stations in China were used to over a 50-year period (1952-2013). The monthly burned area profiles of each sub-regions exhibit a distinctive seasonality. Spring and autumn are two peak

fire seasons in every year for the entire of China. Fire season duration and fire severity are close related to modes of regional climate variability in Northeast, Southwest and Inner Mongolia China. Crop residues burning play an important role in in southeast and north China, especially concentrated in the middle and lower Yangtze River and North China plains. Therefore, the fire activities are dominantly governed by agricultural activities, with less affected by regional climate in southeast and north China.

Future efforts should be addressed to explore spatial variations of specific fire metrics, and analyze relations between human and biophysical variables at regional scales. Additionally, an work should be made to analyze the different ecological and social implications of the different fire groups.

Chapter 3 developed a Fire Disturbance Index (FDI) algorithm to capture long-term variations in the ratio of Land Surface Temperature (LST) and Enhanced Vegetation Index (EVI) on a pixel-by-pixel basis. There is a dramatic difference of the LST-EVI relationship between pre-fire and post-fire in the fire case occurred in 2003. The algorithm was tested by Moderate Resolution Imaging Spectroradiometer (MODIS) fire product data explore continuous spatiotemporal patterns of fire disturbance. The findings suggest that FDI can be used to detect the burned pixels but often overestimates the fire affected area with large amount of noise. The fire disturbance spatial and temporal patterns are also analyzed with meterological parameters in Northeast China. The climate scenario in Northeast china with great spatial differences from the Changbai mountain to the Great Xing'an Mountain. The climate in Changbai Mountain belongs to temperate continental monsoon climate with total

annual precipitation of 600mm to 1000mm. It is wetter than other region in Northeast china, therefore, there is no larger fire even though amount of forests in Changbai Mountain. While the climate in Great Xing'an Mountain belongs to cold temperate continental monsoon climate with low precipitation less than 400mm and strong wind in spring and autumn. Therefore, fire regime is characterized by large and frequent forest fires in Great Xing'an Mountain. The peak of the fire season occurs during the relative drier seasons in spring and autumn of the climatological annual cycle in Northeast region.

Chapter 4 improved strategies that optimize input information by combining explicit spatio-temporal remote-sensing data with models to obtain reliable emissions information. Biomass burning emissions in boreal region yield an important contribution to the chemical budget of the troposphere. To assess the contribution of biomass burning to the emissions of atmospheric trace species in the Great Xing'an Mountain (GXM), which is the most severe fire-prone area in China, we estimated various biomass burning activities by combining explicit spatio-temporal remote sensing data with models. We derived 9998 fire scars with a total 4,6096 km^2 in Great Xing'an Mountain between the year of 1986 and 2010. The year of 1987 and 2003 contributes 33.2% and 22.9% in burned area during the 25 years, respectively. Fire activity is strongest in May. Most of large fires occurred north region of Great Xing'an Mountain between 50ºN and 54ºN latitude due to much drier weather and higher fire danger in north than the south part. Evergreen and deciduous needleaf forest and Deciduous broadleaf forest are main sources of emissions, accounting for 84%, 87%, 84%, 88%, 90%, 74%, 91% and 96% of the total annual CO_2, CH_4, CO,

PM_{10}, $PM_{2.5}$, NOx, NH_3, SO_2 and BC emissions, respectively. Fire emissions from Shrubland, Grassland and Cropland only account for a small fraction of total level (approximately 4%-11%). Comparisons of our results with other published estimates of biomass burning emissions show reasonable agreement, but substantial uncertainties remain in the modelling parameters. Variability in emission factors contributed more to the un-certainty. There is an urgent need to obtain more accurate biomass burning estimates because of its considerable contribution to the regional and global carbon balance and the atmosphere.

Chapter 5 described the long-term effects on vegetation of a catastrophic fire on the northern Great Xing'an Mountain in 1987 that were observed using a nonparametric Mann-Kendall (MK) statistics method and analyzing the AVHRR GIMMS 15-day composite NDVI dataset. Both temporal and spatial characteristics were analyzed under natural regeneration and tree planting scenarios from 1984 to 2006.

Regressing post-fire NDVI values on pre-fire values helped identify the NDVI for completely burned pixels in vegetation stands; this value was subsequently used in an index to quantify stand differences in fire damage. October was established as a relatively better month compared with the other months to distinguish the post- and pre-fire vegetation conditions using NDVI signals because grasses and shrubs lose their colored leaves, while the leaves on healthy trees remain green. The Mann-Kendall (MK) statistics method is capable of detecting vegetation trends in relatively long time series. Because tree planting primarily occurred in the severely burned areas (approximately equal to the Medium, High and Very High fire damage areas combined), this region exhibited a better recovery trend than the lightly burned

locations. Reasonable tree planting can substantially quicken the recovery process and shorten the restoration time of target species. This research involves a large area and long time span (1984-2006). Therefore, it is unfeasible to perform real field validation for such a study. More detailed satellite analyses and field data are required in the future for a more convincing validation of the results.

Reference

1. Aldersley, A., Murray, S.J., Cornell, S.E., 2011. Global and regional analysis of climate and human drivers of wildfire. Science of The Total Environment 409, 3472-3481.

2. Anaya, J.A., Chuvieco, E., Palacios-Orueta, A., 2009. Aboveground biomass assessment in Colombia: A remote sensing approach. Forest Ecology and Management 257, 1237-1246.

3. Andreae, M.O., Merlet, P., 2001. Emission of trace gases and aerosols from biomass burning. Global Biogeochemical Cycles 15, 955-966.

4. Anyamba, A., Tucker, C.J., 2005. Analysis of Sahelian vegetation dynamics using NOAA-AVHRR NDVI data from 1981-2003. Journal of Arid Environments 63, 596-614.

5. Ardizzone, S., Doldo, P., Ranzi, T., Sturniolo, G.C., Giglio, L.A., Annese, V., D'Arienzo, A., Gaia, E., Gullini, S., Riegler, G., Valentini, M., Massa, P., Del Piano, M., Rossini, F., Guidetti, C.S., Pera, A., Greinwald, R., Porro, G.B., Grp, S.-S., 1999. Mesalazine foam (Salofalk (R) foam) in the treatment of active distal ulcerative colitis. A comparative trial vs Salofalk (R) enema. Ital J Gastroenterol 31, 677-684.

6. Balzter, H., Gonzalez, M.C., Gerard, F., Ria, x00F, o, D., 2007. Post-fire vegetation phenology in Siberian burn scars. Geoscience and Remote Sensing Symposium, 2007. IGARSS 2007. IEEE International, pp. 4652-4655.

7. Bastos, A., Gouveia, C.M., DaCamara, C.C., Trigo, R.M., 2011. Modelling post-fire vegetation recovery in Portugal. Biogeosciences 8, 3593-3607.

8. Beck, P.S.A., Goetz, S.J., Mack, M.C., Alexander, H.D., Jin, Y., Randerson, J.T., Loranty, M.M., 2011. The impacts and implications of an intensifying fire regime on Alaskan boreal forest composition and albedo. Global Change Biology 17, 2853-2866.

9. Borak, J.S., Lambin, E.F., Strahler, A.H., 2000. The use of temporal metrics for land cover change detection at coarse spatial scales. International Journal of Remote Sensing 21, 1415-1432.

10. Brewer, N.W., Smith, A.M.S., Hatten, J.A., Higuera, P.E., Hudak, A.T., Ottmar, R.D., Tinkham, W.T., 2013. Fuel moisture influences on fire-altered carbon in masticated fuels: An experimental study. J Geophys Res-Biogeo 118, 30-40.

11. Cahoon, D.R., Stocks, B.J., Levine, J.S., Cofer, W.R., Pierson, J.M., 1994. Satellite analysis of the severe 1987 forest fires in northern China and

southeastern Siberia. Journal of Geophysical Research: Atmospheres (1984–2012) 99, 18627-18638.

12. Cao, G.L., Zhang, X.Y., Wang, Y.Q., Zheng, F.C., 2008. Estimation of emissions from field burning of crop straw in China. Chinese Sci Bull 53, 784-790.

13. Carlson, T.N., Gillies, R.R., Schmugge, T.J., 1995. An Interpretation of Methodologies for Indirect Measurement of Soil-Water Content. Agricultural and Forest Meteorology 77, 191-205.

14. Chen, H., Hu, Y., Chang, Y., Bu, R., Li, Y., Liu, M., 2011. Simulating impact of larch caterpillar (Dendrolimus superans) on fire regime and forest landscape in Da Hinggan Mountains, Northeast China. Chinese Geographical Science 21, 575-586.

15. Cheng, T.T., Han, Z.W., Zhang, R.J., Du, H.H., Jia, X.A., Wang, J.J., Yao, J.Y., 2010. Black carbon in a continental semi-arid area of Northeast China and its possible sources of fire emission. J Geophys Res-Atmos 115.

16. Chuvieco, E., Giglio, L., Justice, C., 2008. Global characterization of fire activity: toward defining fire regimes from Earth observation data. Global Change Biology 14, 1488-1502.

17. Chuvieco, E., Riano, D., Aguado, I., Cocero, D., 2002. Estimation of fuel moisture content from multitemporal analysis of Landsat Thematic Mapper reflectance data: applications in fire danger assessment. International Journal of Remote Sensing 23, 2145-2162.

18. Coops, N.C., Wulder, M.A., Iwanicka, D., 2009. Large area monitoring with a MODIS-based Disturbance Index (DI) sensitive to annual and seasonal variations. Remote Sensing of Environment 113, 1250-1261.

19. Crimmins, M.A., 2004. Wildfire and climate interactions across the Southwest United States. The University of Arizona, United States -- Arizona, pp. 129-129 p.

20. Cuevas-GonzÁLez, M., Gerard, F., Balzter, H., RiaÑO, D., 2009. Analysing forest recovery after wildfire disturbance in boreal Siberia using remotely sensed vegetation indices. Global Change Biology 15, 561-577.

21. Diaz-Delgado, R., Lloret, F., Pons, X., Terradas, J., 2002. Satellite evidence of decreasing resilience in Mediterranean plant communities after recurrent wildfires. Ecology 83, 2293-2303.

22. Eck, T.F., Holben, B.N., Ward, D.E., Dubovik, O., Reid, J.S., Smirnov, A., Mukelabai, M.M., Hsu, N.C., O'Neill, N.T., Slutsker, I., 2001. Characterization of the optical properties of biomass burning aerosols in Zambia during the 1997 ZIBBEE field campaign. J Geophys Res-Atmos 106, 3425-3448.

23. Fang, J., Chen, A., Peng, C., Zhao, S., Ci, L., 2001. Changes in forest biomass carbon storage in China between 1949 and 1998. Science 292, 2320-2322.

24. FAO, 2006. world fire management global assessment. FAO Forestry Paper.

25. Fensholt, R., Sandholt, I., Stisen, S., Tucker, C., 2006. Analysing NDVI for the African continent using the geostationary meteosat second generation SEVIRI sensor. Remote Sensing of Environment 101, 212-229.

26. Floyd, M.L., Hanna, D., Romme, W.H., Crews, T.E., 2006. Predicting and mitigating weed invasions to restore natural post-fire succession in Mesa Verde National Park, Colorado, USA. International Journal of Wildland Fire 15, 247-259.

27. Frey, K.E., Smith, L.C., 2005. Amplified carbon release from vast West Siberian peatlands by 2100. Geophysical Research Letters 32.

28. Gabban, A., San‐Miguel‐Ayanz, J., Viegas, D.X., 2008. A comparative analysis of the use of NOAA‐AVHRR NDVI and FWI data for forest fire risk assessment. International Journal of Remote Sensing 29, 5677-5687.

29. Galtié, J.-F., 2006. Remotely based fuels water content assessment applied to operational fire risk prevision: Requirements, situation and perspectives. Forest Ecology and Management 234, Supplement, S35.

30. Giglio, L., Csiszar, I., Justice, C.O., 2006. Global distribution and seasonality of active fires as observed with the Terra and Aqua Moderate Resolution Imaging Spectroradiometer (MODIS) sensors. Journal of Geophysical Research 111.

31. Giglio, L., Loboda, T., Roy, D.P., Quayle, B., Justice, C.O., 2009. An active-fire based burned area mapping algorithm for the MODIS sensor. Remote Sensing of Environment 113, 408-420.

32. Gillies, R.R., Carlson, T.N., 1995. Thermal Remote-Sensing of Surface Soil-Water Content with Partial Vegetation Cover for Incorporation into Climate-Models. J Appl Meteorol 34, 745-756.

33. Gillies, R.R., Carlson, T.N., Cui, J., Kustas, W.P., Humes, K.S., 1997. A verification of the 'triangle' method for obtaining surface soil water content and energy fluxes from remote measurements of the Normalized Difference Vegetation Index (NDVI) and surface radiant temperature. International Journal of Remote Sensing 18, 3145-3166.

34. Girardin, M.P., Ali, A.A., Carcaillet, C., Gauthier, S., Hély, C., Le Goff, H., Terrier, A., Bergeron, Y., Fire in managed forests of eastern Canada: Risks and options. Forest Ecology and Management.

35. Goetz, S.J., Fiske, G.J., Bunn, A.G., 2006. Using satellite time-series data sets to analyze fire disturbance and forest recovery across Canada. Remote Sensing of Environment 101, 352-365.

36. Gottschalck, J.C., Gillies, R.R., Carlson, T.N., 2001. The simulation of canopy transpiration under doubled CO2: The evidence and impact of feedbacks on transpiration in two 1-D soil-vegetation-atmosphere-transfer models. Agricultural and Forest Meteorology 106, 1-21.

37. Gouveia, C., DaCamara, C.C., Trigo, R.M., 2010. Post-fire vegetation recovery in Portugal based ¥newline on spot/vegetation data. Nat Hazard Earth Sys 10, 673-684.

38. Han, Y., Wang, Y., Zhao, Y., 2010. Estimating Soil Moisture Conditions of the Greater Changbai Mountains by Land Surface Temperature and NDVI. Ieee T Geosci Remote 48, 2509-2515.

39. Hansen, M., DeFries, R., Townshend, J.R., Sohlberg, R., 2000. Global land cover classification at 1 km spatial resolution using a classification tree approach. International Journal of Remote Sensing 21, 1331-1364.

40. Hasanbeigi, A., Morrow, W., Masanet, E., Sathaye, J., Xu, T.F., 2013. Energy efficiency improvement and CO2 emission reduction opportunities in the cement industry in China. Energ Policy 57, 287-297.

41. Hoelzemann, J.J., 2004. Global Wildland Fire Emission Model (GWEM): Evaluating the use of global area burnt satellite data. Journal of Geophysical Research 109.

42. Hope, A., Albers, N., Bart, R., 2012. Characterizing post-fire recovery of fynbos vegetation in the Western Cape Region of South Africa using MODIS data. International Journal of Remote Sensing 33, 979-999.

43. Huang, X., Li, M.M., Friedli, H.R., Song, Y., Chang, D., Zhu, L., 2011. Mercury Emissions from Biomass Burning in China. Environmental science & technology 45, 9442-9448.

44. Ito, A., Penner, J.E., 2004. Global estimates of biomass burning emissions based on satellite imagery for the year 2000. J Geophys Res-Atmos 109.

45. Jacobson, L.V., Hacon, S., Ignotti, E., Castio, H., Artaxo, P., de Leon, A.P., 2009. Effects of Air Pollution from Biomass Burning in Amazon: A Panel Study of Schoolchildren. Epidemiology 20, S90-S90.

46. Julien, Y., Sobrino, J.A., Verhoef, W., 2006. Changes in land surface temperatures and NDVI values over Europe between 1982 and 1999. Remote Sensing of Environment 103, 43-55.

47. Justice, C.O., Giglio, L., Korontzi, S., Owens, J., Morisette, J.T., Roy, D., Descloitres, J., Alleaume, S., Petitcolin, F., Kaufman, Y., 2002. The MODIS fire products. Remote Sensing of Environment 83, 244-262.

48. Justice, C.O., Vermote, E., Townshend, J.R.G., Defries, R., Roy, D.P., Hall, D.K., Salomonson, V.V., Privette, J.L., Riggs, G., Strahler, A., Lucht, W., Myneni, R.B., Knyazikhin, Y., Running, S.W., Nemani, R.R., Wan, Z.M., Huete, A.R., van Leeuwen, W., Wolfe, R.E., Giglio, L., Muller, J.P., Lewis, P., Barnsley, M.J., 1998. The Moderate Resolution Imaging Spectroradiometer (MODIS): Land remote sensing for global change research. Ieee T Geosci Remote 36, 1228-1249.

49. Kang, S., Kimball, J.S., Running, S.W., 2006. Simulating effects of fire disturbance and climate change on boreal forest productivity and evapotranspiration. The Science of the total environment 362, 85-102.

50. Karnieli, A., Agam, N., Pinker, R.T., Anderson, M., Imhoff, M.L., Gutman, G.G., Panov, N., Goldberg, A., 2010. Use of NDVI and Land Surface Temperature for Drought Assessment: Merits and Limitations. Journal of Climate 23, 618-633.

51. Kendall, M.G., 1975. Rank correlation methods.

52. Kennedy, R.E., Yang, Z., Cohen, W.B., Pfaff, E., Braaten, J., Nelson, P., 2012. Spatial and temporal patterns of forest disturbance and regrowth within the area of the Northwest Forest Plan. Remote Sensing of Environment.

53. Keywood, M., Kanakidou, M., Stohl, A., Dentener, F., Grassi, G., Meyer, C.P., Torseth, K., Edwards, D., Thompson, A.M., Lohmann, U., Burrows, J., 2013. Fire in the Air: Biomass Burning Impacts in a Changing Climate. Critical Reviews in Environmental Science and Technology 43, 40-83.

54. Knox, K.J.E., Clarke, P.J., 2012. Fire severity, feedback effects and resilience to alternative community states in forest assemblages. Forest Ecology and Management 265, 47-54.

55. Kurz, W.A., Stinson, G., Rampley, G.J., Dymond, C.C., Neilson, E.T., 2008. Risk of natural disturbances makes future contribution of Canada's forests to the global carbon cycle highly uncerain. P Natl Acad Sci USA 105, 1551-1555.

56. Lambin, E.F., Ehrlich, D., 1995. COMBINING VEGETATION INDEXES AND SURFACE-TEMPERATURE FOR LAND-COVER MAPPING AT BROAD SPATIAL SCALES. International Journal of Remote Sensing 16, 573-579.

57. Lambin, E.F., Ehrlich, D., 1996. The surface temperature-vegetation index space for land cover and land-cover change analysis. International Journal of Remote Sensing 17, 463-487.

58. Lampainen, J., Kuuluvainen, T., Wallenius, T.H., Karjalainen, L., Vanha-Majamaa,

I., 2004. Long-term forest structure and regeneration after wildfire in Russian Karelia. Journal of Vegetation Science 15, 245-256.

59. Lee, S.-W., Lee, M.-B., Lee, Y.-G., Won, M.-S., Kim, J.-J., Hong, S.-k., 2009. Relationship between landscape structure and burn severity at the landscape and class levels in Samchuck, South Korea. Forest Ecology and Management 258, 1594-1604.

60. Leon, J.R.R., van Leeuwen, W.J.D., Casady, G.M., 2012. Using MODIS-NDVI for the Modeling of Post-Wildfire Vegetation Response as a Function of Environmental Conditions and Pre-Fire Restoration Treatments. Remote Sensing 4, 598-621.

61. Levine, J.S., Cofer, W.R., Cahoon, D.R., Winstead, E.L., 1995. Biomass Burning - a Driver for Global Change. Environmental science & technology 29, A120-A125.

62. Li, X., He, H., Wang, X., Xie, F., Hu, Y., Li, Y., 2010. Tree planting: How fast can it accelerate post-fire forest restoration? — A case study in Northern Da Hinggan Mountains, China. Chinese Geographical Science 20, 481-490.

63. Li, X., He, H.S., Wu, Z., Liang, Y., Schneiderman, J.E., 2013. Comparing Effects of Climate Warming, Fire, and Timber Harvesting on a Boreal Forest Landscape in Northeastern China. PloS one 8.

64. Liang, L., Li, L., Liu, Q., 2011. Precipitation variability in Northeast China from 1961 to 2008. Journal of Hydrology 404, 67-76.

65. Lin, y., Wang, l., 2007. Typical cases of forest fire in China from 1953 to 2005. Chinese Forestry Press

66. Liu, Y., L. Goodrick, S., A. Stanturf, J., Future U.S. wildfire potential trends projected using a dynamically downscaled climate change scenario. Forest Ecology and Management.

67. Liu, Z., Yang, J., Chang, Y., Weisberg, P.J., He, H.S., 2012. Spatial patterns and drivers of fire occurrence and its future trend under climate change in a boreal forest of Northeast China. Global Change Biology 18, 2041-2056.

68. Lu, A.F., Tian, H.Q., Liu, M.L., Liu, J.Y., Melillo, J.M., 2006. Spatial and temporal patterns of carbon emissions from forest fires in China from 1950 to 2000. J Geophys Res-Atmos 111.

69. Lyons, E.A., Jin, Y., Randerson, J.T., 2008. Changes in surface albedo after fire in boreal forest ecosystems of interior Alaska assessed using MODIS satellite observations. Journal of Geophysical Research: Biogeosciences 113, G02012.

70. Mann, H.B., 1945. Nonparametric tests against trend. Econometrica: Journal of the Econometric Society, 245-259.

71. Marshall, S., Taylor, J.A., Oglesby, R.J., Larson, J.W., Erickson, D.J., 1996. Climatic effects of biomass burning. Environ Softw 11, 53-58.

72. Matthews, S., Sullivan, A., Gould, J., Hurley, R., Ellis, P., Larmour, J., 2012. Field evaluation of two image-based wildland fire detection systems. Fire Safety Journal 47, 54-61.

73. Mildrexler, D.J., Zhao, M., Running, S.W., 2009. Testing a MODIS Global Disturbance Index across North America. Remote Sensing of Environment 113, 2103-2117.

74. Mildrexler, D.J., Zhao, M.S., Heinsch, F.A., Running, S.W., 2007. A new satellite-based methodology for continental-scale disturbance detection. Ecol Appl 17, 235-250.

75. Neeti, N., Eastman, J.R., 2011. A Contextual Mann‐Kendall Approach for the Assessment of Trend Significance in Image Time Series. Transactions in GIS 15, 599-611.

76. Nemani, R., Pierce, L., Running, S., Goward, S., 1993. Developing Satellite-Derived Estimates of Surface Moisture Status. J Appl Meteorol 32, 548-557.

77. Nemani, R.R., Running, S.W., 1989. Estimation of Regional Surface-Resistance to Evapotranspiration from Ndvi and Thermal-Ir Avhrr Data. J Appl Meteorol 28, 276-284.

78. Nielsen, E.M., Prince, S.D., Koeln, G.T., 2008. Wetland change mapping for the US mid-Atlantic region using an outlier detection technique. Remote Sensing of Environment 112, 4061-4074.

79. Nishida, K., Nemani, R.R., Glassy, J.M., Running, S.W., 2003. Development of an evapotranspiration index from aqua/MODIS for monitoring surface moisture status. Ieee T Geosci Remote 41, 493-501.

80. Oberheitmann, A., 2010. A new post-Kyoto climate regime based on per-capita cumulative CO2-emission rights-rationale, architecture and quantitative assessment of the implication for the CO2-emissions from China, India and the Annex-I countries by 2050. Mitig Adapt Strat Gl 15, 137-168.

81. Oberheitmann, A., 2012. CO2-emission reduction in China's residential building sector and contribution to the national climate change mitigation targets in 2020. Mitig Adapt Strat Gl 17, 769-791.

82. Owen, T.W., Carlson, T.N., Gillies, R.R., 1998. An assessment of satellite

remotely-sensed land cover parameters in quantitatively describing the climatic effect of urbanization. International Journal of Remote Sensing 19, 1663-1681.

83. Palacios-Orueta, A., Chuvieco, E., Parra, A., Carmona-Moreno, C., 2005. Biomass Burning Emissions: A Review of Models Using Remote-Sensing Data. Environmental monitoring and assessment 104, 189-209.

84. Parsons, A., 2003. Burned Area Emergency Rehabilitation (BAER) soil burn severity definitions and mapping guidelines Draft. USDA Forest Service, Rocky Mountain Research Station, Missoula.

85. Pausas, J.G., Bradstock, R.A., Keith, D.A., Keeley, J.E., Network, G.F., 2004. Plant functional traits in relation to fire in crown-fire ecosystems. Ecology 85, 1085-1100.

86. Peckham, S.D., Ahl, D.E., Serbin, S.P., Gower, S.T., 2008. Fire-induced changes in green-up and leaf maturity of the Canadian boreal forest. Remote Sensing of Environment 112, 3594-3603.

87. Pouliot, D., Latifovic, R., Olthof, I., 2009. Trends in vegetation NDVI from 1km AVHRR data over Canada for the period 1985-2006. International Journal of Remote Sensing 30, 149-168.

88. Prasad, V.K., Kant, Y., Gupta, P.K., Elvidge, C., Badarinath, K.V.S., 2002. Biomass burning and related trace gas emissions from tropical dry deciduous forests of India: A study using DMSP-OLS data and ground-based measurements. International Journal of Remote Sensing 23, 2837-2851.

89. PRC, S.F.A.o., 2000. china forest fire report 2000

90. Qin, Y., Xie, S.D., 2011. Historical estimation of carbonaceous aerosol emissions from biomass open burning in China for the period 1990-2005. Environ Pollut 159, 3316-3323.

91. Quarmby, N.A., Milnes, M., Hindle, T.L., Silleos, N., 1993. The Use of Multitemporal Ndvi Measurements from Avhrr Data for Crop Yield Estimation and Prediction. International Journal of Remote Sensing 14, 199-210.

92. Raffa, K.F., Aukema, B.H., Bentz, B.J., Carroll, A.L., Hicke, J.A., Turner, M.G., Romme, W.H., 2008. Cross-scale drivers of natural disturbances prone to anthropogenic amplification: The dynamics of bark beetle eruptions. Bioscience 58, 501-517.

93. Randerson, J.T., Chen, Y., van der Werf, G.R., Rogers, B.M., Morton, D.C., 2012. Global burned area and biomass burning emissions from small fires. J Geophys Res-Biogeo 117.

94. Randerson, J.T., Liu, H., Flanner, M.G., Chambers, S.D., Jin, Y., Hess, P.G., Pfister, G., Mack, M.C., Treseder, K.K., Welp, L.R., Chapin, F.S., Harden, J.W., Goulden, M.L., Lyons, E., Neff, J.C., Schuur, E.A., Zender, C.S., 2006. The impact of boreal forest fire on climate warming. Science 314, 1130-1132.

95. Renkin, R.A., Despain, D.G., 1992. Fuel Moisture, Forest Type, and Lightning-Caused Fire in Yellowstone-National-Park. Can J Forest Res 22, 37-45.

96. Roy, D.P., Boschetti, L., Justice, C.O., Ju, J., 2008. The collection 5 MODIS burned area product — Global evaluation by comparison with the MODIS active fire product. Remote Sensing of Environment 112, 3690-3707.

97. Roy, D.P., Jin, Y., Lewis, P.E., Justice, C.O., 2005. Prototyping a global algorithm for systematic fire-affected area mapping using MODIS time series data. Remote Sensing of Environment 97, 137-162.

98. Santin-Janin, H., Garel, M., Chapuis, J.L., Pontier, D., 2009. Assessing the performance of NDVI as a proxy for plant biomass using non-linear models: a case study on the Kerguelen archipelago. Polar Biology 32, 861-871.

99. Schelhaas, M.-J., Nabuurs, G.-J., Schuck, A., 2003. Natural disturbances in the European forests in the 19th and 20th centuries. Global Change Biology 9, 1620-1633.

100. Schmiegelow, F.K.A., Stepnisky, D.P., Stambaugh, C.A., Koivula, M., 2006. Reconciling Salvage Logging of Boreal Forests with a Natural-Disturbance Management Model
101. Reconciliación de la Cosecha de Salvamento de Bosques Boreales con un Modelo de Gestión de Perturbación Natural. Conserv Biol 20, 971-983.

102. Segah, H., Tani, H., Hirano, T., 2010. Detection of fire impact and vegetation recovery over tropical peat swamp forest by satellite data and ground-based NDVI instrument. International Journal of Remote Sensing 31, 5297-5314.

103. Sheng, Y.W., Smith, L.C., MacDonald, G.M., Kremenetski, K.V., Frey, K.E., Velichko, A.A., Lee, M., Beilman, D.W., Dubinin, P., 2004. A high-resolution GIS-based inventory of the west Siberian peat carbon pool. Global Biogeochemical Cycles 18.

104. Shoshany, M., Karnibad, L., 2011. Mapping shrubland biomass along Mediterranean climatic gradients: The synergy of rainfall-based and NDVI-based models. International Journal of Remote Sensing 32, 9497-9508.

105. Simoneit, B.R.T., 2002. Biomass burning - A review of organic tracers for smoke from incomplete combustion. Appl Geochem 17, 129-162.

106. Sobrino, J.A., Julien, Y., 2013. Trend Analysis of Global MODIS-Terra

Vegetation Indices and Land Surface Temperature Between 2000 and 2011. Ieee J-Stars 6, 2139-2145.

107. Song, Y., Liu, B., Miao, W., Chang, D., Zhang, Y., 2009a. Spatiotemporal variation in nonagricultural open fire emissions in China from 2000 to 2007. Global Biogeochemical Cycles 23.

108. Song, Y., Liu, B., Miao, W.J., Chang, D., Zhang, Y.H., 2009b. Spatiotemporal variation in nonagricultural open fire emissions in China from 2000 to 2007. Global Biogeochemical Cycles 23.

109. Sousa, W.P., 1984. THE ROLE OF DISTURBANCE IN NATURAL COMMUNITIES. Annual Review of Ecology and Systematics 15, 353-391.

110. Stephens, S.L., 2005. Forest fire causes and extent on United States Forest Service lands. International Journal of Wildland Fire 14, 213-222.

111. Stocks, B.J., Mason, J.A., Todd, J.B., Bosch, E.M., Wotton, B.M., Amiro, B.D., Flannigan, M.D., Hirsch, K.G., Logan, K.A., Martell, D.L., Skinner, W.R., 2002. Large forest fires in Canada, 1959-1997. J Geophys Res-Atmos 108.

112. Streets, D.G., Canty, T., Carmichael, G.R., de Foy, B., Dickerson, R.R., Duncan, B.N., Edwards, D.P., Haynes, J.A., Henze, D.K., Houyoux, M.R., Jacobi, D.J., Krotkov, N.A., Lamsal, L.N., Liu, Y., Lu, Z., Martini, R.V., Pfister, G.G., Pinder, R.W., Salawitch, R.J., Wechti, K.J., 2013. Emissions estimation from satellite retrievals: A review of current capability. Atmospheric Environment 77, 1011-1042.

113. Tan, K., Piao, S., Peng, C., Fang, J., 2007a. Satellite-based estimation of biomass carbon stocks for northeast China's forests between 1982 and 1999. Forest Ecology and Management 240, 114-121.

114. Tan, K., Piao, S.L., Peng, C.H., Fang, J.Y., 2007b. Satellite-based estimation of biomass carbon stocks for northeast China's forests between 1982 and 1999. Forest Ecology and Management 240, 114-121.

115. Tang, X., Wang, Z., Liu, D., Song, K., Jia, M., Dong, Z., Munger, J.W., Hollinger, D.Y., Bolstad, P.V., Goldstein, A.H., Desai, A.R., Dragoni, D., Liu, X., 2012. Estimating the net ecosystem exchange for the major forests in the northern United States by integrating MODIS and AmeriFlux data. Agricultural and Forest Meteorology 156, 75-84.

116. Tang, X.G., Liu, D.W., Song, K.S., Munger, J.W., Zhang, B., Wang, Z.M., 2011. A new model of net ecosystem carbon exchange for the deciduous-dominated forest by integrating MODIS and flux data. Ecological Engineering 37, 1567-1571.

117. Telesca, L., Lasaponara, R., 2006. Pre- and post-fire behavioral trends revealed in satellite NDVI time series. Geophysical Research Letters 33.

118. Thompson, M.P., Calkin, D.E., 2011. Uncertainty and risk in wildland fire management: a review. Journal of environmental management 92, 1895-1909.

119. Tian, X.-r., Shu, L.-f., Zhao, F.-j., Wang, M.-y., McRae, D.J., 2011. Future impacts of climate change on forest fire danger in northeastern China. Journal of Forestry Research 22, 437-446.

120. Trowbridge, R., Feller, M.C., 1988. Relationships between the Moisture-Content of Fine Woody Fuels in Lodgepole Pine Slash and the Fine Fuel Moisture Code of the Canadian Forest Fire Weather Index System. Can J Forest Res 18, 128-131.

121. Tucker, C.J., Pinzon, J.E., Brown, M.E., Slayback, D.A., Pak, E.W., Mahoney, R., Vermote, E.F., El Saleous, N., 2005. An extended AVHRR 8-km NDVI dataset compatible with MODIS and SPOT vegetation NDVI data. International Journal of Remote Sensing 26, 4485-4498.

122. Turner, M.G., Romme, W.H., Gardner, R.H., Hargrove, W.W., 1997. Effects of fire size and pattern on early succession in Yellowstone National Park. Ecol Monogr 67, 411-433.

123. Urbanski, S.P., Salmon, J.M., Nordgren, B.L., Hao, W.M., 2009. A MODIS direct broadcast algorithm for mapping wildfire burned area in the western United States. Remote Sensing of Environment 113, 2511-2526.

124. van Leeuwen, W.J.D., 2008. Monitoring the effects of forest restoration treatments on post-fire vegetation recovery with MODIS multitemporal data. Sensors 8, 2017-2042.

125. Vasileva, A., Moiseenko, K., 2013. Methane emissions from 2000 to 2011 wildfires in Northeast Eurasia estimated with MODIS burned area data. Atmospheric Environment 71, 115-121.

126. Veraverbeke, S., Gitas, I., Katagis, T., Polychronaki, A., Somers, B., Goossens, R., 2012a. Assessing post-fire vegetation recovery using red-near infrared vegetation indices: Accounting for background and vegetation variability. ISPRS Journal of Photogrammetry and Remote Sensing 68, 28-39.

127. Veraverbeke, S., Verstraeten, W.W., Lhermitte, S., Van De Kerchove, R., Goossens, R., 2012b. Assessment of post-fire changes in land surface temperature and surface albedo, and their relation with fire - burn severity using multitemporal MODIS imagery. International Journal of Wildland Fire 21, 243.

128. Verbesselt, J., Somers, B., Lhermitte, S., Jonckheere, I., van Aardt, J., Coppin, P., 2007. Monitoring herbaceous fuel moisture content with SPOT VEGETATION

time-series for fire risk prediction in savanna ecosystems. Remote Sensing of Environment 108, 357-368.

129. Viedma, O., Melia, J., Segarra, D., GarciaHaro, J., 1997. Modeling rates of ecosystem recovery after fires by using Landsat TM data. Remote Sensing of Environment 61, 383-398.

130. Wang, J., Meng, J.J., Cai, Y.L., 2008a. Assessing vegetation dynamics impacted by climate change in the southwestern karst region of China with AVHRR NDVI and AVHRR NPP time-series. Environ Geol 54, 1185-1195.

131. Wang, X., He, H.S., Li, X., 2007. The long-term effects of fire suppression and reforestation on a forest landscape in Northeastern China after a catastrophic wildfire. Landscape and Urban Planning 79, 84-95.

132. Wang, X.P., Fang, J.Y., Zhu, B., 2008b. Forest biomass and root-shoot allocation in northeast China. Forest Ecology and Management 255, 4007-4020.

133. Westerling, A.L., Gershunov, A., Brown, T.J., Cayan, D.R., Dettinger, M.D., 2003. Climate and Wildfire in the Western United States. Bulletin of the American Meteorological Society 84, 595-604.

134. Wiedinmyer, C., Quayle, B., Geron, C., Belote, A., McKenzie, D., Zhang, X., O'Neill, S., Wynne, K.K., 2006. Estimating emissions from fires in North America for air quality modeling. Atmospheric Environment 40, 3419-3432.

135. Woodcock, C.E., Allen, R., Anderson, M., Belward, A., Bindschadler, R., Cohen, W., Gao, F., Goward, S.N., Helder, D., Helmer, E., Nemani, R., Oreopoulos, L., Schott, J., Thenkabail, P.S., Vermote, E.F., Vogelmann, J., Wulder, M.A., Wynne, R., Team, L.S., 2008. Free access to Landsat imagery. Science 320, 1011-1011.

136. Wu, Z.W., He, H.S., Chang, Y., Liu, Z.H., Chen, H.W., 2011. Development of customized fire behavior fuel models for boreal forests of northeastern China. Environmental management 48, 1148-1157.

137. Wulder, M.A., White, J.C., Alvarez, F., Han, T., Rogan, J., Hawkes, B., 2009. Characterizing boreal forest wildfire with multi-temporal Landsat and LIDAR data. Remote Sensing of Environment 113, 1540-1555.

138. Yan, X.Y., Ohara, T., Akimoto, H., 2006. Bottom-up estimate of biomass burning in mainland China. Atmospheric Environment 40, 5262-5273.

139. Yang, F.H., White, M.A., Michaelis, A.R., Ichii, K., Hashimoto, H., Votava, P., Zhu, A.X., Nemani, R.R., 2006. Prediction of continental-scale evapotranspiration by combining MODIS and AmeriFlux data through support vector machine. Ieee T Geosci Remote 44, 3452-3461.

140. Yebra, M., Chuvieco, E., Riano, D., 2008. Estimation of live fuel moisture content from MODIS images for fire risk assessment. Agricultural and Forest Meteorology 148, 523-536.

141. Zhang, X., Kondragunta, S., 2008. Temporal and spatial variability in biomass burned areas across the USA derived from the GOES fire product. Remote Sensing of Environment 112, 2886-2897.

142. Zhang, Y., Hu, H.-q., Wang, Q., 2011. Carbon Emissions from Forest Fires in Great Xing'an Mountains from 1980 to 2005. Procedia Environmental Sciences 10, Part C, 2505-2510.

143. Zhong, M., Fan, W., Liu, T., Li, P., 2003. Statistical analysis on current status of China forest fire safety. Fire Safety Journal 38, 257-269.

144. Zhou, L., Tian, Y., Baidya Roy, S., Dai, Y., Chen, H., 2012. Diurnal and seasonal variations of wind farm impacts on land surface temperature over western Texas. Clim Dynam, 1-20.

145. Zhou, L.M., Tucker, C.J., Kaufmann, R.K., Slayback, D., Shabanov, N.V., Myneni, R.B., 2001. Variations in northern vegetation activity inferred from satellite data of vegetation index during 1981 to 1999. J Geophys Res-Atmos 106, 20069-20083.

Terminology

biomass

(1) The amount of living matter in a given habitat, expressed either as the weight of organisms per unit area or as the volume of organisms per unit volume of habitat. (2) Organic matter that can be converted to fuel and is therefore regarded as a potential energy source. Note: Organisms include plant biomass (phytomass) and animal biomass (zoomass). (3) In fire science the term biomass is often used synonymously with the term "fuel" and includes both living and dead phytomass (necromass); the zoomass is usually excluded.

combustion

Consumption of fuels by oxidation, evolving heat and generally flame (neither necessarily sensible) and/or incandescence. Combustion can be divided into four phases: pre-ignition (or preheating), flaming, smouldering, and glowing.

dead fuel

Fuels with no living tissue in which moisture content is governed almost entirely by atmospheric moisture (relative humidity and precipitation), dry-bulb temperature, and solar radiation (cf. Live Fuel).

fine fuel

Fast-drying dead fuels, generally characterized by a comparatively high surface area-to-volume ratio, which are less than 0.5 cm in diameter and have a timelag of one hour or less. These fuels (grass, leaves, needles, etc.) ignite readily and are consumed rapidly by fire when dry. (cf. flash fuel, medium fuel, heavy fuel).

fire behaviour

The manner in which fuel ignites, flame develops, and fire spreads and exhibits other related phenomena as determined by the interaction of fuels, weather, and topography. Some common terms used to describe fire behaviour include the following:

fire danger

A general term used to express an assessment of both fixed and variable factors of the fire environment that determine the ease of ignition, rate of spread, difficulty of control, and fire impact; often expressed as an index.

fire ecology

The study of the relationships and interactions between fire, living organisms, and the environment.

fire frequency

The average number of fires or regularly occurring fire events per unit time in a designated area.

fire history

The reconstruction and interpretation of the chronological record, causes and impacts of fire occurrence in an ecosystem in relation to changes of past environmental, cultural and socio-economic conditions. Fire history evidence is based on analysis of charcoal deposits in soils, sediments, and ice, dendrochronology (fire scar analysis), historical documents, and fire reports.

fire interval or fire-return interval

The number of years between two successive fires documented in a designated area (i.e., the interval between two successive fire occurrences); the size of the area must be clearly specified.

fire management

All activities required for the protection of burnable forest and other vegetation values from fire and the use of fire to meet land management goals and objectives. It involves the strategic integration of such factors as a knowledge of fire regimes, probable fire effects, values-at-risk, level of forest protection required, cost of fire-related activities, and prescribed fire technology into multiple-use planning, decision making, and day-to-day activities to accomplish stated resource management objectives. Successful fire management depends on effective fire prevention, detection, and pre-suppression, having an adequate fire suppression capability, and consideration of fire ecology relationships.

fire regime

The patterns of fire occurrence, size, and severity - and sometimes, vegetation and fire effects as well - in a given area or ecosystem. It integrates various fire characteristics. A natural fire regime is the total pattern of fires over time that is characteristic of a natural region or ecosystem. The classification of fire regimes includes variations in ignition, fire intensity and behaviour, typical fire size, fire return intervals, and ecological effects.

fire season

(1) Period(s) of the year during which wildland fires are likely to occur and affect resources sufficiently to warrant organized fire management activities; (2) a legally enacted time during which burning activities are regulated by State or local authority.

fire suppression

All activities concerned with controlling and extinguishing a fire following its detection. (Syn. Fire Control, Fire Fighting).

fire weather

Weather conditions which influence fire ignition, behaviour, and suppression. Weather parameters are dry-bulb temperature, relative humidity, wind speed and direction, precipitation, atmospheric stability, winds aloft.

surface fire

A fire that burns in the surface fuel layer, excluding the crowns of the trees, as either a head fire, flank fire, or backfire.

crown fire

A fire that advances through the crown fuel layer, usually in conjunction with the surface fire.

fuel

All combustible organic material in forests and other vegetation types, including agricultural bio-mass such as grass, branches and wood, infrastructure in urban interface areas; which create heat during the combustion process.

fuel accumulation

Process or result of build-up of those elements of a vegetation complex which are not subject to biological decay, reduction by fire, animal grazing and browsing, or harvest by humans; used in characterizing fuel dynamics between two fires and implications on fire behaviour.

fuel consumption

The amount of a specified fuel type or strata that is removed through the fire process, often expressed as a percentage of the pre-burn fuel weight (or fuel load). It includes available fuel plus fuel consumed after the fire front passes.

fuel loading

The amount of fuel present expressed quantitatively in terms of weight of fuel per unit area. This may be available fuel (consumable fuel) or total fuel, usually expressed as ovendry weight.

prescribed fire

A management-ignited wildland fire or a wildfire that burns within prescription, i.e. the fire is confined to a predetermined area and produces the fire behavior and fire characteristics required to attain planned fire treatment and/or resource management objectives. The act or procedure of setting a prescribed fire is called prescribed burning (cf. Prescribed Burning). A wildfire burning within prescription may result from a human-caused fire or a natural fire (cf. prescribed natural fire, integrated forest fire management, wildfire).

rehabilitation

The activities necessary to repair damage or disturbance caused by wildfire or the wildfire suppression activity (cf. restoration).

residence time

(1) The time required for the flaming zone of a fire to pass a stationary point. (2) The time an emission component is in the air between emission and removal from the air or change into another chemical configuration.

restoration

Restoration of biophysical capacity of ecosystems to previous (desired) conditions. Restoration includes rehabilitation measures after fire, or prescribed burning where certain fire effects are desired (cf. rehabilitation, reclamation burning).

risk

(1) The probability of fire initiation due to the presence and activity of a causative agent. (2) A causative agent.

stand replacement fire

Fire which kills all or most living overstory trees in a forest and initiates secondary succession or regrowth.

wildfire

(1) Any unplanned and uncontrolled wildland fire which regardless of ignition source may require suppression response, or other action according to agency policy. (2) Any free burning wildland fire unaffected by fire suppression measures which meets

management objectives (cf. wildland, wildland fire, prescribed natural fire, prescribed fire).

wildland

Vegetated and non-vegetated land in which development is essentially non-existent, except for roads, railroads, powerlines, and similar transportation facilities; structures, if any, are widely scattered. In fire management terminology this general term includes all burnable vegetation resources including managed forests and forest plantations (cf. residential/wildland interface, wildfire).

Abbreviations

AVHRR: Advanced Very High Resolution Radiometer

CH_4: Methane

CO_2: Carbon dioxide

CO: Carbon monoxide

ETM+: Enhanced Thematic Mapper Plus

EVI: Enhanced Vegetation Index

FDI: Fire Disturbance Index

FMC: Fuel Moisture Content

GHG: Greenhouse gases

GIMMS: Global Inventory Modeling and Mapping Studies

GLC: Global Land Cover

LAI: Leaf Area Index

LST: Land Surface Temperature

MK: Mann-Kendall

MODIS: Moderate resolution Imaging Spectroradiometer

N_2O: Nitrous Oxide

NASA: National Aeronautics and Space Administration

NCDC: National Climatic Data Center

NDVI: Normalized difference vegetation index

NIR: Near Infrared

NOAA: National Oceanic and Atmospheric Administration

NO_X: Nitrogen Oxide

NPP: Net Primary Production

PM 2.5: particulate matter with a diameter of 2.5 micrometer or less

PM 10: particulate matter with a diameter of 10 micrometer or less

RRI: Relative Regrowth Index

SO_2: Sulfur Dioxide

SWIR: Shortwave Infrared

SRI: Stand Regrowth Index

TIR: Thermal Infrared

TM: Thematic Mapper

USGS: U.S. Geological Survey

VI: Vegetation Index

Helpful websites to this study

National Aeronautics and Space Administration (NASA)

https://earthdata.nasa.gov/

National Oceanic and Atmospheric Administration (NOAA)

http://www.noaa.gov/

U.S. Geological Survey (USGS)

http://www.usgs.gov/

Global Web Portal: The Global Fire Monitoring Center (GFMC):

http://www.fire.uni-freiburg.de

FAO Forest Fire Website

http://www.fao.org/forestry/foris/webview/forestry2/index.jsp?siteId=1520&langId=1&97038584

FAO Global Forest Fire Assessment 1990-2000:

http://www.fire.uni-freiburg.de/programmes/un/fao/Wp55_eng.pdf

Global Wildland Fire Network:

http://www.fire.uni-freiburg.de/GlobalNetworks/globalNet.html

WHO Health Guidelines on Vegetation Fire Events:

http://www.who.int/peh/air/vegetation_fires.htm

Global Observation of Forest Cover/Global Observation of Landcover Dynamics (GOFC/GOLD), Fire Mapping and Monitoring:

http://gofc-fire.umd.edu/

Wildland Fire Assessment System (WFAS)

http://www.wfas.net/